UNIVERSITY OF CALIFORNIA SAN DIEGO

Rgnef promotes ovarian tumor progression and confers protection from oxidative stress

A dissertation submitted in partial satisfaction of the requirements for the degree of Doctor of Philosophy

in

Biomedical Sciences

by

Elizabeth G. Kleinschmidt

Committee in charge:

Professor David Schlaepfer, Chair
Professor Kun-Liang Guan
Professor Pamela Mellon
Professor Dwayne Stupack
Professor JoAnn Trejo

2018

The dissertation of Elizabeth G. Kleinschmidt is approved, and it is acceptable in quality and form for publication on microfilm and electronically:

_____

_____

_____

_____

_____

Chair

University of California, San Diego

2018

DEDICATION

This thesis is dedicated to my parents Thomas and Julie Kleinschmidt, who fostered my love of learning and have always supported me along the way.

EPIGRAPH

"I regret only one thing, which is that the days are so short and that they pass so quickly. One never notices what has been done; one can only see what remains to be done, and if one didn't like the work it would be very discouraging. "

-Marie Curie

TABLE OF CONTENTS

LIST OF ABBREVIATIONS

3D	3-Dimensional
ChEA	Chip Enrichment Analysis
CNA	Copy Number Alterations
COSMIC	Catalogue of Somatic Mutations in Cancer
CRISPR	Clustered Regularly Interspaced Short Palindromic Repeats
CSC	Cancer Stem Cell
DH	Dbl Homology
ECM	Extracellular Matrix
FA	Focal Adhesion
FAK	Focal Adhesion Kinase
GDP	Guanosine Diphosphate
GEF	Guanine Nucleotide Exchange Factor
GFP	Green Fluorescence Protein
GSEA	Gene Set Enrichment Analysis
GTP	Guanosine Triphosphate
HGSOC	High-grade Serous Ovarian Cancer
IP	Intraperitoneal
KO	Knockout
MEFs	Mouse Embryonic Fibroblasts
MOVCAR	Murine Ovarian Carcinoma
NF-kB	Nuclear Factor Kappa B

OSE	Ovarian Surface Epithelium
PARP	Poly ADP Ribose Polymerase
PH	Pleckstrin Homology
PROVEAN	Protein Variation Effect Analyzer
RGNEF	Rho Guanine Nucleotide Exchange Factor
RNA-Seq	Whole mRNA Transcriptome Sequencing
SEE-FIM	Sectioning and Extensively Examining the Fimbriated End
SIFT	Sorting intolerant from tolerant
TAg	T-Antigen
TILs	Tumor-Infiltrating Lymphocytes
TME	Tumor Microenvironment
WES	Whole Exome Sequencing

LIST OF FIGURES

LIST OF TABLES

ACKNOWLEDGEMENTS

I'd like to thank my thesis advisor Dr. David Schlaepfer for the opportunity to work in this lab, and for his patience and support as a mentor and scientific advisor. Thanks also to all past and current member of the Schlaepfer lab for all the help, advice, and support, as well as members of the Stupack, Cheresh, and Gutkind labs who have advised with experiments. I'd also like to thank Susie Morris for helping the lab run smoothly, and for all the tiramisu. Thanks the members of my thesis committee, Drs. Dwayne Stupack, JoAnn Trejo, Kun-Liang Guan, and Pamela Mellon for their helpful feedback. I'd also like to thank BMS coordinators Leanne, Gina, and Pat, who have helped make the program a supportive environment for graduate students.

My parents, Tom and Julie Kleinschmidt, and my brothers Andrew and James have been incredibly supportive of me for my entire life, for which I am so indebted. My wife Lindsay Freeman has been a source of unwavering support and always helps me keep things in perspective. I'm so grateful for the friends I've met in graduate school, especially the BMS kids, the Rosewood crew, and the Burning Kernels crew. Without family and friends to celebrate, commiserate, watch football, and explore California with I would never have had the energy to make it through this journey.

Chapter 2, in full, is being prepared for submission: Kleinschmidt, E. G., Miller, N. L. G., Tancioni, I., Osterman C. D., Barrie A. M., Taylor K. N., Jiang S., Connolly D. C., Stupack D. G., Schlaepfer D. D. 2018. "Rgnef

promotes ovarian tumor progression and confers protection from oxidative stress.” The dissertation author was the primary investigator and author of this material.

Chapter 3 is an adaptation of material in preparation for submission in collaboration with Carlos Díaz-Osterman, Allison Barrie, Adam Mark, and Kathleen Fisch. The dissertation author was a co-primary investigator and author of this material.

VITA

2011 Bachelor of Science, University of Notre Dame

2018 Doctor of Philosophy, University of California San Diego

PUBLICATIONS

Kleinschmidt EG, Miller NLG, Tancioni I, Diaz-Osterman CJ, Barrie AM, Taylor KN, Jiang S, Connolly DCC, Stupack DG, Schlaepfer DD. Rgnef promotes ovarian cancer progression and confers protection from oxidative stress. *In preparation*.

Diaz-Osterman CJ*, **Kleinschmidt EG*,** Sulzmaier FJ, Taylor KN, Barrie AM, Tancioni I, Jean C, Jiang SA, Anderson K, Chen XL, Uryu S, Cordasco EA, Mark A, Fisch K, Kolev VN, Weaver DT, Pachter JA, McHale MT, Connolly DC, Molinolo A, Stupack DG, Schlaepfer DD. Targeting platinum-resistant ovarian cancer by FAK inhibition. *In preparation.*

Kleinschmidt EG, Schlaepfer DD. (2017). Focal adhesion kinase signaling in unexpected places. *Curr Opin Cell Biol*. *45*, 24-40.

Tancioni I, Miller NLG, Uryu S, Lawson C, Jean C, Chen XL, **Kleinschmidt EG**, Schlaepfer DD. (2015). FAK activity protects nucleostemin in facilitating breast cancer spheroid and tumor growth. *Breast Cancer Res. 17*(47).

Miller NLG, **Kleinschmidt EG**, Schlaepfer DD. (2014). RhoGEFs in cell motility: Novel links between Rgnef and Focal Adhesion Kinase. *Curr. Mol. Med. 14*(2), 221-234.

Miller NLG, Lawson C, **Kleinschmidt EG**, Tancioni I, Uryu S, Schlaepfer DD. (2013). A non-canonical role for Rgnef in promoting integrin-stimulated focal adhesion kinase activation. *J. Cell Sci*. *126*(21), 5074-5085.

FIELDS OF STUDY

Major Field: Biomedical Sciences

Professor David Schlaepfer

ABSTRACT OF THE DISSERTATION

Rgnef promotes ovarian tumor progression and confers protection from oxidative stress

by

Elizabeth G. Kleinschmidt

Doctor of Philosophy in Biomedical Sciences

University of California, San Diego, 2018

Professor David Schlaepfer, Chair

Ovarian cancer is the most deadly gynecological malignancy, with few treatment options. High mortality is largely due to late diagnosis after the disease

has metastasized. Ovarian tumor cells typically metastasize by detachment from the primary tumor into the peritoneal cavity. Aggressive tumor cells form multicellular spheroids, which attach and invade at distant sites. Preventing tumor spheroid survival, attachment, and invasion may provide therapeutic benefit.

Rgnef is a Rho guanine nucleotide exchange factor that canonically activates Rho GTPases, key coordinators of adhesion, migration, and contractility. Rgnef is activated downstream of integrin engagement with the extracellular matrix, and also binds directly to focal adhesion kinase (FAK). While Rgnef has been shown to promote colon carcinoma growth and invasiveness, the role of Rgnef in other types of cancer is unknown. In this thesis, I explore the role of Rgnef in ovarian carcinoma.

In Chapter 2, I demonstrate that Rgnef is overexpressed in late-stage serous ovarian cancer, and that high Rgnef expression corresponds to poor prognosis in late-stage patients. I use a genetically engineered mouse model and murine ovarian cancer cell lines to investigate the role of Rgnef in ovarian cancer tumor progression, demonstrating that Rgnef promotes both primary ovarian tumor formation and metastatic dissemination. Furthermore, I find that Rgnef is required for anchorage-independent spheroid growth. Finally, I reveal a novel role for Rgnef in promoting an NF-kB-mediated antioxidant gene signature, which may protect cells from reactive oxygen species induced in anchorage-independent conditions. In Chapter 3, I characterize a novel aggressive murine cell line that models human ovarian cancer. In Chapter 4, I explore how the

interaction between Rgnef and FAK promotes growth and contractility when attached to extracellular matrix.

Chapter 1

Introduction

1.1 Ovarian cancer

Ovarian cancer is the most deadly gynecological malignancy, with an estimated 47% five-year survival rate (Siegel, Miller, and Jemal 2018). High-grade serous ovarian carcinoma (HGSOC) is the most deadly and common ovarian cancer subtype, and typically presents at an advanced stage after the disease has spread into the peritoneal cavity (Lengyel 2010; Narod 2016). The 10-year survival rate for patients diagnosed with advanced-stage HGSOC is only 15% (Narod 2016), largely due to recurrence after initial treatment. Therefore, it is essential to develop biomarkers for earlier diagnosis and targeted therapeutics to treat recurrent disease.

Until recently, the site of origin for HGSOC was under debate. Many early theories proposed the ovarian surface epithelium (OSE) as the site of origin, despite the observation that HGSOC tumor histology more closely resembles the fallopian epithelium than the OSE (Kurman and Shih 2010). However, as it became standard practice for women with pathogenic *BRCA1/2* germline mutations to undergo risk-reducing salpingo-oophorectomy surgery, dysplastic lesions were identified in the fimbriae of removed fallopian tubes (Perets and Drapkin 2016; Karnezis et al. 2016; Labidi-Galy et al. 2017). Adoption of the SEE-FIM (Sectioning and Extensively Examining the Fimbriated End) protocol in these fallopian tube specimens led to development of a HGSOC initiation model. First, a “p53 signature” distinguished by *TP53* mutations and DNA damage is observed in fallopian tube, followed by development of a dysplastic precursor

STIC (serous tubal intraepithelial carcinoma) lesion (Perets and Drapkin 2016). Using mathematical models of genomic data from patients presenting with both STIC and ovarian cancer, the average estimated time between initiation and ovarian cancer is 6.5 years, although the estimated time for patients that present with advanced diseased is only 2 years (Labidi-Galy et al. 2017).

The rapid development from precursor lesion to metastasis in ovarian cancer is likely due to the unique metastatic progression of ovarian cancer (Fig 1.1a). In the classic model of ovarian cancer progression, primary tumors spread to adjacent sites through localized migration in early stages. In advanced stages, tumor cells are shed into the peritoneal cavity, either as single cells or multicellular sheets. Surviving cells form multicellular spheroids that are passively diffused by peritoneal fluid and attach to distant peritoneal sites, preferentially the omentum (Naora and Montell 2005; Shield et al. 2009; Ahmed and Stenvers 2013; Al Habyan et al. 2018). Thus, there are fewer barriers to metastasis in HGSOC than in other solid tumors, many of which disseminate by invading matrix and spreading through hematogenous routes. As residual microscopic spheroids that survive cytoreductive surgery are often more resistant to chemotherapeutics, discovering novel ways to eradicate residual peritoneal tumor cells is essential in order to prevent tumor recurrence (Narod 2016; Shield et al. 2009).

Patients with HGSOC are typically responsive to the standard platinum- and taxane- based chemotherapeutics first administered as neo-adjuvant or adjuvant chemotherapy (Matulonis et al. 2016; Narod 2016). However, about

80% of patients diagnosed at advanced stages will experience tumor recurrence, which often becomes resistant to chemotherapy (Matulonis et al. 2016). As HGSOC is a disease characterized by low mutational burden but high levels of copy number alterations (CNAs), it is difficult to use targeted therapeutics to treat classically “druggable” driver mutations. Instead, research efforts often focus on methods of targeting functional vulnerabilities in HGSOC. For example, about half of HGSOC tumors have a defect in the homologous recombination (HR) DNA repair pathway, usually due to mutations in *BRCA1/2*. PARP (poly(ADP-ribose)) inhibitors such as olaparib that further disrupt DNA repair have been approved for use in patients with HR-defective tumors (Bowtell et al. 2015). Novel therapeutic approaches involve selectively targeting cancer cells by increasing stressors already present in tumor cells, such as metabolic or oxidative stress (Raj et al. 2011; Shaukat et al. 2015). Identifying tumor-specific CNA signatures that render tumors more sensitive to targeted drugs and chemotherapeutics is an important task for ovarian cancer researchers (McLornan, List, and Mufti 2014).

1.2 Focal adhesion kinase (FAK)

Cell migration is a highly regulated process required for both normal development and tumor metastasis. Many signaling pathways controlling cell migration converge on the actin cytoskeleton, which determines cell shape, adhesion, and tension generation. During cell migration, the actin cytoskeleton is

physically linked to the extracellular environment through cell-matrix contacts called focal adhesions. Focal adhesion formation is initiated by integrins, a family of heterodimeric transmembrane receptor proteins. While integrins do not have inherent signaling ability, their engagement with ECM proteins triggers clustering and permits the recruitment of adaptor and signaling proteins (Hynes 2002; Parsons, Horwitz, and Schwartz 2010). These multiprotein focal adhesion complexes serve as hubs for signal transduction, traction, and mechanosensing throughout the cell (Geiger, Spatz, and Bershadsky 2009; Mitra, Hanson, and Schlaepfer 2005; Plotnikov and Waterman 2013).

FAK (focal adhesion kinase) is one of the first proteins to be recruited to nascent focal adhesions, mediated by its interaction with paxillin, talin, and Rgnef (Hildebrand, Schaller, and Parsons 1993; Lawson et al. 2012; Miller et al. 2013). Mutational and knockout analyses demonstrate that all three proteins contribute to, but are not sufficient for, FAK localization to nascent adhesions (Lawson and Schlaepfer 2012; Miller et al. 2013). Evidence suggests that FAK is recruited in an inactive, autoinhibited state (Walkiewicz, Girault, and Arold 2015). Following localization, the FAK autoinhibitory FERM domain binds $PI(4,5)P_2$ lipids generated by PIPKIγ, resulting in a “relaxed” conformation that promotes FAK clustering and an equilibrium shift towards transient dimerization (Goñi et al. 2014). Transient FAK dimerization has been proposed to facilitate FAK autophosphorylation at Y397 in *trans* (Brami-Cherrier et al. 2014). FAK autophosphorylation and further phosphorylation by Src creates a binding site for SH2- and SH3-containing adaptor proteins such as Grb2 and p130Cas(D D

Schlaepfer et al. 1994). By binding various adaptor proteins, FAK is connected to signal transduction pathways throughout the cell, such as the PI3K-AKT and MAPK-JNK signaling pathways (David D Schlaepfer and Mitra 2004; Parsons, Horwitz, and Schwartz 2010; Sulzmaier, Jean, and Schlaepfer 2014).

While most research has focused on the role of FAK at focal adhesions, recent studies have revealed novel roles for FAK at additional subcellular sites (Kleinschmidt and Schlaepfer 2017) (Fig 1.1b). New evidence suggests that FAK is recruited to endosomal membranes, where it facilitates maintenance of integrin activation and suppresses anoikis in detached conditions (Alanko et al. 2015). FAK also localizes to adherens junctions following VEGF treatment, resulting in increased vascular permeability and tumor cell transmigration (Chen et al. 2012; Jean et al. 2014). FAK also plays several roles in the nucleus. As an adaptor, FAK provides a scaffold that connects E3 ubiquitin ligases and transcription factors such as p53 and GATA4, promoting their ubiquitination and degradation (Lim et al. 2008, 2012). FAK has also been shown to bind directly to a core component of the TFIID complex that is recruited to sites of active transcription (Serrels et al. 2015). Unlike many other non-receptor tyrosine kinases, FAK is not myristoylated or palmitoylated to promote membrane targeting, but instead relies on protein-protein and protein-lipid interactions to modulate its cellular localization (Goñi et al. 2014; Mitra, Hanson, and Schlaepfer 2005). Thus, understanding the interaction between FAK and its many protein binding partners is key to understanding FAK spatiotemporal activation in these many subcellular localizations.

FAK is amplified or overexpressed in a number of human cancers. Consistent with its position at the intersection of many signaling pathways controlling motility, survival, and transcriptional pathways, many studies have demonstrated a role for FAK in promoting tumor progression (Sulzmaier, Jean, and Schlaepfer 2014). FAK is amplified or overexpressed in over 50% of ovarian cancer cases (Cerami et al. 2012). Data from our lab suggests that pharmacological inhibition of FAK can sensitize cisplatin-resistant tumor cells to cisplatin treatment both *in vitro* and *in vivo*, and FAK inhibitors are being used in several clinical trials for ovarian cancer (NCT03287271, NCT01778803). This provides further support for the study of proteins that regulate and bind to FAK.

1.3 Rgnef (Arhgef28/p190RhoGEF)

Rho GTPases are key coordinators of the actin cytoskeleton, regulating adhesion, migration, and actomyosin contractility. In cancer cells, these processes are required for local spread and metastasis. Rho GTPases function as bi-molecular switches that alternate between an inactive GDP-bound state and an active GTP-bound state. GTP binding triggers a conformational shift that allows Rho GTPases to interact with a variety of effector proteins (Jaffe and Hall 2005). Interestingly, although mutations in canonical Ras GTPases occur in about 30% of human cancers, Rho GTPases are rarely mutated in cancer (Fernández-Medarde and Santos 2011; Barrio-Real and Kazanietz 2012).

Rho GTPase activation by exchange of -GDP for -GTP is facilitated by a

family of guanine nucleotide exchange factors (GEFs) that are under strict spatiotemporal control. Like Rho GTPases, GEFs are not usually mutated in human cancers, although they are often overexpressed and correlate with higher Rho GTPase activation (Barrio-Real and Kazanietz 2012). While most GEFs activate specific isoforms of one of three main Rho GTPase subfamilies; Rho; Rac; and Cdc42; others interact more promiscuously (Fig 1.2a). Notably, phosphorylation of RhoA regulatory proteins was found to be the pathway most significantly correlated with short survival (< 3 years) in HGSOC patients (Zhang et al. 2016), yet only two Rho-specific GEFs have been implicated in ovarian cancer progression (Earp et al. 2018; Wakahashi et al. 2013). Examining the role of the GEFs responsible for Rho activation in ovarian cancer could guide future pharmacological studies.

In canonical models of focal adhesion formation, GEFs are proposed to function far downstream of integrin signaling. An exception is Rgnef (also named Arhgef28 or p190RhoGEF), which localizes to focal adhesions and binds directly to phosphoinositide lipids at the plasma membrane (Fig 1.2b-c). Rgnef is a ubiquitously-expressed protein which was first identified as a RhoA-specific GEF that prevents neurite outgrowth (Gebbink et al. 1997). Rgnef contains a tandem DH-PH (Dbl-homology/pleckstrin-homology) domain that is conserved across the Dbl GEF family, and several putative regulatory domains, including an N-terminal leucine-rich region, putative zinc-finger domain, and PDZ-binding motif.

While *in vitro* experiments suggest that the Rgnef DH-PH domain specifically activates RhoA, RhoB, and RhoC, experiments with full-length Rgnef

have only revealed Rgnef-specific activation of RhoA and RhoC (Miller et al. 2012; Bravo-Cordero et al. 2011). Rgnef is activated within an hour of fibronectin-induced integrin activation, as measured by binding and affinity precipitation with a nucleotide-free mutant of RhoA (G17A) (Miller et al. 2012). Consistent with a role in Rho GTPase activation, depletion of Rgnef decreases wound closure time, and overexpression induces the formation of actin stress fibers (Miller et al. 2012; van Horck et al. 2001). In mammary tumor cells, Rgnef is required for localized spatial activation of RhoC surrounding invadopodia, and promotes localized RhoC activation just behind the leading edge of a migrating cell (Bravo-Cordero et al. 2011; Bravo-Cordero, Hodgson, and Condeelis 2012).

While the DH and PH catalytic domains are both required for GEF nucleotide exchange, the PH domain alone possesses several unique properties in Rgnef function. The Rgnef PH domain binds phosphoinositide lipids through residues R1098/K1100, preferentially to PI(4)P, PI(4,5)P_2, and phosphatidic acid. Functionally, mutation of these residues abrogates PH domain-phosphoinositide binding and prevents Rgnef localization to the leading edge of a spreading cell (Miller et al. 2013). Furthermore, recent evidence demonstrates that active (GTP-bound) RhoA and Rac1 bind to a conserved hydrophobic patch on the Rgnef PH domain (Fig 1.2c), which stimulates Rgnef-RhoA exchange activity in both cases (Medina et al. 2013; Dada et al. 2017). While Rac1-GTP interaction with the GEF family members most similar to Rgnef (ARHGEF11, ARHGEF12, AKAP13, ARHGEF18) moderately stimulates RhoA exchange activity, Rac1-GTP-stimulated RhoA activation is vastly increased upon Rac1-Rgnef interaction

(Dada et al. 2017). This is noteworthy because it suggests that Rgnef is preferentially involved in mediating Rac-Rho crosstalk, despite the fact that Rgnef does not stimulate Rac GTPase activity.

Unlike most other GEFs, Rgnef binds directly to FAK through residues 1292-1301, which are adjacent to the putative Rgnef coiled-coil domain (Fig 1.2b) (Zhai et al. 2003). Rgnef co-localizes with FAK at nascent adhesions at the periphery of a spreading cell, and deletion of the Rgnef FAK-binding domain (*Rgnef* $^{\Delta 1292}$) or mutation of the PH domain phosphoinositide-binding residues (*Rgnef* $^{R1098A/K1100A}$) impairs FAK localization to nascent adhesions. FAK activation following integrin stimulation is also diminished by Rgnef knockout or by *Rgnef* $^{\Delta 1292}$ or *Rgnef* $^{R1098A/K1100A}$ re-expression in *Rgnef* $^{-/-}$ mouse embryonic fibroblasts (MEFs). Interestingly, this FAK recruitment and activation is independent of Rgnef GEF activity, as determined by re-expression of the catalytically inactive *Rgnef* ^{Y1003A} mutant in *Rgnef* $^{-/-}$ cells (Miller et al. 2013). Conversely, FAK activation promotes Rgnef phosphorylation and RhoA activation (Zhai et al. 2003), suggesting that the FAK-Rgnef interaction is critical for both proteins at the early stages of focal adhesion initiation. Overexpression of the C-terminal end of Rgnef (amino acids 1279-1582) prevents the Rgnef-FAK interaction in a dominant-negative manner, and decreases tumor size and invasiveness in an orthotopic mouse model of colon carcinoma (Yu et al. 2011). This indicates that the Rgnef-FAK connection is also important for invasiveness and tumor progression *in vivo*.

1.4 Conclusions and overview

Rgnef has been shown to play a role in colon carcinoma progression. Furthermore, Rgnef promotes the activation of both FAK and Rho GTPases, two proteins involved in motility and ovarian tumor progression. While Rgnef has not previously been studied in ovarian carcinoma, its place at the intersection of two migration and adhesion pathways makes this protein a good candidate for further studies. In this thesis, I will explore the role of Rgnef in ovarian tumor progression. In Chapter 2, I show that Rgnef is overexpressed in ovarian cancer, promotes primary and metastatic tumor formation, and confers protection from oxidative stress in anchorage-independent conditions. In Chapter 3, I characterize a new model of aggressive ovarian cancer, demonstrating that these cells retain characteristics similar to HGSOC such as low mutational burden but numerous copy number alterations. In Chapter 4, I demonstrate that the Rgnef-FAK connection in is needed for growth and contractility in extracellular matrix-attached conditions.

1.5 References

Ahmed, N., and K. L. Stenvers. 2013. “Getting to Know Ovarian Cancer Ascites: Opportunities for Targeted Therapy-Based Translational Research.” *Front Oncol* 3 (September): 1–12. doi.org/10.3389/fonc.2013.00256.

Alanko, J., A. Mai, G. Jacquemet, K. Schauer, R. Kaukonen, M. Saari, B. Goud, and J. Ivaska. 2015. “Integrin Endosomal Signalling Suppresses Anoikis.” *Nat Cell Biol* 17 (11). doi.org/10.1038/ncb3250.

Barrio-Real, L., and M. G. Kazanietz. 2012. “Rho GEFs and Cancer: Linking Gene Expression and Metastatic Dissemination.” *Sci Signal* 5 (244): pe43. doi.org/10.1126/scisignal.2003543.

Bowtell, D. D., S. Böhm, A. A. Ahmed, P.-J. Aspuria, R. C. Bast, V. Beral, J. S. Berek, et al. 2015. “Rethinking Ovarian Cancer II: Reducing Mortality from High-Grade Serous Ovarian Cancer.” *Nat Rev Cancer* 15 (11): 668–79. doi.org/10.1038/nrc4019.

Brami-Cherrier, K., N. Gervasi, D. Arsenieva, K. Walkiewicz, M. C. Boutterin, A. Ortega, P. G. Leonard, et al. 2014. “FAK Dimerization Controls Its Kinase-Dependent Functions at Focal Adhesions.” *EMBO J* 33 (4): 356–70. doi.org/10.1002/embj.201386399.

Bravo-Cordero, J. J., L. Hodgson, and J. Condeelis. 2012. “Directed Cell Invasion and Migration during Metastasis.” *Curr Opin Cell Biol* 24 (2): 277–83. doi.org/10.1016/j.ceb.2011.12.004.

Bravo-Cordero, J. J., M. Oser, X. Chen, R. Eddy, L. Hodgson, and J. Condeelis. 2011. “A Novel Spatiotemporal RhoC Activation Pathway Locally Regulates Cofilin Activity at Invadopodia.” *Curr Biol* 21 (8): 635–44. doi.org/10.1016/j.cub.2011.03.039.A.

Cerami, E., J. Gao, U. Dogrusoz, B. E. Gross, S. O. Sumer, B. A. Aksoy, A. Jacobsen, et al. 2012. “The cBio Cancer Genomics Portal: An Open Platform for Exploring Multidimensional Cancer Genomics Data.” *Cancer Discov* 2 (5): 401–4. doi.org/10.1158/2159-8290.CD-12-0095.

Chen, X. L., J.-O. Nam, C. Jean, C. Lawson, C. T. Walsh, E. Goka, S.-T. Lim, et al. 2012. “VEGF-Induced Vascular Permeability Is Mediated by FAK.” *Dev Cell* 22 (1): 146–57. doi.org/10.1016/j.devcel.2011.11.002.

Dada, O., S. Gutowski, C. A. Brautigam, Z. Chen, and P. C. Sternweis. 2017. “Direct Regulation of p190RhoGEF by Activated Rho and Rac GTPases.” *J Struct Biol*, no. July: 0–1. doi.org/10.1016/j.jsb.2017.11.014.

Earp, M., J. P. Tyrer, S. J. Winham, H.-Y. Lin, G. Chornokur, J. Dennis, K. K. H. Aben, et al. 2018. “Variants in Genes Encoding Small GTPases and Association with Epithelial Ovarian Cancer Susceptibility.” *PLoS One* 13 (7): e0197561. doi.org/10.1371/journal.pone.0197561.

Fernández-Medarde, A., and E. Santos. 2011. “Ras in Cancer and Developmental Diseases.” *Genes and Cancer* 2 (3): 344–58. doi.org/10.1177/1947601911411084.

Gebbink, M. F., O. Kranenburg, M. Poland, F. P. van Horck, B. Houssa, and W. H. Moolenaar. 1997. “Identification of a Novel, Putative Rho-Specific GDP/GTP Exchange Factor and a RhoA-Binding Protein: Control of Neuronal Morphology.” *J Cell Biol* 137 (7): 1603–13.

Geiger, B., J. P. Spatz, and A. D. Bershadsky. 2009. “Environmental Sensing through Focal Adhesions.” *Nat Rev Mol Cell Biol* 10 (1): 21–33. doi.org/10.1038/nrm2593.

Goñi, G. M., C. Epifano, J. Boskovic, M. Camacho-Artacho, J. Zhou, A. Bronowska, M. T. Martín, et al. 2014. “Phosphatidylinositol 4,5-Bisphosphate Triggers Activation of Focal Adhesion Kinase by Inducing Clustering and Conformational Changes.” *Proc Natl Acad Sci U S A* 111 (31): E3177-86. doi.org/10.1073/pnas.1317022111.

Habyan, S. Al, C. Kalos, J. Szymborski, and L. McCaffrey. 2018. “Multicellular Detachment Generates Metastatic Spheroids during Intra-Abdominal Dissemination in Epithelial Ovarian Cancer.” *Oncogene*, no. 1: 1–9. doi.org/10.1038/s41388-018-0317-x.

Hildebrand, J. D., M. D. Schaller, and J. T. Parsons. 1993. “Identification of Sequences Required for the Efficient Localization of the Focal Adhesion Kinase, pp125 FAK, to Cellular Focal Adhesions.” *Cell* 123 (4): 993–1005.

Horck, F. P. van, M. R. Ahmadian, L. C. Haeusler, W. H. Moolenaar, and O. Kranenburg. 2001. “Characterization of p190RhoGEF, a RhoA-Specific Guanine Nucleotide Exchange Factor That Interacts with Microtubules.” *J Biol Chem* 276 (7): 4948–56. doi.org/10.1074/jbc.M003839200.

Hynes, R. O. 2002. “Integrins: Bidirectional, Allosteric Signaling Machines.” *Cell* 110 (6): 673–87. doi.org/10.1016/S0092-8674(02)00971-6.

Jaffe, A. B., and A. Hall. 2005. “Rho GTPases: Biochemistry and Biology.” *Annu Rev Cell Dev Biol* 21 (January): 247–69. doi.org/10.1146/annurev.cellbio.21.020604.150721.

Jean, C., X. L. Chen, J.-O. Nam, I. Tancioni, S. Uryu, C. Lawson, K. K. Ward, et al. 2014. “Inhibition of Endothelial FAK Activity Prevents Tumor Metastasis by Enhancing Barrier Function.” *J Cell Biol* 204 (2): 247–63. doi.org/10.1083/jcb.201307067.

Karnezis, A. N., K. R. Cho, C. B. Gilks, C. L. Pearce, and D. G. Huntsman. 2016. “The Disparate Origins of Ovarian Cancers: Pathogenesis and Prevention Strategies.” *Nat Rev Cancer*. doi.org/10.1038/nrc.2016.113.

Kleinschmidt, E. G., and D. D. Schlaepfer. 2017. “Focal Adhesion Kinase Signaling in Unexpected Places.” *Curr Opin Cell Biol* 45: 24–30. doi.org/10.1016/j.ceb.2017.01.003.

Kurman, R. J., and I.-M. Shih. 2010. “The Origin and Pathogenesis of Epithelial Ovarian Cancer: A Proposed Unifying Theory.” *Am J Surg Pathol* 34 (3): 433–43. doi.org/10.1097/PAS.0b013e3181cf3d79.

Labidi-Galy, S. I., E. Papp, D. Hallberg, N. Niknafs, V. Adleff, M. Noe, R. Bhattacharya, et al. 2017. “High Grade Serous Ovarian Carcinomas Originate in the Fallopian Tube.” *Nat Commun* 8 (1): 1093. doi.org/10.1038/s41467-017-00962-1.

Lawson, C., S.-T. Lim, S. Uryu, X. L. Chen, D. a Calderwood, and D. D. Schlaepfer. 2012. “FAK Promotes Recruitment of Talin to Nascent Adhesions to Control Cell Motility.” *J Cell Biol* 196 (2): 223–32. doi.org/10.1083/jcb.201108078.

Lawson, C., and D. D. Schlaepfer. 2012. “Integrin Adhesions: Who’s on First? What’s on Second? Connections between FAK and Talin.” *Cell Adhes Migr*, no. August: 1–5.

Lengyel, E. 2010. “Ovarian Cancer Development and Metastasis.” *Am J Pathol* 177 (3): 1053–64. doi.org/10.2353/ajpath.2010.100105.

Lim, S.-T., X. L. Chen, Y. Lim, D. A. Hanson, T.-T. Vo, K. Howerton, N. Larocque, S. J. Fisher, D. D. Schlaepfer, and D. Ilic. 2008. “Nuclear FAK Promotes Cell Proliferation and Survival through FERM-Enhanced p53 Degradation.” *Mol Cell* 29 (1): 9–22. doi.org/10.1016/j.molcel.2007.11.031.

Lim, S.-T., N. L. G. Miller, X. L. Chen, I. Tancioni, C. T. Walsh, C. Lawson, S. Uryu, S. M. Weis, D. a Cheresh, and D. D. Schlaepfer. 2012. “Nuclear-Localized Focal Adhesion Kinase Regulates Inflammatory VCAM-1 Expression.” *J Cell Biol* 197 (7): 907–19. doi.org/10.1083/jcb.201109067.

Matulonis, U. A., A. K. Sood, L. Fallowfield, B. E. Howitt, J. Sehouli, and B. Y.

Karlan. 2016. “Ovarian Cancer.” *Nat Rev Dis Prim* 2: 1–22. doi.org/10.1038/nrdp.2016.61.

McLornan, D. P., A. List, and G. J. Mufti. 2014. “Applying Synthetic Lethality for the Selective Targeting of Cancer.” *N Engl J Med* 371 (18): 1725–35. doi.org/10.1056/NEJMra1407390.

Medina, F., A. M. Carter, O. Dada, S. Gutowski, J. Hadas, Z. Chen, and P. C. Sternweis. 2013. “Activated RhoA Is a Positive Feedback Regulator of the Lbc Family of RhoGEFs.” *J Biol Chem*, no. 5(March): 1–19. doi.org/10.1074/jbc.M113.450056.

Miller, N. L. G., C. Lawson, X. L. Chen, S.-T. Lim, and D. D. Schlaepfer. 2012. “Rgnef (p190RhoGEF) Knockout Inhibits RhoA Activity, Focal Adhesion Establishment, and Cell Motility Downstream of Integrins.” *PLoS One* 7 (5): e37830. doi.org/10.1371/journal.pone.0037830.

Miller, N. L. G., C. Lawson, E. G. Kleinschmidt, I. Tancioni, S. Uryu, and D. D. Schlaepfer. 2013. “A Non-Canonical Role for Rgnef in Promoting Integrin-Stimulated Focal Adhesion Kinase Activation.” *J Cell Sci* 126 (Pt 21): 5074–85. doi.org/10.1242/jcs.135509.

Mitra, S. K., D. a Hanson, and D. D. Schlaepfer. 2005. “Focal Adhesion Kinase: In Command and Control of Cell Motility.” *Nat Rev Mol Cell Biol* 6 (1): 56–68. doi.org/10.1038/nrm1549.

Naora, H., and D. J. Montell. 2005. “Ovarian Cancer Metastasis: Integrating Insights from Disparate Model Organisms.” *Nat Rev Cancer* 5 (5): 355–66. doi.org/10.1038/nrc1611.

Narod, S. 2016. “Can Advanced-Stage Ovarian Cancer Be Cured?” *Nat Rev Clin Oncol* 13 (4): 255–61. doi.org/10.1038/nrclinonc.2015.224.

Parsons, J. T., A. R. Horwitz, and M. a Schwartz. 2010. “Cell Adhesion: Integrating Cytoskeletal Dynamics and Cellular Tension.” *Nat Rev Mol Cell Biol* 11 (9): 633–43. doi.org/10.1038/nrm2957.

Perets, R., and R. Drapkin. 2016. “It’s Totally Tubular···. Riding the New Wave of Ovarian Cancer Research.” *Cancer Res* 76 (1): 10–17. doi.org/10.1158/0008-5472.CAN-15-1382.

Plotnikov, S. V, and C. M. Waterman. 2013. “Guiding Cell Migration by Tugging.” *Curr Opin Cell Biol* 25 (5): 619–26. doi.org/10.1016/j.ceb.2013.06.003.

Raj, L., T. Ide, A. U. Gurkar, M. Foley, M. Schenone, X. Li, N. J. Tolliday, et al.

2011. “Selective Killing of Cancer Cells by a Small Molecule Targeting the Stress Response to ROS.” *Nature* 475 (7355): 231–34. doi.org/10.1038/nature10167.

Schlaepfer, D. D., S. K. Hanks, T. Hunter, and P. van der Geer. 1994. “Integrin-Mediated Signal Transduction Linked to Ras Pathway by GRB2 Binding to Focal Adhesion Kinase.” *Nature*. doi.org/10.1038/372786a0.

Schlaepfer, D. D., and S. K. Mitra. 2004. “Multiple Connections Link FAK to Cell Motility and Invasion.” *Curr Opin Genet Dev* 14 (1): 92–101. doi.org/10.1016/j.gde.2003.12.002.

Serrels, A., T. Lund, B. Serrels, S. M. Anderton, R. J. B. Nibbs, M. C. Frame, A. Byron, et al. 2015. “Nuclear FAK Controls Chemokine Transcription, Tregs, and Evasion of Anti-Tumor Immunity.” *Cell* 163: 160–73. doi.org/10.1016/j.cell.2015.09.001.

Shaukat, Z., D. Liu, A. Choo, R. Hussain, L. O’Keefe, R. Richards, R. Saint, and S. L. Gregory. 2015. “Chromosomal Instability Causes Sensitivity to Metabolic Stress.” *Oncogene* 34 (31): 4044–55. doi.org/10.1038/onc.2014.344.

Shield, K., M. L. Ackland, N. Ahmed, and G. E. Rice. 2009. “Multicellular Spheroids in Ovarian Cancer Metastases: Biology and Pathology.” *Gynecol Oncol* 113 (1): 143–48. doi.org/10.1016/j.ygyno.2008.11.032.

Siegel, R. L., K. D. Miller, and A. Jemal. 2018. “Cancer Statistics, 2018.” *CA Cancer J Clin* 68 (1): 7–30. doi.org/10.3322/caac.21442.

Sulzmaier, F. J., C. Jean, and D. D. Schlaepfer. 2014. “FAK in Cancer: Mechanistic Findings and Clinical Applications.” *Nat Rev Cancer* 14 (9): 598–610. doi.org/10.1038/nrc3792.

Wakahashi, S., T. Sudo, N. Oka, S. Ueno, S. Yamaguchi, K. Fujiwara, C. Ohbayashi, and R. Nishimura. 2013. “VAV1 Represses E-Cadherin Expression through the Transactivation of Snail and Slug: A Potential Mechanism for Aberrant Epithelial to Mesenchymal Transition in Human Epithelial Ovarian Cancer.” *Transl Res* 162 (3): 181–90. doi.org/10.1016/j.trsl.2013.06.005.

Walkiewicz, K. W., J.-A. Girault, and S. T. Arold. 2015. “How to Awaken Your Nanomachines: Site-Specific Activation of Focal Adhesion Kinases through Ligand Interactions.” *Prog Biophys Mol Biol* 119 (1): 60–71. doi.org/10.1016/j.pbiomolbio.2015.06.001.

Yu, H.-G., J.-O. Nam, N. L. G. Miller, I. Tanjoni, C. Walsh, L. Shi, L. Kim, et al. 2011. “p190RhoGEF (Rgnef) Promotes Colon Carcinoma Tumor Progression via Interaction with Focal Adhesion Kinase.” *Cancer Res* 71 (2): 360–70. doi.org/10.1158/0008-5472.CAN-10-2894.

Zhai, J., H. Lin, Z. Nie, J. Wu, R. Cañete-Soler, W. W. Schlaepfer, and D. D. Schlaepfer. 2003. “Direct Interaction of Focal Adhesion Kinase with p190RhoGEF.” *J Biol Chem* 278 (27): 24865–73. doi.org/10.1074/jbc.M302381200.

Zhang, H., T. Liu, Z. Zhang, D. W. Chan, K. D. Rodland, H. Zhang, T. Liu, et al. 2016. “Integrated Proteogenomic Characterization of Human High-Grade Serous Ovarian Cancer Resource Integrated Proteogenomic Characterization of Human High-Grade Serous Ovarian Cancer.” *Cell*, 1–11. doi.org/10.1016/j.cell.2016.05.069.

1.6 Figures

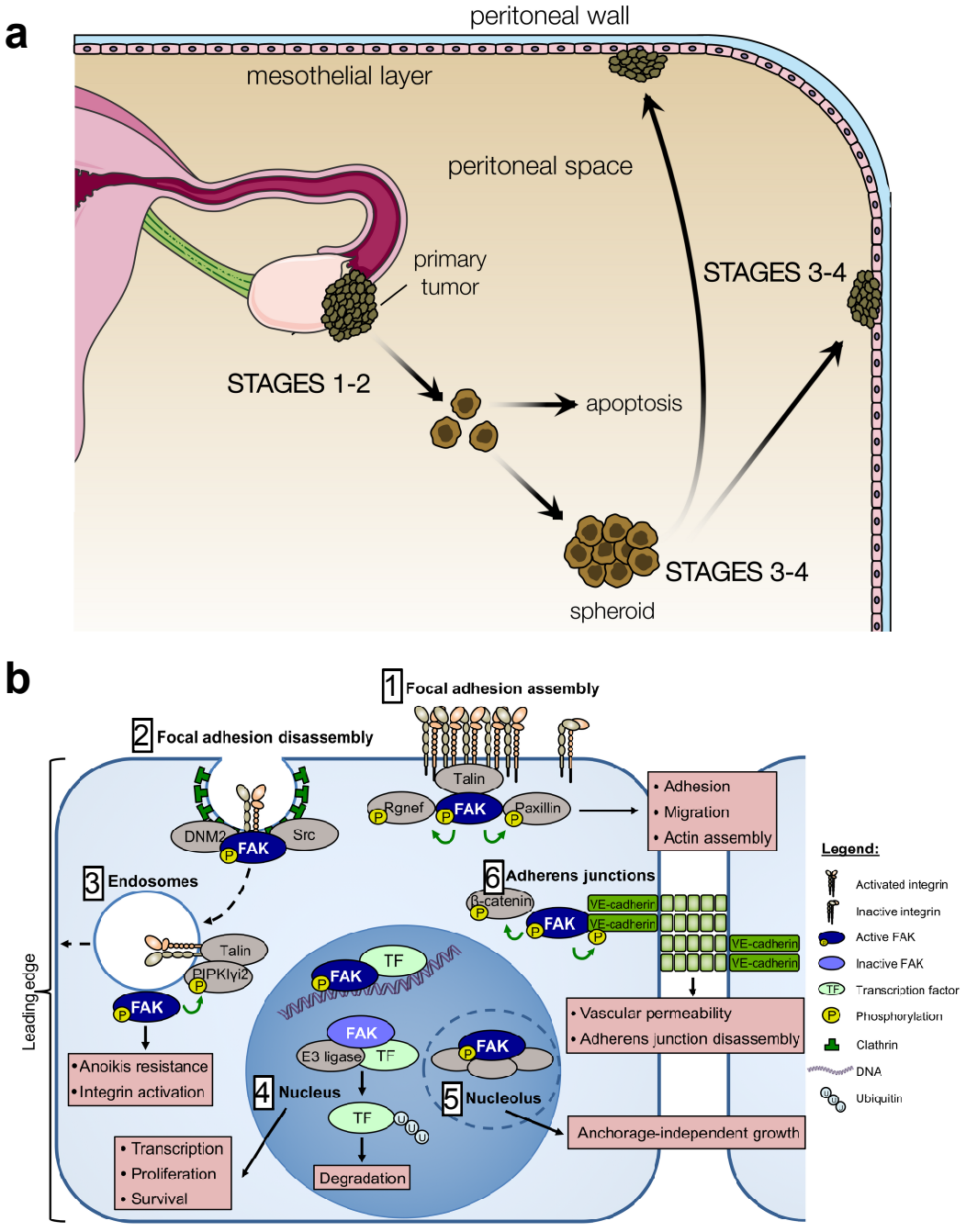

Figure 1.1: Models of ovarian cancer and FAK. **(a)** Model of ovarian cancer progression. Ovarian cancer can originate in the fallopian tube. In early stages, tumor cells spread locally or shed into the peritoneal cavity and often undergo anoikis. In stages III-IV, shed tumor cells form multicellular spheroids that are passively diffused throughout the peritoneal cavity and attach at distant sites such as the omentum. **(b)** Sites of FAK localization throughout the cell, including 1) focal adhesions assembly and 2) disassembly, 3) endosomes, 4) the nucleus and 5) nucleolus, and 6) adherens junctions.

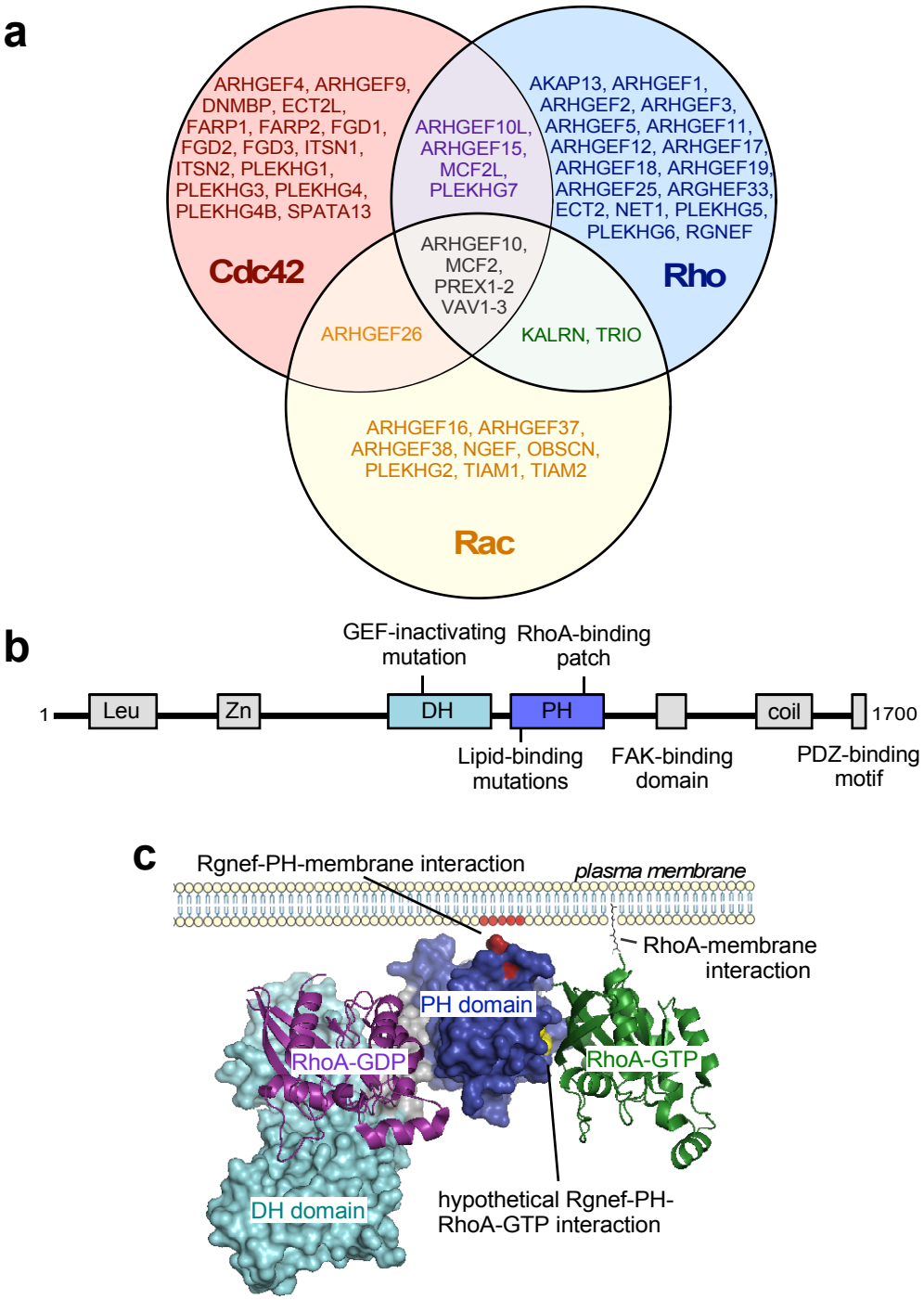

Figure 1.2: Dbl Family GEFs. **(a)** Dbl family GEFs, with their selectivity for substrate GTPases in the Cdc42, Rho, or Rac family. Figure adapted from Jaiswal et. al., 2013. **(b)** Rgnef protein structure. Rgnef contains a leucine-rich domain (Leu), zinc-finger motif (Zn), tandem Dbl-homology (DH) and pleckstrin-homology (PH) domains, a FAK-binding domain, predicted coil-coil domain (coil), and a PDZ-binding motif. **(c)** Theoretical Rgnef DH-PH model created in Swiss-Model. RhoA-GDP crystal structure PDB 1X86, RhoA-GTP crystal structure PDB 3KZ1. Theoretical Rgnef DH-PH model generated in Swiss-Model based on AKAP13 crystal structure.

Chapter 2

Rgnef promotes ovarian tumor progression and confers protection from oxidative stress

2.1 Abstract

Ovarian cancer is the fifth-leading cause of cancer death among women. High mortality is associated with the formation and dissemination of tumor spheroids. *In vitro*, ovarian tumor cell spheroids can exhibit elevated resistance to environmental stressors such as hypoxia and reactive oxygen species (ROS). Homeostatic balance of the antioxidant response is a protective mechanism supporting ovarian cancer spheroid growth and preventing from anoikis, a form of programmed cell death. Matrix proteins, integrin receptors, and integrin-activated signaling proteins suppress anoikis. Rgnef (Arhgef28/p190RhoGEF) is a guanine nucleotide exchange factor (GEF) that is activated downstream of integrins. Here we show that Rgnef protein levels are elevated in late-stage ovarian cancer and that high Rgnef mRNA levels are associated with decreased patient survival. Using transgenic and transplantable Rgnef knockout mouse models, we find that Rgnef is essential for supporting ovarian spheroid growth *in vitro* and ovarian tumor growth in mice. Using RNA-sequencing and bioinformatic analyses, we identify an antioxidant gene signature in Rgnef-expressing compared to Rgnef-knockout cells. We identify a novel non-canonical role for Rgnef in facilitating NF-kB-mediated protection from oxidative stress, which is needed for optimal three-dimensional spheroid growth. These studies reveal that Rgnef is an important regulator of ovarian tumor progression.

2.2 Introduction

Ovarian cancer is the fifth-leading cause of cancer death among women (Siegel, Miller, and Jemal 2018). The high mortality rate is largely due to the fact that most patients are diagnosed after tumors have metastasized (Lengyel 2010). Ovarian cancer exhibits a unique pattern of metastasis whereby cells detach from the primary tumor into the peritoneal space, which can trigger a form of programmed cell death called anoikis (Lengyel 2010). More aggressive cancer cells resist anoikis, can proliferate anchorage-independently as multicellular spheroids, and can become resistant to chemotherapy (Shield et al. 2009). Preventing peritoneal spheroid survival and triggering anoikis may provide therapeutic benefit (Kenny et al. 2009, Al Habyan et al. 2018).

Ovarian cancer tumors growing within the peritoneal space must adapt to environmental stresses from hypoxia, anchorage independence, and metabolic challenges (Roy and Cowden Dahl 2018). Several of these events trigger increased oxidative stress within cells (Cairns, Harris, and Mak 2011, Gorrini, Harris, and Mak 2013). Oxidative stress occurs when the generation of cellular reactive oxygen species (ROS) cells is not sufficiently balanced by ROS-scavenging pathways (Gorrini, Harris, and Mak 2013, Trachootham, Alexandre, and Huang 2009, Schieber and Chandel 2014). Notably, platinum- and taxane-based chemotherapies elevate ROS generation, which is associated with increased ovarian cancer cell senescence and cytotoxicity (Alexandre et al. 2007, Marullo et al. 2013). Correspondingly, antioxidants that lower cellular ROS levels can enhance tumor initiation and progression (Schafer et al. 2009, Harris et al.

2015). Ovarian cancer cells often exhibit elevated endogenous antioxidant gene expression, driven by transcription factors such as nuclear factor-like 2 (NRF2) and nuclear factor kappa-light-chain-enhancer of activated B cells (NF-kB) (Morgan and Liu 2011, van der Wijst, Brown, and Rots 2014). Although upregulation of NRF2- and NF-kB-driven pathways is a prognostic for poor survival in ovarian cancer (Konstantinopoulos et al. 2008), the regulator upstream factors for these signaling pathways in ovarian cancer remain undefined.

Integrins are cell surface receptors that facilitate extracellular matrix attachment and initiate signals that promote cell survival (Seguin et al. 2015). Loss of matrix attachment can increase ROS levels in ovarian cancer cells (Reddig and Juliano 2005, Schafer et al. 2009). Rgnef (Arhgef28/p190RhoGEF) is a Rho-specific guanine nucleotide exchange factor (GEF) that is activated downstream of integrins in a complex with focal adhesion kinase (FAK) (Miller, Kleinschmidt, and Schlaepfer 2014). In primary fibroblasts, Rgnef facilitates RhoA GTPase activation, actin stress fiber formation, and paxillin tyrosine phosphorylation needed for the control of cell motility (Lim et al. 2008, Miller et al. 2012). In advanced-stage colon cancer, Rgnef expression is elevated and promotes tumor growth through its interaction with FAK (Yu et al. 2011, Masia-Balague et al. 2015). In high grade serous ovarian cancer, RhoA activation regulators are phosphoproteomic predictors of poor survival (Zhang et al. 2016). However, the role of Rgnef in ovarian cancer remains undefined.

Here we show that Rgnef expression levels are elevated in late-stage serous ovarian cancer and are associated with decreased ovarian cancer patient

survival. Using transgenic and transplantable Rgnef knockout ovarian cancer tumor models, we find that Rgnef expression is essential for promoting ovarian tumor growth in mice. We identify a novel role for Rgnef in facilitating three-dimensional spheroid growth and Rgnef-NF-kB-mediated protection from oxidative stress *in vitro*. This signaling linkage is needed for optimal three-dimensional ovarian cancer spheroid growth. These studies reveal that Rgnef is an important regulator of ovarian cancer tumor progression.

2.3 Results

Rgnef expression is elevated in late-stage serous ovarian cancer

Rgnef (Arhgef28/p190RhoGEF) is a ubiquitously-expressed protein with elevated protein levels detected in the murine ovary, brain, lung, and spleen (Miller et al. 2012). Polyclonal antibodies have been generated against Rgnef and validated using tissues from *Rgnef*$^{+/+}$ and *Rgnef*$^{-/-}$ mice (Yu et al. 2011). Human ovarian serous adenocarcinomas tumor microarrays were analyzed by anti-Rgnef immunohistochemical staining (Fig. 2.1a) and revealed a wide range of expression (Fig. 2.1b). Significantly increased Rgnef staining was detected in stage 3-4 compared to stage I-II tumors (P<0.01, Fig. 2.1b). Surprisingly, analyses of Rgnef mRNA levels in the TCGA dataset did not reveal differences with regard to overall survival (data not shown). However, Kaplan-Meier analyses of combined mRNA datasets (Lanczky et al. 2016) limited to stage III-IV tumors (>400 patient samples)

revealed that elevated Rgnef mRNA levels were associated with a significant decrease in both progression-free and overall survival (Figs. 2.1c-d). Together, these findings support the notion that Rgnef may be important in late-stage serous ovarian cancer biology.

Rgnef knockout inhibits spontaneous ovarian tumor formation

Mice null for *Rgnef* (*Rgnef*$^{-/-}$) are born smaller than wildtype (*Rgnef*$^{+/+}$) littermates and are present at less than expected Mendelian ratios (Miller et al. 2012). However, by 6 to 8 weeks, *Rgnef*$^{-/-}$ mice are phenotypically normal and fertile. In high-grade serous ovarian cancer, the p53 tumor suppressor is mutated or inactivated in >95% of cases, and the RB1 signaling pathway is deregulated in 67% of cases (Cancer Genome Atlas Research 2011). Simian Virus 40 T antigen (TAg) protein binds and functionally inactivates p53 and RB1 in cells (Bargonetti et al. 1992, Quinn et al. 2010) and female mice expressing *TAg* under the control of the Müllerian inhibiting substance type II receptor (*MISIIR*) develop spontaneous ovarian tumors with complete penetrance (Connolly et al. 2003). As early as 4 weeks of age, TAg staining can be detected within cells of the oviduct and ovary (Quinn et al. 2010, Gabbasov et al. 2018) (Fig. 2.2a). To test the effect of Rgnef knockout (KO) in the *MISIIR-TAg* model, pure C57Bl6 *MISIIR-TAg*$^{+}$ mice were crossed with C57Bl6 Rgnef$^{-/-}$ mice (Fig. 2.2b) to generate *Rgnef*$^{+/+}$*;MISIIR-TAg*$^{+}$ and *Rgnef*$^{-/-}$*;MISIIR-TAg*$^{+}$ mice. Female littermate mice were monitored for spontaneous ovarian tumor formation by ultrasound (Fig. 2.2c). Some *Rgnef*$^{+/+}$

mice formed large tumors by week 15, and all mice were euthanized by 18 weeks. Ovarian mass was used to measure tumor burden (Fig. 2.2d), and *Rgnef*$^{+/+}$ mice formed significantly larger (P<0.05) tumors than Rgnef$^{-/-}$ mice (Fig. 2.2e). TAg expression was confirmed by immunofluorescent staining of tumor-bearing ovarian tissue from *Rgnef*$^{+/+}$ and *Rgnef*$^{-/-}$ mice (Fig 2.2f). These results demonstrate that Rgnef supports TAg-driven ovarian primary tumor growth.

Tumor cell-intrinsic role for Rgnef in vivo

In the spontaneous *MISIIR-TAg*$^{+}$ model, Rgnef is deleted in all cells. To determine if Rgnef expression is required for tumor cell-intrinsic growth, cells were collected from peritoneal wash of either *Rgnef*$^{+/+}$ or *Rgnef*$^{-/-}$ *MISIIR-TAg*$^{+}$ tumor-bearing mice at 17 weeks and expanded by growth in adherent culture (Fig. 2.3a). Pooled populations of murine ovarian carcinoma (MOVCAR) cells were generated and the presence or absence of Rgnef expression was verified by DNA genotyping (Fig. 2.3b), anti-Rgnef immunoblotting (Fig. 2.3c), and verified positive for TAg expression by immunoblotting (data not shown). Surprisingly, *Rgnef*$^{-/-}$ MOVCARs proliferated faster than *Rgnef*$^{+/+}$ MOVCARs in adherent cell culture (Fig. 2.3d).

To test growth differences between pooled *Rgnef*$^{+/+}$ and *Rgnef*$^{-/-}$ MOVCARs *in vivo*, cells were injected into the ovarian bursa (Figs. 2.3e-g) of wild-type syngeneic C57Bl/6 *MISIIR-TAg-Low* mice (Quinn et al. 2010). At 15 weeks, ovaries of mice injected with *Rgnef*$^{+/+}$ MOVCARs exhibited extensive tumor burden whereas no tumors were detected in mice injected with an equal number of *Rgnef*

$^{-/-}$ MOVCARs (Fig. 2.3f). To monitor changes in tumor cell survival in the peritoneal space, *Rgnef*$^{+/+}$ and *Rgnef*$^{-/-}$ MOVCARs were transduced with a luciferase reporter and evaluated for differences in intraperitoneal growth (Fig. 2.3g). Within 4 weeks, the bioluminescent signal from *Rgnef*$^{-/-}$ MOVCARs was reduced to background whereas *Rgnef*$^{+/+}$ MOVCAR signal continued to increase over time. After 14 weeks, *Rgnef*$^{+/+}$ MOVCAR cells had formed large ovarian tumors, omentum infiltration, and non-adherent spheroids collected with ascites (Figs. 2.3h-j). Notably, *Rgnef* $^{-/-}$ MOVCAR cells failed to form ovarian or omental tumors and few ascites-associated tumor cells were recovered at 14 weeks (Figs. 2.3h-j). Taken together, these results support the importance of a tumor-intrinsic role for Rgnef *in vivo*.

CRISPR/Cas9-mediated Rgnef knockout in ID8-IP cells

To test the role of Rgnef in a transplantable C57Bl/6 ovarian tumor model, we utilized the aggressive murine ID8-IP cell line, generated by passage of ID8 cells in C57Bl/6 mice (Ward et al. 2013). Clustered Regularly Interspaced Short Palindromic Repeat (CRISPR)/Cas9-mediated genome editing was used to target murine *Rgnef* exon 6 for within ID8-IP cells, single cells were isolated by dilution cloning, and Rgnef knockout (KO) ID8-IP clones containing deletions in exon 6 were screened by genomic DNA PCR analyses (Fig. 2.4a). Several Rgnef KO clones exhibited cell senescence upon expansion and adherent cell growth analyses were performed to identify Rgnef KO clones that proliferated equally to

parental ID8-IP cells (Fig. 2.4b). Rgnef clones KO-10, KO-12, and KO-13 grew equally to parental ID8-IP cells and Rgnef KO-13 cells were validated to contain two deletions in Rgnef exon 6, predicted to result in translational reading frame shifts and stop codon introduction (Fig. 2.4c). Interestingly, despite equivalent growth in adherent cell culture conditions, ID8-IP KO-13 cells (hereafter termed ID8-IP Rgnef-KO) were unable to grow as three-dimensional colonies embedded in Matrigel (Figs. 2.4d and e) and exhibited limited cell proliferation as spheroids in serum-free anchorage-independent culture conditions (Fig. 2.4f).

Rgnef promotes ID8-IP spheroid growth in vitro and in vivo

To confirm that anchorage-independent Rgnef-KO growth defects were caused by Rgnef loss, GFP-Rgnef was stably re-expressed in ID8-IP Rgnef-KO cells and enriched by fluorescence-activated cell sorting. Full-length GFP-Rgnef expression was confirmed by immunoblotting (Fig. 2.5a) and by fluorescent enrichment of GFP-Rgnef in the leading edge of cells as compared to diffuse distribution of GFP alone (Fig. 2.5b). Previous studies showed that GFP-Rgnef rescues signaling defects of primary *Rgnef*$^{-/-}$ fibroblasts (Miller et al. 2012, Miller et al. 2013). Notably, whereas no adherent growth differences were observed between Rgnef-KO and GFP-Rgnef re-expression (Fig. 2.5c), 3D colony growth of ID8-IP Rgnef-KO cells in Matrigel was significantly increased by GFP-Rgnef re-expression (Figs. 2.5d-e).

This enhanced anchorage-independent survival phenotype was also observed *in vivo*, as luciferase-labeled GFP-Rgnef ID8-IP cells produced a significantly higher bioluminescent signal 5 weeks following intraperitoneal injection compared to labeled ID8-IP Rgnef-KO + GFP cells (Figs. 2.5f-g). Increased numbers of GFP-Rgnef cells were recovered from the peritoneal cavity of C57Bl/6 mice at 39 days compared to mice injected with ID8-IP Rgnef-KO cells (Fig. 2.5h). Rgnef-KO ID8-IP cell infiltration was detected within the omentum fat by sectioning and H&E staining (Fig. 2.5i). In general, Rgnef-KO ID8-IP omental tumor implants were smaller than tumors detected in mice injected with GFP-Rgnef ID8-IP cells. However, although there was a trend in increased total omentum mass, the data was not significantly different between the two groups (Fig. 2.5j). Together, these results support the notion that Rgnef expression contributes to anchorage-independent ID8-IP cell growth, and this may underlie the enhanced tumor-promoting role for Rgnef *in vivo*.

Rgnef enhances an antioxidant gene signature

To explore whether Rgnef supports altered mRNA changes that may enhance anchorage-independent growth, RNA array hybridization analyses were performed with *Rgnef*$^{+/+}$ and *Rgnef*$^{-/-}$ MOVCARs (Figs. 2.6a-b) and RNA sequencing was performed with Rgnef-KO and GFP-Rgnef re-expressing ID8-IP cells (Figs. 2.6c-f). In MOVCARs, 394 genes were upregulated and 774 genes were downregulated between *Rgnef*$^{+/+}$ vs *Rgnef*$^{-/-}$ cells. Gene set enrichment

analysis (GSEA) revealed transcript enrichment in several molecular pathways including oxidoreductase activity (Fig. 2.6a). Parallel analyses using Kyoto Encyclopedia of Genes and Genomes (KEGG) enrichment revealed enhancement of several signaling pathways, including glutathione metabolism in *Rgnef*$^{+/+}$ MOVCARs (Fig. 2.6b).

In ID8-IP cells, 670 genes were upregulated and 1142 genes were downregulated in GFP-Rgnef re-expressing compared to Rgnef-KO ID8-IP cells (Fig. 2.6c). Rgnef had the highest global top fold-change in ID8-IP cells, as expected for GFP-Rgnef re-expression (Fig. 2.6d). Notably, oxidoreductase activity and glutathione metabolism were also enriched in GFP-Rgnef cells by GO and KEGG pathway analyses, respectively (Fig. 2.6e-f). The alterations shared between MOVCAR and ID8-IP cells reinforce the potential importance of Rgnef in regulating these pathways.

Glutathione is the largest pool of antioxidant reducing equivalents in the cell, and reduced glutathione is used as a substrate for antioxidant enzymes that protect against oxidative stress (Gorrini, Harris, and Mak 2013). Therefore, we investigated differential expression of antioxidant genes in ID8-IP GFP-Rgnef vs Rgnef-KO cells using a curated list that includes glutathione peroxidases, thioredoxins, peroxiredoxins, superoxide dismutases, and members of the glutathione metabolism pathway (Table 2.1). Twenty-four of these transcripts were upregulated and four were downregulated in response to Rgnef expression (Fig. 2.6g). Increased expression of targets such as Nqo1 (reductase), Gsta4 (glutathione transferase), and Gpx4 (glutathione peroxidase) were confirmed by

immunoblotting (Fig. 2.6h). Together, these results demonstrate that Rgnef supports the expression of an antioxidant gene signature.

Increased ROS in Rgnef-KO cells is rescued by antioxidant treatment

Loss of matrix attachment can increase ROS levels in ovarian carcinoma cells, which may trigger anoikis (Reddig and Juliano 2005, Schafer et al. 2009). As Rgnef loss prevents ID8-IP growth as spheroids and alters antioxidant-associated mRNA levels, ROS levels in suspended Rgnef-KO and GFP-Rgnef ID8-IP cells were measured using a redox-sensitive fluorescent probe (Fig. 2.7a). Elevated ROS levels were present in Rgnef-KO cells as compared to cells expressing Rgnef. The addition of the antioxidant Trolox, a water-soluble vitamin E analog, restored ROS equilibrium to the cells (Fig. 2.7a). Importantly, Trolox addition rescued the anchorage-independent growth of Rgnef-KO cells under defined serum-free media conditions (Fig. 2.7b). Trolox addition had no effect on anchorage-independent GFP-Rgnef ID8-IP cell growth, supporting the notion that these cells do not gain added benefit from antioxidant treatment. These results show that oxidative stress is a limiting factor for anchorage-independent Rgnef-KO ID8-IP cell growth.

Rgnef supports NFκB transcription factor activation

To explore possible regulatory mechanisms underlying the Rgnef-associated antioxidant mRNA changes, we queried the ChEA (Chip Enrichment Analysis) database using the 670 transcripts upregulated in the ID8-IP GFP-Rgnef re-expressing cells. ChEA calculates overrepresented transcription factor targets in a gene set against a database of mammalian Chip-X experiments (Lachmann et al. 2010). Transcription factors with the most significant target overlap with genes upregulated by GFP-Rgnef included NRF2, KLF1, RELA, and SOX2 (Table 2.2). NRF2 is a known master regulator of the antioxidant response (Rojo de la Vega, Chapman, and Zhang 2018) and GFP-Rgnef ID8-IP cells express elevated NRF2 levels compared to Rgnef-KO cells by immunoblotting (Fig. 7c). However, transient over-expression of GFP-Rgnef cells was not sufficient to activate a NRF2 transcriptional reporter (Fig 7d).

RELA, a component of the NF-kB transcription factor complex, is activated by ROS and can protect cells from oxidative stress (Morgan and Liu 2011). Notably, twelve of the twenty-four antioxidant gene targets identified as differentially upregulated in GFP-Rgnef ID8-IP cells are targets of NF-kB (Fig. 6g, starred), including NRF2. Additionally, RELA was one of the transcription factors identified by ChEA analysis (Table 2.2). NF-kB can promote interleukin-6 (IL-6) gene expression (Baccam et al. 2003) and GFP-Rgnef over-expression activated an IL-6 transcriptional reporter. This activation was dependent on NF-kB DNA binding site integrity (Fig. 7e). This result supports the notion that Rgnef can facilitate NF-kB-mediated gene expression (Lee, Ha, and Kim 2003).

Importance of NF-kB in ID8-IP spheroid growth

ID8-IP are aggressive cells that exhibit up-regulated FAK expression and FAK activation in anchorage-independent conditions (Ward et al. 2013, Tancioni et al. 2015). As Rgnef can function upstream to promote FAK activation (Miller et al. 2013), and FAK inhibitor treatment prevents ID8-IP anchorage-independent growth (Ward et al. 2013), pathways downstream of Rgnef-FAK were tested for effects on ID8-IP anchorage-independent spheroid growth (Fig. 7f). ID8-IP three-dimensional spheroid growth remain unchanged after 24-hour pre-treatment of cells with wortmannin or UO126, inhibitors of phosphatidylinositol kinase and mitogen-activated protein kinases, respectively. However, ID8-IP growth was inhibited by pre-treatment with inhibitors of NF-kB signaling, Bay 11-7082 and TPCA-1 (Fig. 7e). Together, these results support the importance of NF-kB activation downstream of Rgnef in the regulation of oxidative stress and anchorage-independent growth.

2.4 Discussion

Here, we demonstrate that Rgnef expression is elevated in late-stage ovarian cancer, and that high Rgnef expression corresponds to poor prognosis in late-stage ovarian cancer patients. Using a transgenic mouse ovarian cancer model and two syngeneic ovarian cancer cell lines, we determine that Rgnef promotes ovarian primary tumor formation, peritoneal growth, and metastasis. Our

results support a model in which Rgnef knockout increases cellular ROS, which limits tumor spheroid growth (Fig. 7g). Rgnef expression confers protection from oxidative stress by mediating an NF-kB driven antioxidant signature (Fig. 7g). Antioxidant treatment can also rescue cell growth defects observed upon loss of Rgnef. These results support a role for Rgnef as a novel mediator of ovarian tumorigenesis.

Survival and growth of peritoneal spheroids in advanced-stage ovarian cancer is associated with recurrence and chemoresistance (Shield et al. 2009, Al Habyan et al. 2018). Here, we find that Rgnef expression supports increased ovarian tumor spheroid growth both *in vitro* and *in vivo*, and that this advantage is specific to anchorage-independent tumor spheroid growth. How Rgnef is activated in spheroids remains unclear, although Rgnef activation can be mediated by integrins and by FAK in adherent conditions (Miller et al. 2012, Zhai et al. 2003). Inhibition of both integrins and FAK have been shown to inhibit spheroid survival (Lengyel 2010, Tancioni et al. 2015), suggesting that these proteins may be upstream of Rgnef activation in spheroids. Furthermore, the spheroid growth advantage in Rgnef-expressing cells reflects the poor prognosis for patients with high Rgnef expression in late-stage ovarian cancer.

Anchorage-independent survival is a hallmark of oncogenic transformation (Guadamillas, Cerezo, and Del Pozo 2011) and is critical to ovarian cancer progression. One of the barriers to achieving anchorage-independent survival is mitigating cellular ROS levels after matrix detachment (Schafer et al. 2009). We show that Rgnef expression protects the cell from increased ROS in anchorage-

independent conditions. Cheung et al. recently reported that Rgnef promotes cell survival after induction of oxidative stress by a chemical agent (Cheung et al. 2017). Additionally, Rgnef has been shown to protect cells from other types of stress, including osmotic-, heat-, and drug-induced stress (Cheung et al. 2017, Wu et al. 2003). Together, this suggests that Rgnef may play a more general role in protection from cellular stress in addition to its function in cancer cell biology. In addition to its role in inducing expression of antioxidant transcripts, NF-kB activation downstream of Rgnef may confer protection through increased expression of antiapoptotic transcripts.

Upregulation of the NF-kB pathway prior to chemotherapy has been shown to be a predictor of poor survival in ovarian cancer (Konstantinopoulos et al. 2008). We demonstrate that Rgnef is a novel regulator upstream of NF-kB activation. How Rgnef signaling connects to NF-kB activation remains unclear, although both RhoA and FAK have been shown to promote NF-kB activation (Tong and Tergaonkar 2014, You et al. 2015). Our results are consistent with a previous report linking Rgnef overexpression to NF-kB activation in B cells, which was dependent on Rgnef GEF activity (Lee, Ha, and Kim 2003). Further functional studies characterizing Rgnef mutants may determine if Rgnef-mediated NF-kB activation relies on a scaffolding role or GEF activity.

In our study, Rgnef knockout reduced primary and metastatic tumor burden, increased cellular ROS, and impaired anchorage-independent growth, suggesting that targeting oxidative stress protection pathways is a viable therapeutic target. Several studies have shown that increased levels of oxidative stress sensitize

cancer cells to radio- and chemotherapeutic treatment (Trachootham, Alexandre, and Huang 2009, Mateescu et al. 2011, Diehn et al. 2009). Additionally, resistance to paclitaxel has been shown to correlate with cellular antioxidant capacity (Ramanathan et al. 2005). Therefore, therapeutic inhibition of Rgnef (Diviani et al. 2016) to render cells more vulnerable to oxidative stress is a possible avenue for future studies.

2.5 Materials and Methods

Antibodies, Plasmids, and Reagents

Rabbit polyclonal affinity-purified antibodies to the C-terminal region of Rgnef (clone 1397) were created and used as described (Yu et al. 2011). Antibody to β-actin (AC-17) was from Sigma. GAPDH (GT239) antibody was from GeneTex. NRF2 (A-10) and SV40 TAg (Pab 101) antibodies were from Santa Cruz. GFP (B34) was from Biolegend. NQO1 (A180), GPX4 (EPNCIR144), and Ki67 (SP6) were from Abcam. GSTA4 (ABS1652) was from Millipore. AlexaFluor-488 and AlexaFluor-647 labeled antibodies were from ThermoFisher. Matrigel (GFR, 356231) used in *in vitro* and *in vivo* experiments was from Corning. D-Luciferin for IVIS imaging was from PerkinElmer. Trolox, wortmannin, U0126, and Bay 11-7082 were from Sigma-Aldrich. TPCA-1 was from Abcam. Cre-driven Rgnef recombination in *Rgnef*$^{-/-}$ MOVCARs was determined by PCR using forward (5'-ACTGCAGATCAGCATGTCTTG-3' and reverse (5'-GCTGCTATCTCCAAACGCTAT-3') primers. PCR for TOPO-TA cloning in ID8-IP

Rgnef-KO clones was performed using forward (5'-CTGGGAAGCTGTGTGGATTT-3') and reverse (5'-AGGACATGGGGTTAGAGCCT-3') primers. The dTomato-luciferase (pUltra-Chili-Luc) vector was a gift from Malcolm Moore (Addgene #48688). dTomato-luciferase and pCDH-CMV-MCS1-eGFP were used to produce lentivirus as described (Lim et al. 2008) and cells were transduced according to standard methods (System Biosciences) and enriched by fluorescence-activated cell sorting. High-concentration lentivirus using pCDH-CMV-MCS1-eGFP-Rgnef (Lim et al. 2008) was produced by Systems Biosciences. CRISPR gRNA construct was from GenScript (5'-CCGACTGCGTCTTAACGAAG-3' in pSpCas9 BB-2A Puro PX459). The pmIL-6 FL and pmIL-6 mut NFkB plasmids were from Addgene (#61286 and #61293, respectively). pTK-Green Renilla Luc Vector was from ThermoFisher.

Reporter assays

All 293T Lenti-X cells used in reporter assays were seeded at 30k cells/well in 96-well white polystyrene microplates (Corning) 24 hours before transfection. For the NF-kB reporter assay, cells were transiently transfected with pTK-Green Renilla Luc plus either pCDH-MCS1-mCherry or pCDH-MCS1-mCherry-Rgnef, and either pMIL-6 FL or pmIL-6 mut NF-kB using jetPRIME (Polyplus). Transfection media was removed after 4 hours. The ARE Cignal Reporter Assay was performed according to standard manufacturer instructions (Qiagen). For both assays, luciferase signal was measured 32 hours after transfection using the Dual-Glo Luciferase System (Promega). Signal was analyzed on a plate reader, and the

ratio of firefly:renilla luciferase signal was calculated.

Cells

Mouse ovarian carcinoma (MOVCAR) cells were isolated from ascites of tumor-bearing *MISIIR-TAg*+;*Rgnef*$^{+/+}$ or Rgnef$^{-/-}$ mice and expanded by adherent growth, as described (Connolly et al. 2003). ID8-IP cells were isolated from ID8 peritoneal ascites and expanded in suspension, as described (Ward et al. 2013). 293T Lenti-X cells were from Clontech. For adherent growth, ID8-IP and 293T Lenti-X cells were maintained in DMEM (Corning) supplemented with 10% FBS, 100 µM non-essential amino acids, 100 U/ml penicillin, and 100 µg/ml streptomycin on tissue culture-treated plastic plates (Corning). MOVCAR cells were maintained in DMEM (Corning) supplemented with 4% FBS, 100 µM non-essential amino acids, 100 U/ml penicillin, 100 µg/ml streptomycin, and 1x insulin-transferrin-selenium (Mediatech). For anchorage-independent growth, cells were seeded at 50k/well in ultra-low attachment plates (Corning) in serum-free Tumorsphere Medium XF (PromoCell). For growth assays, cells were counted using a ViCell XR counter (Beckman). CRISPR/Cas9-mediated knockout was performed as previously described (Ran et al. 2013) using a guide RNA in the PX459 vector. Confirmation of *Rgnef* early stop codon generation in ID8-IP Rgnef-KO clones was performed using TOPO-TA cloning (Thermo Fisher) followed by Sanger sequencing.

Mice and tumor experiments

All animal experiments were performed in accordance with The Association for the Assessment and Accreditation for Laboratory Animal Care (AALAC) guidelines and were approved by the University of California San Diego Institutional Animal Care and Use Committee (IACUC). *Rgnef*$^{-/-}$ mice were developed and genotyped as described (Miller et al. 2012). Briefly, *Rgnef* exon 24-floxed mice were crossed with cytomegalovirus (CMV)-driven Cre recombinase transgenic mice, resulting in loss of Rgnef expression (*Rgnef*$^{-/-}$). *MISIIR-TAg*+ and *MISIIR-TAg-Low* mice were developed as described previously (Connolly et al. 2003, Quinn et al. 2010). Orthotopic bursa injections were performed as described (Connolly and Hensley 2009). Briefly, MOVCAR cells were mixed with Matrigel (GFR, Corning), at a concentration of 0.5 x 10^6 cells per 7 μL and injected into the ovarian bursal space using a Hamilton syringe, 29.5-gauge needle. Incisions were closed with surgical stables, and mice were evaluated for health daily. For intraperitoneal injection, were mixed with PBS + 25% Matrigel (GFR, Corning) for a final concentration of 7.5 x 10^6 (MOVCAR) or 5 x 10^6 (ID8-IP) cells per 250 μL. Ascites-associated cells in were recovered by peritoneal washings performed with 5 mL of PBS, followed by erythrocyte lysis using RBC lysis buffer (eBioscience), trypsinization, and enumeration on a ViCell XR counter (Beckman). Prior to initiation of tumor experiments, ID8-IP and MOVCAR cells were transduced with a lentiviral vector expressing dTomato and luciferase (pUltra-Chili-Luc) or and fluorescent cells were enriched by fluorescence sorting. Ultrasound imaging of MISIIR-TAg+ mice was performed at the IVISR in the Moores Cancer Center. Mice were euthanized when tumors reached standards for humane endpoint, or by 18

weeks. For orthotopic or intraperitoneal MOVCAR and ID8-IP tumor experiments, tumor growth was monitored weekly via bioluminescent luciferase imaging (IVIS, Perkin Elmer).

Kaplan Meier TCGA plots

Kaplan-Meier survival analyses using TCGA patient data were performed using KMplotter (Lanczky et al. 2016) (http://kmplot.com/analysis/). Selections were: Affymetrix probe *ARHGEF28* (1560348_at), PFS or OS, follow-up threshold all, auto-select cutoff, stages 3+4, serous histology, exclude outlier arrays.

RNA and bioinformatics analysis

For differential RNA expression from MOVCAR cells, total RNA was isolated from adherently grown *Rgnef*$^{+/+}$ or *Rgnef*$^{-/-}$ MOVCAR cells (n=1) grown adherently using PureLink RNA Mini Kit (ThermoFisher). Sample preparation (Ambion/Illumina TotalPrep RNA amplification kit) and runs (Illumina BeadChip Microarray MouseRef-8 v2.0) were performed at the UCSD/VA/VMRF Gene Core. Differentially-expressed genes had two-fold differences and probes with $p<0.05$.

For RNA-Seq, total RNA was isolated from ID8-IP Rgnef-KO or cells re-expressing GFP-Rgnef growing in an adherent monolayer coated with 0.2% Matrigel (n=3 per group) using PureLink RNA Mini Kit (Thermo Fisher). RNA sequencing was performed by Novogene (Beijing, China). RNA samples were prepared using NEB Next Ultra RNA Library Prep Kit (New England Biolabs) as per manufacturer recommendations. Each transcriptome was sequenced using a

150 bp paired-end protocol on the Illumina HiSeq platform, generating at least 37 million clean reads for all samples. Reads were mapped to the reference genome (reads were >87% mapped in all cases) using TopHat2 (Kim et al. 2013). Differential expression analysis was performed using the DESeq2 R package (Anders and Huber 2010). To test for enriched pathways, we used the online version of GSEA (gene set enrichment analysis) (Subramanian et al. 2005). ChEA analysis was performed using Enrichr (Lachmann et al. 2010, Chen et al. 2013, Kuleshov et al. 2016).

Immunohistochemistry

Human tumor microarrays OV8010, OV8011, and OV807 were obtained from Biomax and stained with a polyclonal Rgnef antibody developed and validated in our lab (Clone 1397 (Yu, Ramena, and Elble 2012)). Two independent researchers scored samples blindly and in a semiquantitative manner from 0 to 4. Results were averaged, and only samples from serous epithelial ovarian cancer were included.

For paraffin-embedded staining, ovary or omentum was removed and fixed in formalin for staining using TAg antibody or hematoxylin and eosin. Human tumor microarrays containing ovary cancer tissue were obtained from Biomax (OV8010, OV8011, and OV807). Tissue deparaffinization, rehydration, antigen unmasking, and peroxidase quenching was performed as described (Ward et al. 2013). Tissues were blocked (10% goat serum, 0,1% TritonX-100 in PBS) for 45 minutes and incubated with anti-TAg (1:200) or anti-Rgnef antibody (Yu et al. 2011) (1:100)

overnight in blocking buffer. Biotinylated goat-anti-mouse/rabbit IgG (1:300 in PBS), Vectastain Elite ABC, and diaminobenzidine (Vector Labs) were used to visualize antibody binding. Slides were counter-stained with hematoxylin or methyl green. Images were captured using an upright microscope (Olympus BX43) with a color camera (Olympus SC100).

For tumor microarrays, two independent researchers scored samples blindly and in a semiquantitative manner from 0 to 4. Scores from samples of serous adenocarcinoma were averaged. For cryosections, ovaries were snap-frozen in Optimal cutting temperature (OCT) compound (Tissue Tek) and thin-sectioned using a cryomicrotome (Leica CM1950) and mounted onto glass slides. For TAg and DNA visualization, slides were fixed in acetone, rehydrated (PBS, 0.5% BSA), blocked (1:50 normal goat serum, 0.5% BSA in PBS), and incubated overnight with TAg antibody (1:100). Slides were incubated with secondary antibody (AlexaFluor 488, 1:300) and Hoechst (1:50,000), and coverslips were mounted with Vectashield Hardset (Vector Labs). For GFP visualization, cells were plated onto glass-bottom dishes (MatTek). All immunofluorescence was visualized using an inverted microscope (IX81, Olympus) and Slidebook software (v5.0, Intelligent Imaging). Images were psuedocolored and overlaid using ImageJ.

Colony growth in Matrigel

Protocol was adapted from the Matrigel-on-top assay (Shapiro et al. 2014). Briefly, a dense layer of Matrigel diluted 1:1 with culture media was allowed to solidify for 30 mins at 37°C. A single-cell suspension consisting of ID8-IP cells

diluted at 3000 cells/cm^2 in a 1:50 Matrigel:culture medium dilution was prepared, and added on top of the base layer at twice the volume of the base layer. Colonies were grown for 10 days and counted using ImageJ.

Cellular ROS levels

ID8-IP Rgnef-KO or GFP-Rgnef re-expressing cells were grown adherently. After trypsinization and counting (ViCell XR), equal numbers of cells were transferred to low-attachment plates in serum-free Tumorsphere Medium XF (PromoCell) for growth in suspension. Cells were treated with vehicle or 100 μM Trolox (Farris et al. 2016) 1 hour prior to CellROX staining. After 24 hours, cells were stained with 750 nM CellROX Deep Red Reagent for 30 mins (Invitrogen). Median fluorescent staining intensity was assessed using flow cytometry on the FL-4 channel (FACScalibur, BD).

Statistics

Statistical difference between ID8-IP clones was determined using one-way ANOVA with Bonferroni post-hoc analysis. Statistical difference between ID8-IP GFP-Rgnef cells treated with inhibitors was determined using one-way ANOVA with Tukey post-hoc analysis. Differences between pairs of data were determined using an unpaired two-tailed Student's t-test. All statistical analyses were performed using Prism (GraphPad Software, v7). P-values of <0.05 were considered significant. All experiments including statistics were performed in triplicate unless otherwise specified.

2.6 References

Al Habyan, S., C. Kalos, J. Szymborski, and L. McCaffrey. 2018. "Multicellular detachment generates metastatic spheroids during intra-abdominal dissemination in epithelial ovarian cancer." *Oncogene*. doi: 10.1038/s41388-018-0317-x.

Alexandre, J., Y. Hu, W. Lu, H. Pelicano, and P. Huang. 2007. "Novel action of paclitaxel against cancer cells: bystander effect mediated by reactive oxygen species." *Cancer Res* 67 (8):3512-7. doi: 10.1158/0008-5472.CAN-06-3914.

Anders, S., and W. Huber. 2010. "Differential expression analysis for sequence count data." *Genome Biol* 11 (10):R106. doi: 10.1186/gb-2010-11-10-r106.

Baccam, M., S. Y. Woo, C. Vinson, and G. A. Bishop. 2003. "CD40-mediated transcriptional regulation of the IL-6 gene in B lymphocytes: involvement of NF-kappa B, AP-1, and C/EBP." *J Immunol* 170 (6):3099-108.

Bargonetti, J., I. Reynisdottir, P. N. Friedman, and C. Prives. 1992. "Site-specific binding of wild-type p53 to cellular DNA is inhibited by SV40 T antigen and mutant p53." *Genes Dev* 6 (10):1886-98.

Cairns, R. A., I. S. Harris, and T. W. Mak. 2011. "Regulation of cancer cell metabolism." *Nat Rev Cancer* 11 (2):85-95. doi: 10.1038/nrc2981.

Cancer Genome Atlas Research, Network. 2011. "Integrated genomic analyses of ovarian carcinoma." *Nature* 474 (7353):609-15. doi: 10.1038/nature10166.

Chen, E. Y., C. M. Tan, Y. Kou, Q. Duan, Z. Wang, G. V. Meirelles, N. R. Clark, and A. Ma'ayan. 2013. "Enrichr: interactive and collaborative HTML5 gene list enrichment analysis tool." *BMC Bioinformatics* 14:128. doi: 10.1186/1471-2105-14-128.

Cheung, K., C. A. Droppelmann, A. MacLellan, I. Cameron, B. Withers, D. Campos-Melo, K. Volkening, and M. J. Strong. 2017. "Rho guanine nucleotide exchange factor (RGNEF) is a prosurvival factor under stress conditions." *Mol Cell Neurosci* 82:88-95. doi: 10.1016/j.mcn.2017.05.003.

Connolly, D. C., R. Bao, A. Y. Nikitin, K. C. Stephens, T. W. Poole, X. Hua, S. S. Harris, B. C. Vanderhyden, and T. C. Hamilton. 2003. "Female mice chimeric for expression of the simian virus 40 TAg under control of the MISIIR promoter develop epithelial ovarian cancer." *Cancer Res* 63 (6):1389-97.

Connolly, D. C., and H. H. Hensley. 2009. "Xenograft and Transgenic Mouse Models of Epithelial Ovarian Cancer and Non Invasive Imaging Modalities to Monitor Ovarian Tumor Growth In situ -Applications in Evaluating Novel Therapeutic Agents." *Curr Protoc Pharmacol* 45:14 12 1-14 12 26.

Diehn, M., R. W. Cho, N. A. Lobo, T. Kalisky, M. J. Dorie, A. N. Kulp, D. Qian, J. S. Lam, L. E. Ailles, M. Wong, B. Joshua, M. J. Kaplan, I. Wapnir, F. M. Dirbas, G. Somlo, C. Garberoglio, B. Paz, J. Shen, S. K. Lau, S. R. Quake, J. M. Brown, I. L. Weissman, and M. F. Clarke. 2009. "Association of reactive oxygen species levels and radioresistance in cancer stem cells." *Nature* 458 (7239):780-3. doi: 10.1038/nature07733.

Diviani, D., F. Raimondi, C. D. Del Vescovo, E. Dreyer, E. Reggi, H. Osman, L. Ruggieri, C. Gonano, S. Cavin, C. L. Box, M. Lenoir, M. Overduin, L. Bellucci, M. Seeber, and F. Fanelli. 2016. "Small-Molecule Protein-Protein Interaction Inhibitor of Oncogenic Rho Signaling." *Cell Chem Biol* 23 (9):1135-1146. doi: 10.1016/j.chembiol.2016.07.015.

Farris, J. C., P. M. Pifer, L. Zheng, E. Gottlieb, J. Denvir, and S. M. Frisch. 2016. "Grainyhead-like 2 Reverses the Metabolic Changes Induced by the Oncogenic Epithelial-Mesenchymal Transition: Effects on Anoikis." *Mol Cancer Res* 14 (6):528-38. doi: 10.1158/1541-7786.MCR-16-0050.

Gabbasov, R., F. Xiao, C. G. Howe, L. E. Bickel, S. W. O'Brien, D. Benrubi, T. V. Do, Y. Zhou, E. Nicolas, K. Q. Cai, S. Litwin, S. Seo, E. A. Golemis, and D. C. Connolly. 2018. "NEDD9 promotes oncogenic signaling, a stem/mesenchymal gene signature, and aggressive ovarian cancer growth in mice." *Oncogene* 37 (35):4854-4870. doi: 10.1038/s41388-018-0296-y.

Gorrini, C., I. S. Harris, and T. W. Mak. 2013. "Modulation of oxidative stress as an anticancer strategy." *Nat Rev Drug Discov* 12 (12):931-47. doi: 10.1038/nrd4002.

Guadamillas, M. C., A. Cerezo, and M. A. Del Pozo. 2011. "Overcoming anoikis--pathways to anchorage-independent growth in cancer." *J Cell Sci* 124 (Pt 19):3189-97. doi: 10.1242/jcs.072165.

Harris, I. S., A. E. Treloar, S. Inoue, M. Sasaki, C. Gorrini, K. C. Lee, K. Y. Yung, D. Brenner, C. B. Knobbe-Thomsen, M. A. Cox, A. Elia, T. Berger, D. W. Cescon, A. Adeoye, A. Brustle, S. D. Molyneux, J. M. Mason, W. Y. Li, K. Yamamoto, A. Wakeham, H. K. Berman, R. Khokha, S. J. Done, T. J. Kavanagh, C. W. Lam, and T. W. Mak. 2015. "Glutathione and thioredoxin antioxidant pathways synergize to drive cancer initiation and progression." *Cancer Cell* 27 (2):211-22. doi: 10.1016/j.ccell.2014.11.019.

Kenny, H. A., S. Dogan, M. Zillhardt, K. Mitra A, S. D. Yamada, T. Krausz, and E. Lengyel. 2009. "Organotypic models of metastasis: A three-dimensional culture mimicking the human peritoneum and omentum for the study of the early steps of ovarian cancer metastasis." *Cancer Treat Res* 149:335-51. doi: 10.1007/978-0-387-98094-2_16.

Kim, D., G. Pertea, C. Trapnell, H. Pimentel, R. Kelley, and S. L. Salzberg. 2013. "TopHat2: accurate alignment of transcriptomes in the presence of insertions, deletions and gene fusions." *Genome Biol* 14 (4):R36. doi: 10.1186/gb-2013-14-4-r36.

Konstantinopoulos, P. A., E. Fountzilas, K. Pillay, L. F. Zerbini, T. A. Libermann, S. A. Cannistra, and D. Spentzos. 2008. "Carboplatin-induced gene expression changes in vitro are prognostic of survival in epithelial ovarian cancer." *BMC Med Genomics* 1:59. doi: 10.1186/1755-8794-1-59.

Kuleshov, M. V., M. R. Jones, A. D. Rouillard, N. F. Fernandez, Q. Duan, Z. Wang, S. Koplev, S. L. Jenkins, K. M. Jagodnik, A. Lachmann, M. G. McDermott, C. D. Monteiro, G. W. Gundersen, and A. Ma'ayan. 2016. "Enrichr: a comprehensive gene set enrichment analysis web server 2016 update." *Nucleic Acids Res* 44 (W1):W90-7. doi: 10.1093/nar/gkw377.

Lachmann, A., H. Xu, J. Krishnan, S. I. Berger, A. R. Mazloom, and A. Ma'ayan. 2010. "ChEA: transcription factor regulation inferred from integrating genome-wide ChIP-X experiments." *Bioinformatics* 26 (19):2438-44. doi: 10.1093/bioinformatics/btq466.

Lanczky, A., A. Nagy, G. Bottai, G. Munkacsy, A. Szabo, L. Santarpia, and B. Gyorffy. 2016. "miRpower: a web-tool to validate survival-associated miRNAs utilizing expression data from 2178 breast cancer patients." *Breast Cancer Res Treat* 160 (3):439-446. doi: 10.1007/s10549-016-4013-7.

Lee, J. R., Y. J. Ha, and H. J. Kim. 2003. "Cutting edge: induced expression of a RhoA-specific guanine nucleotide exchange factor, p190RhoGEF, following CD40 stimulation and WEHI 231 B cell activation." *J Immunol* 170 (1):19-23.

Lengyel, E. 2010. "Ovarian cancer development and metastasis." *Am J Pathol* 177 (3):1053-64. doi: 10.2353/ajpath.2010.100105.

Lim, Y., S. T. Lim, A. Tomar, M. Gardel, J. A. Bernard-Trifilo, X. L. Chen, S. A. Uryu, R. Canete-Soler, J. Zhai, H. Lin, W. W. Schlaepfer, P. Nalbant, G. Bokoch, D. Ilic, C. Waterman-Storer, and D. D. Schlaepfer. 2008. "PyK2 and FAK connections to p190Rho guanine nucleotide exchange factor

regulate RhoA activity, focal adhesion formation, and cell motility." *J Cell Biol* 180 (1):187-203. doi: 10.1083/jcb.200708194.

Marullo, R., E. Werner, N. Degtyareva, B. Moore, G. Altavilla, S. S. Ramalingam, and P. W. Doetsch. 2013. "Cisplatin induces a mitochondrial-ROS response that contributes to cytotoxicity depending on mitochondrial redox status and bioenergetic functions." *PLoS One* 8 (11):e81162. doi: 10.1371/journal.pone.0081162.

Masia-Balague, M., I. Izquierdo, G. Garrido, A. Cordomi, L. Perez-Benito, N. L. Miller, D. D. Schlaepfer, V. Gigoux, and A. M. Aragay. 2015. "Gastrin-stimulated Galpha13 Activation of Rgnef Protein (ArhGEF28) in DLD-1 Colon Carcinoma Cells." *J Biol Chem* 290 (24):15197-209. doi: 10.1074/jbc.M114.628164.

Mateescu, B., L. Batista, M. Cardon, T. Gruosso, Y. de Feraudy, O. Mariani, A. Nicolas, J. P. Meyniel, P. Cottu, X. Sastre-Garau, and F. Mechta-Grigoriou. 2011. "miR-141 and miR-200a act on ovarian tumorigenesis by controlling oxidative stress response." *Nat Med* 17 (12):1627-35. doi: 10.1038/nm.2512.

Miller, N. L., E. G. Kleinschmidt, and D. D. Schlaepfer. 2014. "RhoGEFs in cell motility: novel links between Rgnef and focal adhesion kinase." *Curr Mol Med* 14 (2):221-34.

Miller, N. L., C. Lawson, X. L. Chen, S. T. Lim, and D. D. Schlaepfer. 2012. "Rgnef (p190RhoGEF) knockout inhibits RhoA activity, focal adhesion establishment, and cell motility downstream of integrins." *PLoS One* 7 (5):e37830. doi: 10.1371/journal.pone.0037830.

Miller, N. L., C. Lawson, E. G. Kleinschmidt, I. Tancioni, S. Uryu, and D. D. Schlaepfer. 2013. "A non-canonical role for Rgnef in promoting integrin-stimulated focal adhesion kinase activation." *J Cell Sci* 126 (Pt 21):5074-85. doi: 10.1242/jcs.135509.

Morgan, M. J., and Z. G. Liu. 2011. "Crosstalk of reactive oxygen species and NF-kappaB signaling." *Cell Res* 21 (1):103-15. doi: 10.1038/cr.2010.178.

Quinn, B. A., F. Xiao, L. Bickel, L. Martin, X. Hua, A. Klein-Szanto, and D. C. Connolly. 2010. "Development of a syngeneic mouse model of epithelial ovarian cancer." *J Ovarian Res* 3:24. doi: 10.1186/1757-2215-3-24.

Ramanathan, B., K. Y. Jan, C. H. Chen, T. C. Hour, H. J. Yu, and Y. S. Pu. 2005. "Resistance to paclitaxel is proportional to cellular total antioxidant

capacity." *Cancer Res* 65 (18):8455-60. doi: 10.1158/0008-5472.CAN-05-1162.

Ran, F. A., P. D. Hsu, J. Wright, V. Agarwala, D. A. Scott, and F. Zhang. 2013. "Genome engineering using the CRISPR-Cas9 system." *Nat Protoc* 8 (11):2281-2308. doi: 10.1038/nprot.2013.143.

Reddig, P. J., and R. L. Juliano. 2005. "Clinging to life: cell to matrix adhesion and cell survival." *Cancer Metastasis Rev* 24 (3):425-39. doi: 10.1007/s10555-005-5134-3.

Rojo de la Vega, M., E. Chapman, and D. D. Zhang. 2018. "NRF2 and the Hallmarks of Cancer." *Cancer Cell* 34 (1):21-43. doi: 10.1016/j.ccell.2018.03.022.

Roy, L., and K. D. Cowden Dahl. 2018. "Can Stemness and Chemoresistance Be Therapeutically Targeted via Signaling Pathways in Ovarian Cancer?" *Cancers (Basel)* 10 (8). doi: 10.3390/cancers10080241.

Schafer, Z. T., A. R. Grassian, L. Song, Z. Jiang, Z. Gerhart-Hines, H. Y. Irie, S. Gao, P. Puigserver, and J. S. Brugge. 2009. "Antioxidant and oncogene rescue of metabolic defects caused by loss of matrix attachment." *Nature* 461 (7260):109-13. doi: 10.1038/nature08268.

Schieber, M., and N. S. Chandel. 2014. "ROS function in redox signaling and oxidative stress." *Curr Biol* 24 (10):R453-62. doi: 10.1016/j.cub.2014.03.034.

Seguin, L., J. S. Desgrosellier, S. M. Weis, and D. A. Cheresh. 2015. "Integrins and cancer: regulators of cancer stemness, metastasis, and drug resistance." *Trends Cell Biol* 25 (4):234-40. doi: 10.1016/j.tcb.2014.12.006.

Shapiro, I. M., V. N. Kolev, C. M. Vidal, Y. Kadariya, J. E. Ring, Q. Wright, D. T. Weaver, C. Menges, M. Padval, A. I. McClatchey, Q. Xu, J. R. Testa, and J. A. Pachter. 2014. "Merlin deficiency predicts FAK inhibitor sensitivity: a synthetic lethal relationship." *Sci Transl Med* 6 (237):237ra68. doi: 10.1126/scitranslmed.3008639.

Shield, K., M. L. Ackland, N. Ahmed, and G. E. Rice. 2009. "Multicellular spheroids in ovarian cancer metastases: Biology and pathology." *Gynecol Oncol* 113 (1):143-8. doi: 10.1016/j.ygyno.2008.11.032.

Siegel, R. L., K. D. Miller, and A. Jemal. 2018. "Cancer statistics, 2018." *CA Cancer J Clin* 68 (1):7-30. doi: 10.3322/caac.21442.

Subramanian, A., P. Tamayo, V. K. Mootha, S. Mukherjee, B. L. Ebert, M. A. Gillette, A. Paulovich, S. L. Pomeroy, T. R. Golub, E. S. Lander, and J. P. Mesirov. 2005. "Gene set enrichment analysis: a knowledge-based approach for interpreting genome-wide expression profiles." *Proc Natl Acad Sci U S A* 102 (43):15545-50. doi: 10.1073/pnas.0506580102.

Tancioni, I., N. L. Miller, S. Uryu, C. Lawson, C. Jean, X. L. Chen, E. G. Kleinschmidt, and D. D. Schlaepfer. 2015. "FAK activity protects nucleostemin in facilitating breast cancer spheroid and tumor growth." *Breast Cancer Res* 17:47. doi: 10.1186/s13058-015-0551-x.

Tong, L., and V. Tergaonkar. 2014. "Rho protein GTPases and their interactions with NFkappaB: crossroads of inflammation and matrix biology." *Biosci Rep* 34 (3). doi: 10.1042/BSR20140021.

Trachootham, D., J. Alexandre, and P. Huang. 2009. "Targeting cancer cells by ROS-mediated mechanisms: a radical therapeutic approach?" *Nat Rev Drug Discov* 8 (7):579-91. doi: 10.1038/nrd2803.

van der Wijst, M. G., R. Brown, and M. G. Rots. 2014. "Nrf2, the master redox switch: the Achilles' heel of ovarian cancer?" *Biochim Biophys Acta* 1846 (2):494-509. doi: 10.1016/j.bbcan.2014.09.004.

Ward, K. K., I. Tancioni, C. Lawson, N. L. Miller, C. Jean, X. L. Chen, S. Uryu, J. Kim, D. Tarin, D. G. Stupack, S. C. Plaxe, and D. D. Schlaepfer. 2013. "Inhibition of focal adhesion kinase (FAK) activity prevents anchorage-independent ovarian carcinoma cell growth and tumor progression." *Clin Exp Metastasis* 30 (5):579-94. doi: 10.1007/s10585-012-9562-5.

Wu, J., J. Zhai, H. Lin, Z. Nie, W. W. Ge, L. Garcia-Bermejo, R. J. Muschel, W. W. Schlaepfer, and R. Canete-Soler. 2003. "Cytoplasmic retention sites in p190RhoGEF confer anti-apoptotic activity to an EGFP-tagged protein." *Brain Res Mol Brain Res* 117 (1):27-38.

You, D., J. Xin, A. Volk, W. Wei, R. Schmidt, G. Scurti, S. Nand, E. K. Breuer, P. C. Kuo, P. Breslin, A. R. Kini, M. I. Nishimura, N. J. Zeleznik-Le, and J. Zhang. 2015. "FAK mediates a compensatory survival signal parallel to PI3K-AKT in PTEN-null T-ALL cells." *Cell Rep* 10 (12):2055-68. doi: 10.1016/j.celrep.2015.02.056.

Yu, H. G., J. O. Nam, N. L. Miller, I. Tanjoni, C. Walsh, L. Shi, L. Kim, X. L. Chen, A. Tomar, S. T. Lim, and D. D. Schlaepfer. 2011. "p190RhoGEF (Rgnef) promotes colon carcinoma tumor progression via interaction with focal adhesion kinase." *Cancer Res* 71 (2):360-70. doi: 10.1158/0008-5472.CAN-10-2894.

Yu, Y., G. Ramena, and R. C. Elble. 2012. "The role of cancer stem cells in relapse of solid tumors." *Front Biosci (Elite Ed)* 4:1528-41.

Zhai, J., H. Lin, Z. Nie, J. Wu, R. Canete-Soler, W. W. Schlaepfer, and D. D. Schlaepfer. 2003. "Direct interaction of focal adhesion kinase with p190RhoGEF." *J Biol Chem* 278 (27):24865-73. doi: 10.1074/jbc.M302381200.

Zhang, H., T. Liu, Z. Zhang, S. H. Payne, B. Zhang, J. E. McDermott, J. Y. Zhou, V. A. Petyuk, L. Chen, D. Ray, S. Sun, F. Yang, L. Chen, J. Wang, P. Shah, S. W. Cha, P. Aiyetan, S. Woo, Y. Tian, M. A. Gritsenko, T. R. Clauss, C. Choi, M. E. Monroe, S. Thomas, S. Nie, C. Wu, R. J. Moore, K. H. Yu, D. L. Tabb, D. Fenyo, V. Bafna, Y. Wang, H. Rodriguez, E. S. Boja, T. Hiltke, R. C. Rivers, L. Sokoll, H. Zhu, I. M. Shih, L. Cope, A. Pandey, B. Zhang, M. P. Snyder, D. A. Levine, R. D. Smith, D. W. Chan, K. D. Rodland, and Cptac Investigators. 2016. "Integrated Proteogenomic Characterization of Human High-Grade Serous Ovarian Cancer." *Cell* 166 (3):755-765. doi: 10.1016/j.cell.2016.05.069.

2.7 Figures

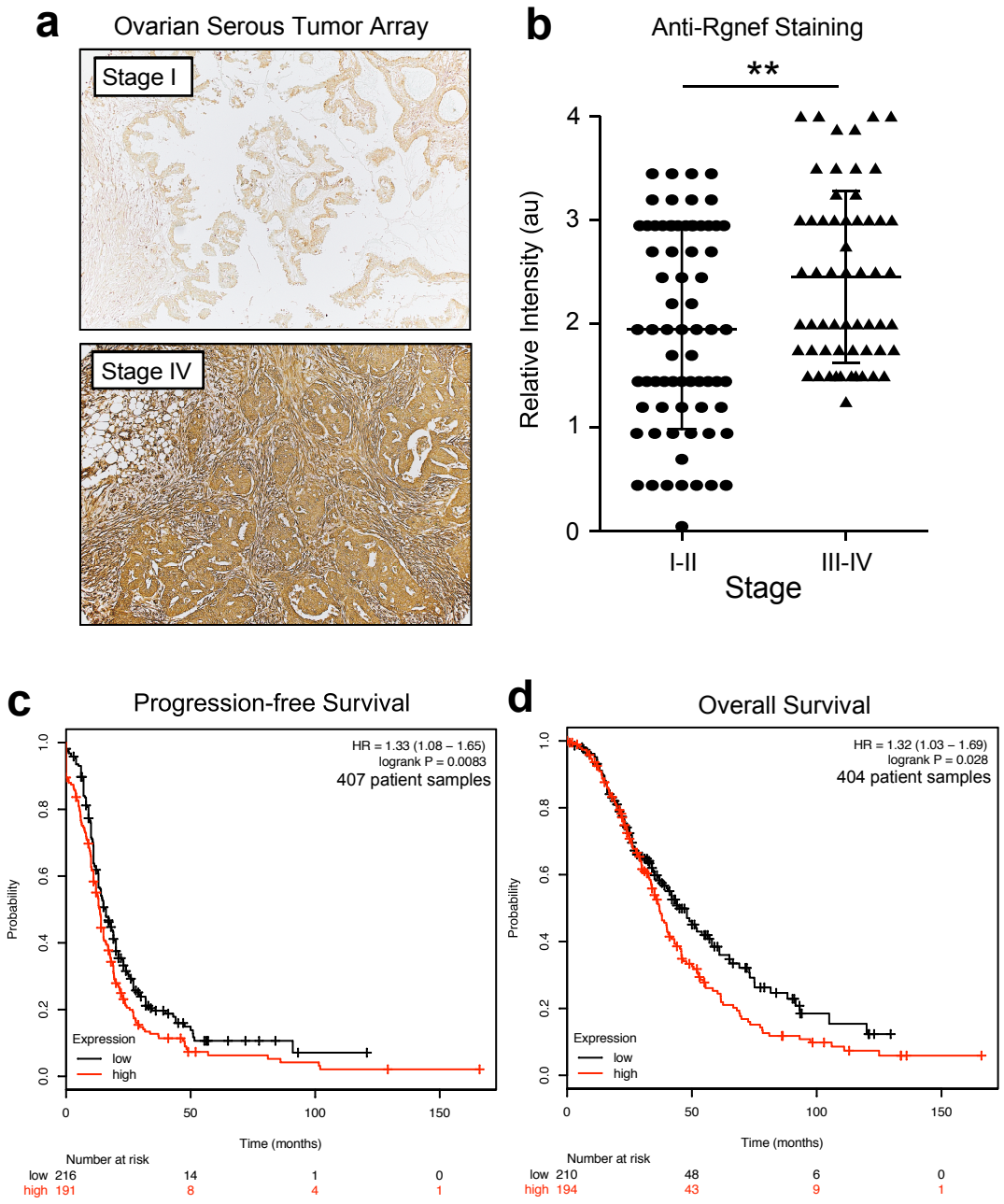

Figure 2.1: Rgnef is overexpressed in late-stage serous ovarian cancer. (a) Representative images of serous ovarian tumor sections stained with a polyclonal anti-Rgnef antibody (brown). (b) Quantification of tumor microarray staining. Expression graded from 0-4 and scored by two independent blinded researchers (**P≤0.01). Plot shows distribution of averaged data. Stage I-II n=71 and stage III-IV n=57. (c) The Kaplan-Meier plotter (http://kmplot.com/ovar) was used to evaluate *RGNEF* mRNA expression in serous ovarian cancer tumor samples from patients with stage III-IV serous ovarian cancer. High *RGNEF* expression was significantly associated with (c) progression-free survival (P=0.0083, n=407) or (d) overall survival (P=0.028, n=404).

Figure 2.2: Rgnef promotes spontaneous ovarian tumor formation. (a) Image of a TAg-stained (brown) ovary and oviduct from a *MISIIR-TAg*+ mouse at week 17. TAg is expressed in the murine ovary and fallopian tubal lesions (green asterisks and dotted lines) and oviduct (yellow asterisk and dotted line), two predicted sites of human ovarian tumor formation. Scale is 1 mm (left) or 100 μM (right). (b) Breeding schematic for generation of *Rgnef*$^{-/-}$ or *Rgnef*$^{+/+}$*;MISIIR;TAg*+ mice. (c) Ovary size was measured by ultrasound. Mice were sacrificed at week 17 or when mice met IACUC humane standards for euthanasia. Each point represents n≥5 mice, error bars represent SEM. (d) Representative pictures of oviducts and ovaries for each group at the experimental endpoint. (e) Tumor burden was significantly higher in *Rgnef*$^{+/+}$ than *Rgnef*$^{-/-}$ mice. Tumor burden was measured by combined ovary mass (*P≤0.05, bar represents mean). (f) Immunofluorescent staining in frozen ovary sections from mice with spontaneous ovarian tumor formation. Stains for TAg (green) and DNA (Hoechst, blue).

Figure 2.2

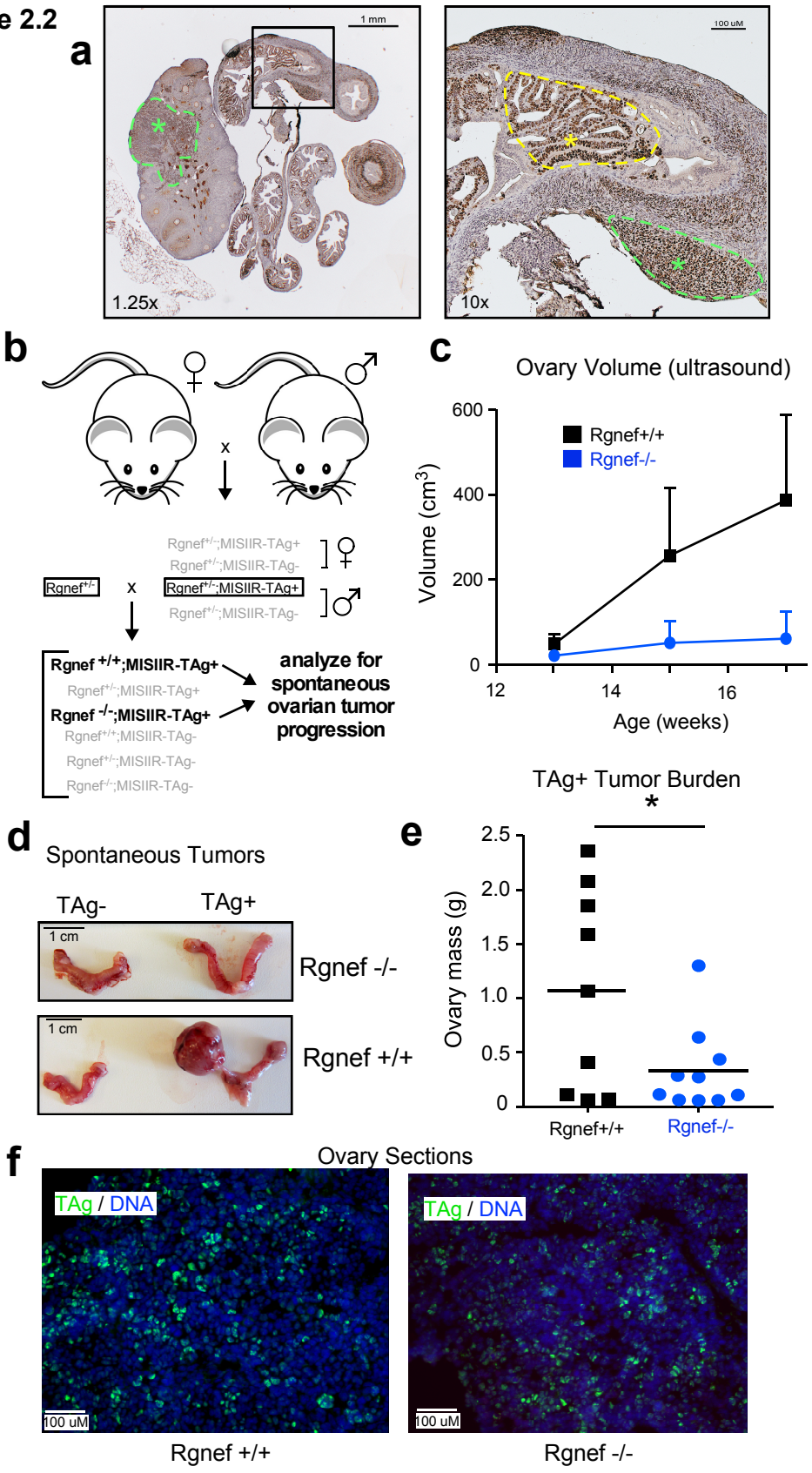
a
1 mm
1.25x
100 uM
10x
b
x
Rgnef+/-;MISIIR-TAg+
Rgnef+/-;MISIIR-TAg-
Rgnef+/- x Rgnef+/-;MISIIR-TAg+
Rgnef+/-;MISIIR-TAg-
Rgnef +/+;MISIIR-TAg+
Rgnef+/-;MISIIR-TAg+
Rgnef -/-;MISIIR-TAg+
Rgnef+/+;MISIIR-TAg-
Rgnef+/-;MISIIR-TAg-
Rgnef-/-;MISIIR-TAg-
analyze for spontaneous ovarian tumor progression
c
Ovary Volume (ultrasound)
Rgnef+/+
Rgnef-/-
Volume (cm3)
600
400
200
0
12
14
16
Age (weeks)
TAg+ Tumor Burden
*
d
Spontaneous Tumors
TAg-
TAg+
1 cm
Rgnef -/-
1 cm
Rgnef +/+
e
Ovary mass (g)
2.5
2.0
1.5
1.0
0.5
0
Rgnef+/+
Rgnef-/-
f
Ovary Sections
TAg / DNA
100 uM
Rgnef +/+
TAg / DNA
100 uM
Rgnef -/-

Figure 2.3: Rgnef promotes tumor formation in a tumor-cell-intrinsic manner. (a) Schematic of *Rgnef*$^{+/+}$ and *Rgnef*$^{-/-}$ MOVCAR generation. (b) Representative PCR of MOVCAR cells from *Rgnef*$^{+/+}$ and Rgnef$^{-/-}$ TAg+ mice confirming genomic Rgnef integrity or deletion in Rgnef murine exon 24. (c) Immunoblotting showing Rgnef loss in *Rgnef*$^{-/-}$ MOVCARs, with GAPDH as loading control. (d) *Rgnef*$^{-/-}$ MOVCARs grow significantly faster in adherent conditions over 4 days (*P≤0.05, **P≤0.01, ***P≤0.001, error bars represent SD, n=3). (e) MOVCAR cells were introduced orthotopically into syngeneic *MISIIR-TAg-Low;Rgnef*$^{+/+}$ mice by intrabursal injection. (f) Orthotopic injection of Rgnef -/- MOVCARs resulted in significantly lower ovarian tumor mass (**P≤0.01, error bars represent SD). (g) Bioluminescent imaging (BLI) readings from mice injected intraperitoneally with *Rgnef*$^{+/+}$ or *Rgnef*$^{-/-}$ MOVCAR cells. Total flux (photons/second) levels are normalized by group to week 1 readings for each cohort (**P≤ 0.01, ****P≤ 0.0001, n=8 for each group, error bars represent SEM). (h) At week 14 following intraperitoneal injection, ascites-associated cells were collected from recipient mice by peritoneal wash, and ovaries and omentum were dissected and weighed. Rgnef loss significantly impaired metastatic potential as measured by (h) ovarian tumor burden, (i) number of ascites-associated cells, and (j) omentum mass (*P≤0.05***P≤0.001, error bars represent SD, n=8 per group).

Figure 2.3

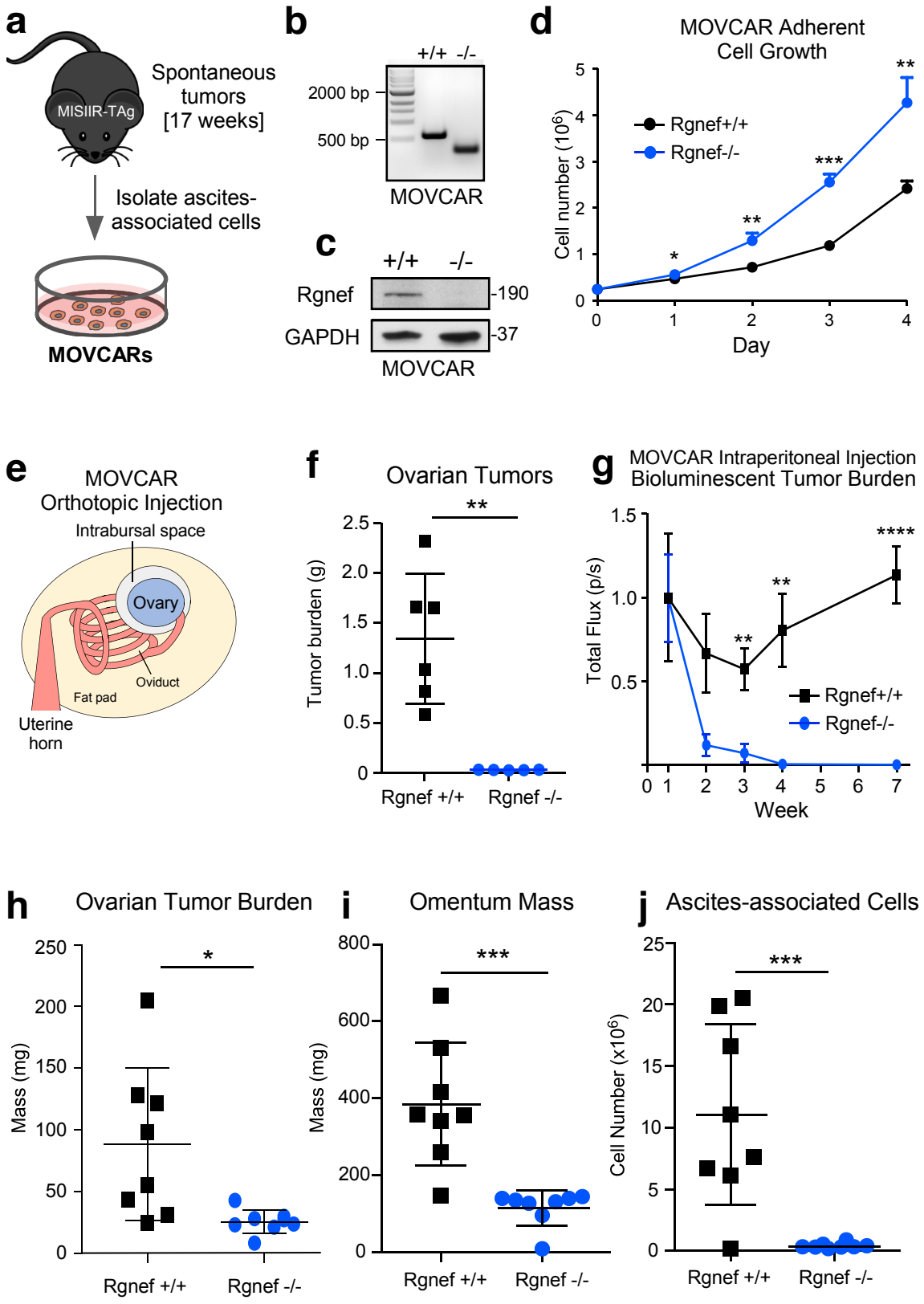
a
MISIIR-TAg
Spontaneous tumors [17 weeks]
Isolate ascites-associated cells
MOVCARs
b
+/+ -/-
2000 bp
500 bp
MOVCAR
c
+/+ -/-
Rgnef
-190
GAPDH
-37
MOVCAR
d
MOVCAR Adherent Cell Growth
Cell number (10^6)
Rgnef+/+
Rgnef-/-
Day
e
MOVCAR Orthotopic Injection
Intrabursal space
Ovary
Oviduct
Fat pad
Uterine horn
f
Ovarian Tumors
Tumor burden (g)
Rgnef +/+
Rgnef -/-
g
MOVCAR Intraperitoneal Injection Bioluminescent Tumor Burden
Total Flux (p/s)
Rgnef+/+
Rgnef-/-
Week
h
Ovarian Tumor Burden
Mass (mg)
Rgnef +/+
Rgnef -/-
i
Omentum Mass
Mass (mg)
Rgnef +/+
Rgnef -/-
j
Ascites-associated Cells
Cell Number (x10^6)
Rgnef +/+
Rgnef -/-

Figure 2.4: Rgnef loss specifically impairs 3D growth and metastasis. (a) Schematic of Rgnef CRISPR/Cas9-mediated knockout. CRISPR/Cas9 gRNA was designed to target murine Rgnef exon 6 (blue text). Also shown are Rgnef protein domains: Zn - zinc finger, DH - double homology, PH - pleckstrin homology, FBD – FAK binding domain, c-c - coiled-coil. Below: PCR of genomic DNA for screening was performed using primers flanking gRNA target, followed by Sanger sequencing. (b) ID8-IP parental cells and CRISPR Rgnef-KO clones were grown adherently for 4 days (n.s.= no significance, *P≤0.05, ***P≤0.001, ****P≤0.0001, n=3, error bars represent SD). 50,000 cells were seeded on day 0 in triplicate. (c) Sanger sequencing of ID8-IP KO-13 genomic DNA was used to confirm deletions in Rgnef. Shown are regions from murine Rgnef exon 6 with biallelic deletions. Predicted mutations and early stop codon (*) resulting from deletions are denoted below, underlined and italicized. (d) Rgnef loss in ID8-IP cells significantly impairs 3D colony growth by day 10 (**P≤0.01, n=2 biological replicates, error bars represent SD). (e) Representative picture from each group. (f) ID8-IP parental cells have an anchorage-independent growth advantage as compared to Rgnef-KO cells. 50,000 cells were seeded in suspension on day 0, and cells were counted in Day 7 (3 biological replicates, error bars represent SD, **P≤0.01).

Figure 2.4

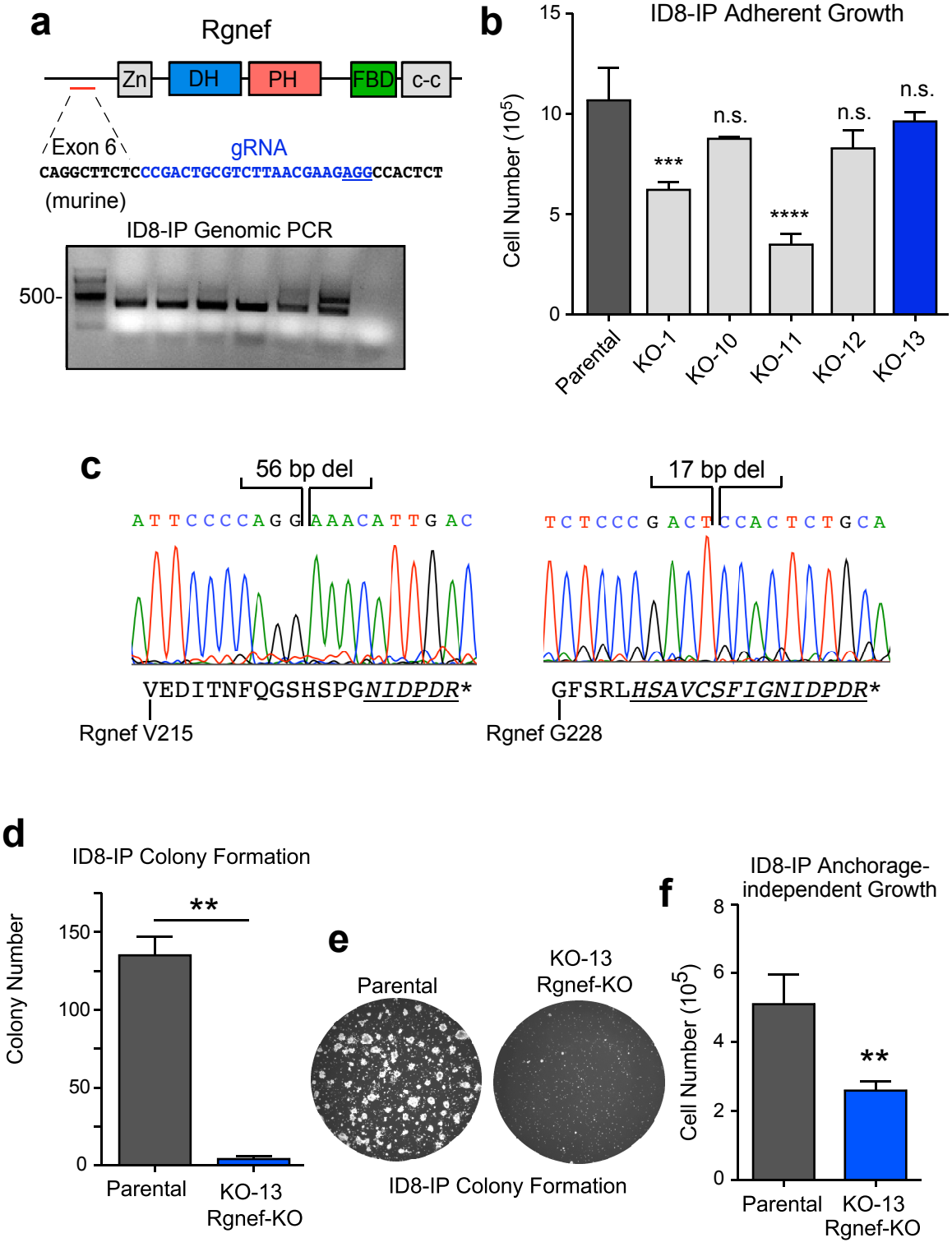
a
Rgnef
Zn
DH
PH
FBD
c-c
Exon 6
gRNA
CAGGCTTCTCCCGACTGCGTCTTAACGAAGAGGCCACTCT
(murine)
ID8-IP Genomic PCR
500-
b
ID8-IP Adherent Growth
Cell Number (10^5)
15
10
5
0
***
n.s.
****
n.s.
n.s.
Parental
KO-1
KO-10
KO-11
KO-12
KO-13
c
56 bp del
ATTCCCCAGGAAACATTGAC
VEDITNFQGSHSPGNIDPDR*
Rgnef V215
17 bp del
TCTCCCGACTCCACTCTGCA
GFSRLHSAVCSFIGNIDPDR*
Rgnef G228
d
ID8-IP Colony Formation
Colony Number
150
100
50
0
**
Parental
KO-13
Rgnef-KO
e
Parental
KO-13
Rgnef-KO
ID8-IP Colony Formation
f
ID8-IP Anchorage-independent Growth
Cell Number (10^5)
8
6
4
2
0
**
Parental
KO-13
Rgnef-KO

Figure 2.5: Rgnef promotes anchorage-independent growth *in vitro* and *in vivo*. (a) Immunoblot showing GFP-Rgnef re-expression in ID8-IP Rgnef-KO cells. (b) GFP-Rgnef or GFP localization in ID8-IP Rgnef-KO cells was visualized by confocal microscopy. (c) ID8-IP Rgnef-KO and GFP-Rgnef re-expressing cells have no significant adherent growth difference by day 4. 50,000 cells were seeded on day 0 in triplicate (n.s.= no significance, error bars represent SD). (d) ID8-IP GFP-Rgnef re-expressing cells grow significantly more 3D colonies by day 10. Representative picture (d) and quantification (e) are shown (**P≤0.01, n=3 biological replicates, error bars represent SD). (f) 5 million ID8-IP Rgnef-KO or GFP-Rgnef re-expressing cells were injected into syngeneic C57Bl/6 mice. Shown are representative pictures from bioluminescent imaging and (g) measurements of total flux on day 34 (**P≤0.01, error bars represent SD). (h) Recipient mice were sacrificed on day 39, and ascites-associated cells were recovered by peritoneal wash and counted. Peritoneal growth of ascites-associated cells was significantly increased in ID8-IP GFP-Rgnef-expressing cells (**P≤0.01, n=6 mice per group, error bars represent SD). (i) H&E staining of ID8-IP Rgnef-KO or GFP-Rgnef cells infiltrating the murine omentum (dotted line). (j) Omentum mass from mice injected with ID8-IP Rgnef-KO or GFP-Rgnef re-expressing cells was not significantly different (n.s. = no significance).

Figure 2.5

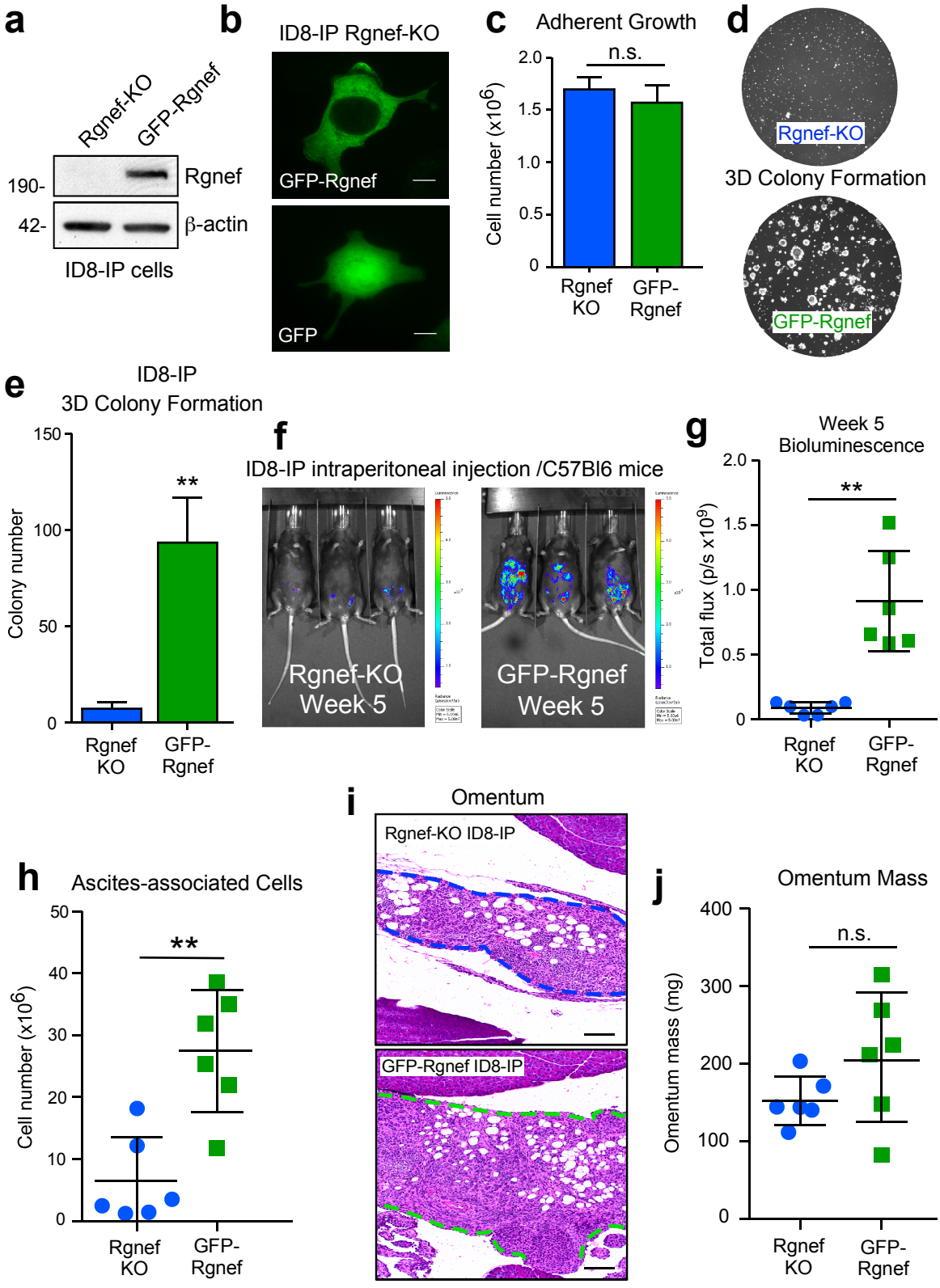
a
Rgnef-KO
GFP-Rgnef
190-
Rgnef
42-
β-actin
ID8-IP cells
b
ID8-IP Rgnef-KO
GFP-Rgnef
GFP
c
Adherent Growth
n.s.
Cell number (x10^6)
2.0
1.5
1.0
0.5
0
Rgnef KO
GFP-Rgnef
d
Rgnef-KO
3D Colony Formation
GFP-Rgnef
e
ID8-IP
3D Colony Formation
Colony number
150
100
50
0
**
Rgnef KO
GFP-Rgnef
f
ID8-IP intraperitoneal injection /C57Bl6 mice
Rgnef-KO Week 5
GFP-Rgnef Week 5
g
Week 5 Bioluminescence
Total flux (p/s x10^9)
2.0
1.5
1.0
0.5
0
**
Rgnef KO
GFP-Rgnef
h
Ascites-associated Cells
Cell number (x10^6)
50
40
30
20
10
0
**
Rgnef KO
GFP-Rgnef
i
Omentum
Rgnef-KO ID8-IP
GFP-Rgnef ID8-IP
j
Omentum Mass
Omentum mass (mg)
400
300
200
100
0
n.s.
Rgnef KO
GFP-Rgnef

Figure 2.6: Rgnef expression promotes an antioxidant gene signature. (a) Differentially upregulated transcripts in MOVCAR *Rgnef*$^{+/+}$ as compared to *Rgnef*$^{-/-}$ were determined using Illumina BeadChip Array. Gene Set Enrichment Analysis (GSEA) was applied to the differentially upregulated mRNA transcripts in *Rgnef*$^{+/+}$ MOVCARs. Top 5 most enriched GO molecular function (a) or KEGG pathways (b) in the set of 313 upregulated transcripts are shown. (c) RNA from ID8-IP Rgnef-KO and GFP-Rgnef re-expressing cells were analyzed by RNA sequencing. 670 differentially-expressed genes were upregulated in the GFP-Rgnef re-expressing cells, and 1142 differentially expressed genes were upregulated in the Rgnef-KO cells. (d) The top $\log_2$ fold changes in the ID8-IP Rgnef-KO or GFP-Rgnef re-expressing cells are shown. (e) Top 5 most enriched GO molecular function or (f) KEGG pathways in the set of 670 upregulated genes in the ID8-IP GFP-Rgnef re-expressing cells. Enrichment score was determined using GSEA. (g) Differentially expressed genes were compared to a curated list of antioxidant genes (Supplemental Table 2). Genes differentially upregulated (green) or downregulated (blue) in ID8-IP GFP-Rgnef cells vs Rgnef-KO cells are shown. (h) Increased levels of Nqo1, Gsta4, and Gpx4 in ID8-IP GFP-Rgnef cells as compared to Rgnef-KO. β-actin is shown as a loading control. Cells were grown for 5 days in anchorage-independent conditions.

Figure 2.6

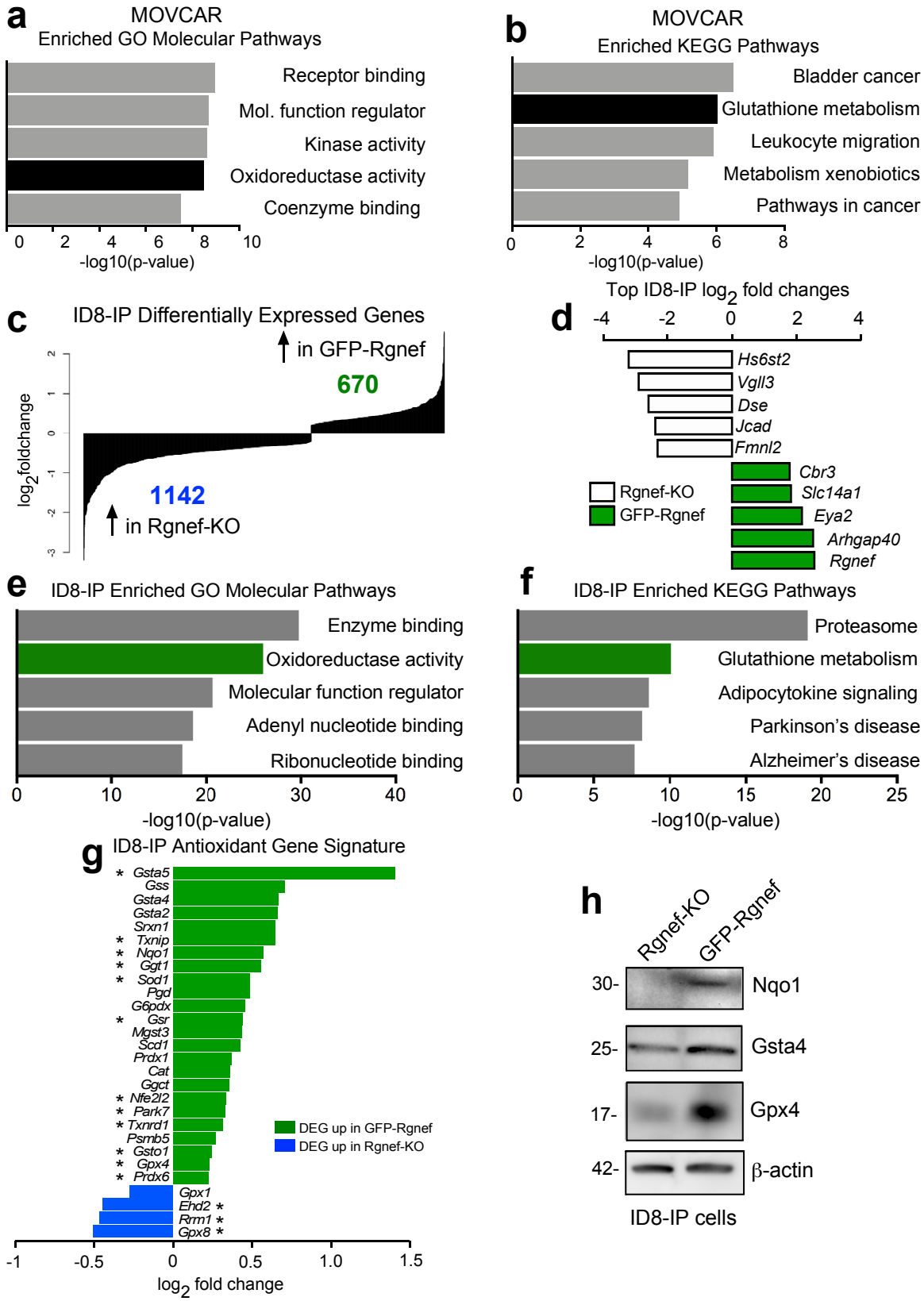
a
MOVCAR
Enriched GO Molecular Pathways
Receptor binding
Mol. function regulator
Kinase activity
Oxidoreductase activity
Coenzyme binding
0 2 4 6 8 10
-log10(p-value)
b
MOVCAR
Enriched KEGG Pathways
Bladder cancer
Glutathione metabolism
Leukocyte migration
Metabolism xenobiotics
Pathways in cancer
0 2 4 6 8
-log10(p-value)
c
ID8-IP Differentially Expressed Genes
in GFP-Rgnef
670
1142
in Rgnef-KO
log2foldchange
d
Top ID8-IP log2 fold changes
-4 -2 0 2 4
Hs6st2
Vgll3
Dse
Jcad
Fmnl2
Cbr3
Slc14a1
Eya2
Arhgap40
Rgnef
Rgnef-KO
GFP-Rgnef
e
ID8-IP Enriched GO Molecular Pathways
Enzyme binding
Oxidoreductase activity
Molecular function regulator
Adenyl nucleotide binding
Ribonucleotide binding
0 10 20 30 40
-log10(p-value)
f
ID8-IP Enriched KEGG Pathways
Proteasome
Glutathione metabolism
Adipocytokine signaling
Parkinson's disease
Alzheimer's disease
0 5 10 15 20 25
-log10(p-value)
g
ID8-IP Antioxidant Gene Signature
* Gsta5
Gss
Gsta4
Gsta2
Srxn1
* Txnip
* Nqo1
* Ggt1
* Sod1
Pgd
G6pdx
* Gsr
Mgst3
Scd1
Prdx1
Cat
Ggct
* Nfe2l2
* Park7
* Txnrd1
Psmb5
* Gsto1
* Gpx4
* Prdx6
Gpx1
Ehd2 *
Rrm1 *
Gpx8 *
DEG up in GFP-Rgnef
DEG up in Rgnef-KO
-1 -0.5 0 0.5 1.0 1.5
log2 fold change
h
Rgnef-KO
GFP-Rgnef
30-
Nqo1
25-
Gsta4
17-
Gpx4
42-
β-actin
ID8-IP cells

Figure 2.7: Endogenous or exogenous antioxidants promote anchorage-independent ovarian tumor cell growth. (a) Cellular ROS levels are higher in Rgnef-KO ID8-IP cells after 24h growth in anchorage-independent conditions, as measured by CellROX. Treatment with 100 uM Trolox for 1h mitigates ROS levels. (b) Trolox administration rescues ID8-IP Rgnef-KO growth in suspension. 50,000 cells were seeded in anchorage-independent conditions on day 0 with or without 100 uM Trolox, and cells were counted in Day 7 (**P≤0.01, n=3 independent experiments, error bars represent SD). (c) Immunoblot of ID8-IP GFP-Rgnef re-expressing or Rgnef-KO cells grown in anchorage-independent conditions, demonstrating increased NRF2 expression in GFP-Rgnef cells. (d) ARE (antioxidant response element) reporter assay for NRF2 transcriptional activity in 293T cells. Overexpression of GFP-Rgnef did not induce expression of the ARE reporter (n.s.=no significance, error bars represent SD). (e) Rgnef expression activates an NFkB reporter. 293T cells were transiently transfected with mCherry or mCherry-Rgnef along with either full-length (FL) IL-6 reporter or an IL-6 reporter with a deletion in the NF-kB reporter region (NF-kB*). Dual-luciferase activity was measured and normalized (***P≤0.001, ****P≤0.0001, error bars represent SD). (f) Adherent ID8-IP GFP-Rgnef cells were pre-treated with DMSO vehicle, 1 uM wortmannin, 10 μM U0126, 10 uM Bay 11-7082, or 10 uM TPCA-1 for 24h, then seeded at 50k/well in anchorage-independent inhibitor-free conditions for 7 days. Shown is cell number normalized to vehicle control (n.s.=no significance, *P≤0.05, ****P≤0.0001, error bars represent SD). (g) Proposed model of Rgnef in ovarian cancer. Upon Rgnef loss, the cell is not able to balance increased ROS resulting from growth in suspension, resulting in oxidative stress. When Rgnef is re-expressed, NF-kB-mediated transcription downstream of Rgnef promotes the expression of an antioxidant gene signature, resulting in redox balance.

Figure 2.7

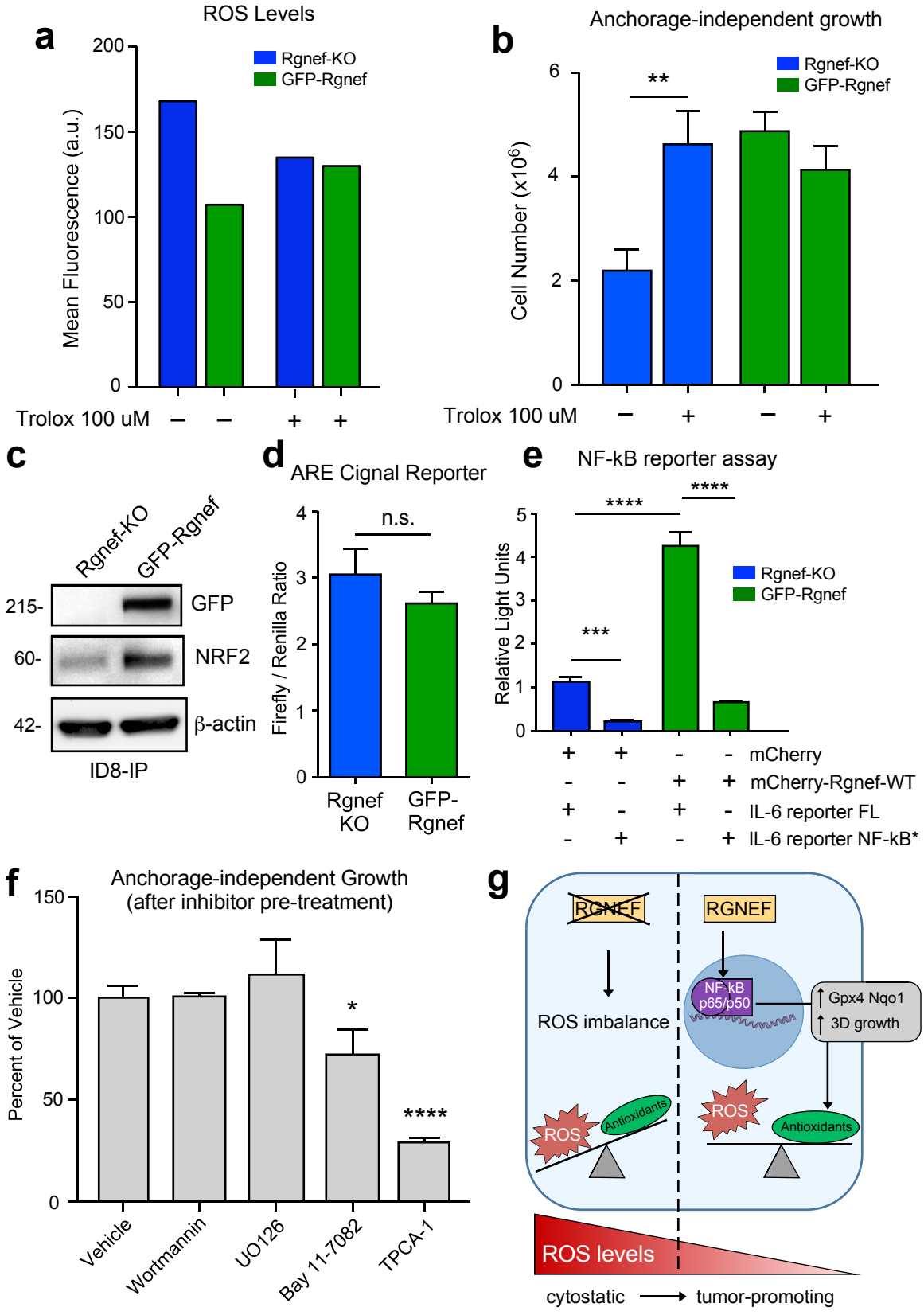
a
ROS Levels
Rgnef-KO
GFP-Rgnef
Mean Fluorescence (a.u.)
200
150
100
50
0
Trolox 100 uM
b
Anchorage-independent growth
Rgnef-KO
GFP-Rgnef
**
Cell Number (x10^6)
6
4
2
0
Trolox 100 uM
c
Rgnef-KO
GFP-Rgnef
215-
GFP
60-
NRF2
42-
β-actin
ID8-IP
d
ARE Cignal Reporter
n.s.
Firefly / Renilla Ratio
Rgnef KO
GFP-Rgnef
e
NF-kB reporter assay
****
****
***
Relative Light Units
Rgnef-KO
GFP-Rgnef
mCherry
mCherry-Rgnef-WT
IL-6 reporter FL
IL-6 reporter NF-kB*
f
Anchorage-independent Growth
(after inhibitor pre-treatment)
Percent of Vehicle
*
****
Vehicle
Wortmannin
UO126
Bay 11-7082
TPCA-1
g
RGNEF
RGNEF
ROS imbalance
NF-kB p65/p50
Gpx4 Nqo1
3D growth
ROS
Antioxidants
ROS
Antioxidants
ROS levels
cytostatic
tumor-promoting

2.8 Tables

Table 2.1: Curated list of antioxidant genes.

Aass	Gpx1	Ift172	Prdx3
Als2	Gpx2	Il19	Prdx4
Anpep	Gpx3	Il22	Prdx5
Apc	Gpx4	Kif9	Prdx6
Apoe	Gpx5	Lap3	Prdx6b
Aqr	Gpx6	Lpo	Prnp
Atr	Gpx7	Mb	Psmb5
Cat	Gpx8	Mgst1	Ptgs1
Ccs	Gsr	Mgst2	Ptgs2
Ctsb	Gss	Mgst3	Rag2
Cyba	Gsta1	Mpo	Recql4
Cymya1	Gsta2	Mpp4	Rrm1
Dnm2	Gsta3	Ncf2	Rrm2
Duox	Gsta4	Nfe2l2	Rrm2B
Ehd2	Gsta5	Ngb	Scd1
Epx	Gstk1	Nos2	Serpinb1b
Ercc2	Gstm1	Nox1	Slc38a1
Ercc6	Gstm2	Nox4	Slc41a3
Fancc	Gstm3	Noxa1	Sms
Fmo2	Gstm4	Noxo1	Sod1
G6pd	Gstm5	Nqo1	Sod2
G6pdx	Gsto1	Nudt15	Sod3
Gab1	Gsto2	Nxn	Srm
Gclc	Gstp1	Odc1	Srxn1
Gclm	Gstt1	Oplah	Tmod1
Ggct	Gstt2	Park7	Tpo
Ggt1	Gstz1	Pgd	Txndc12
Ggt5	Hbq1	Ppp1r15b	Txnip
Ggt6	Idh1	Prdx1	Txnrd1
Ggt7	Idh2	Prdx2	Txnrd2
			Txnrd3
			Ucp3
			Vim
			Xpa
			Zmynd17

Table 2.2: ChEA analysis of differentially-expressed genes

Transcription Factor	Overlap	Adjusted p-value	Combined score	PMID
NRF2	104 / 1331	*1.9e-13*	66.7	26677805
NRF2	83 / 1055	*6.6e-11*	54.2	20460467
KLF1	90 / 1239	*4.1e-10*	47.2	21900194
RELA	82 / 1182	*2.4e-8*	37.6	24523406
SOX2	121 / 2000	*8.8e-9*	34.6	27498859

2.9 Acknowledgements

Chapter 2, in full, is being prepared for submission: Kleinschmidt, E. G., Miller, N. L. G., Tancioni, I., Osterman C. D., Barrie A. M., Taylor K. N., Jiang S., Connolly D. C., Stupack D. G., Schlaepfer D. D. 2018. “Rgnef promotes ovarian tumor progression and confers protection from oxidative stress.” The dissertation author was the primary investigator and author of this material.

The dissertation author designed, performed, and analyzed all experiments except those listed below. Nichol Miller designed, performed, and analyzed: tumor microarray staining, TAg staining, mouse spontaneous tumor experiment, and MOVCAR line generation. Carlos Díaz-Osterman assisted the dissertation author with FACS analysis of CellROX levels. Nichol Miller, Carlos Díaz-Osterman, Isabelle Tancioni, Allison Barrie, and Shulin Jiang assisted with *in vivo* procedures. Work was supported by grants RO1CA180769, RO1CA102310, and P30CA023100 from the NCI, from NIH UL1TR001442, and from charitable donations from Nine Girls Ask. D. Stupack was supported by NIH RO1CA107263. K. Taylor and A. Barrie are fellows of the UCSD Reproductive Medicine Gynecologic Oncology Program D. Connolly was supported by NCI P30 CA006927, NCI CA195723, DOD W81XWH-16-1-0142 and charitable donations from The Roberta Dubrow Fund and The Main Line Chapter of the Board of Associates.

Chapter 3

Characterization of an aggressive model of murine ovarian cancer

3.1 Introduction

There is an urgent need to develop improved ovarian cancer cell lines for use as *in vitro* and *in vivo* models of high-grade serous ovarian carcinoma (HGSOC). Many of the most commonly-used ovarian cancer cell lines do not closely resemble characteristics of HGSOC, due to hypermutation or lack of p53 mutation (Domcke et al. 2013). Furthermore, cancer cell lines derived from humans cannot be transplanted into immunocompetent mice, which precludes study of the immune tumor microenvironment (TME) in ovarian cancer. While the presence of tumor-infiltrating lymphocytes (TILs) correlates to increased ovarian cancer patient survival, no immunotherapies have been approved for use in high-grade serous ovarian cancer (HGSOC) (McCloskey et al. 2018). Therefore, it is important to identify murine ovarian cancer models that 1) reproduce characteristics of human disease and 2) may be transplanted into immunocompetent mice.

HGSOC tumors are characterized by high genomic instability and low mutational tumor burden (Domcke et al. 2013). Correspondingly, while driver mutations are rare, somatic *TP53* mutations are found in >95% of HGSOC cases (Bowtell et al. 2015). A recent study revealed that 75% of HGSOC cases with *TP53* mutations express high levels of p53 protein, and likely correspond to mutations with loss-of-function or gain-of-function phenotypes. About 25% of cases exhibit low or absent p53, mostly caused by frameshift, nonsense, or splicing mutations. Most *TP53* missense mutations map to the DNA-binding

region of the protein, and render the protein unable to bind to its transcriptional response element (Cole et al. 2016).

Two HGSOC models have been developed from spontaneously transformed primary murine epithelial ovarian cells, ID8 and STOSE (Roby et al. 2000; McCloskey et al. 2014). While both lines express the epithelial ovarian cancer markers WT1 and cytokeratin, both retain wild-type p53. Additionally, both lines form primary tumors, metastatic disease, and ascites when injected orthotopically into syngeneic C57Bl/6J and FVB/N mice, respectively. However, the more widely-used ID8 cells form tumors slowly (90-114 days to lethal tumor burden), and do not survive when cultured in *in vitro* anchorage-independent conditions (Roby et al. 2000; Ward et al. 2013). Our lab has generated an aggressive ID8 subline, ID8-IP, through intraperitoneal passage in syngeneic C57Bl/6J mice. These cells form tumors more quickly, and grow in anchorage-independent conditions. In this chapter, I characterize this ID8-IP cell line using a combination of whole exome sequencing (WES), whole transcriptome sequencing (RNA-Seq), and functional assays.

3.2 Results

Validation of the original ID8 parental line

Our lab previously generated the ID8-IP line through intraperitoneal passage in C57Bl/6J mice followed by anchorage-independent growth of the

pooled ascites-associated cell population (Ward et al. 2013) (Fig. 3.1a). When injected orthotopically into syngeneic C57Bl/6J mice, ID8-IP cells are more aggressive than ID8 parental cells, forming larger tumors, large numbers of ascites-associated spheroids, and a lethal tumor burden in less than half the time of ID8 parental cells. In order to characterize the ID8-IP cells as a model of HGSOC and investigate why ID8-IP cells are more aggressive, I assessed the genetic changes between ID8 and ID8-IP cells. Additionally, I sought to validate the original ID8 parental cells, as cell line contamination or misidentification is a common problem in biological research (Horbach and Halffman 2017).

Whole exome (WES) and whole transcriptome (RNA-Seq) sequencing was performed on early-passage ID8 and ID8-IP cells. WES covered 221,784 exons at an average sequencing depth >280x, and RNA-Seq identified ~17,200 different genes with a total of >50 million reads. I first sought to validate the ID8 cell line by comparing variants identified in our ID8 cells to those published by the Walton lab, which also performed WES on ID8 cells (Walton et al. 2016). Total ID8 variants were filtered to include only exonic non-synonymous mutations that were transcribed according to RNA-Seq analysis (Fig 3.1c). I also filtered out SNPs identified on dbSNP version 138. Most of these SNPs corresponded to mutations in C57Bl/6JN mice, implying that ID8 cells were likely generated from this specific C57Bl/6J strain. After filtering, 12 variants remained, 9 of which were previously identified by the other lab (Fig. 3.1c and Table 3.1) (Walton et al. 2016). The three variants unique to our ID8 cells were in the Hjurp and Usf3 genes. The two variants in Hjurp were predicted to be harmful by SIFT analysis

(Table 3.2) (Choi, Chan, and Craig 2015), while the Usf3 variant was predicted to be neutral. However, these Hjurp mutations are not likely to promote a different phenotype in our ID8 cells, as Hjurp is already highly mutated in ID8 cells, according to our pre-filtered data and that from the Walton lab (Walton et al. 2016). In summary, our parental ID8 cells have a low number of functional mutations, and most of these mutations are identical to previously published mutations in ID8 cells.

Analysis of ID8-IP mutational burden

HGSOC tumors have a low mutation burden of about 1-5 mutations per million bases, whereas hypermutated tumors typically have 15+ mutations per million bases. Hypermutated ovarian cancer cell lines such as IGROV1 are not predicted to be good models for HGSOC (Domcke et al. 2013). By comparing the total number of mutations determined by WES in ID8 cells to the estimated genome size based on karyotype analysis of the original polyploid ID8 cells (Roby et al. 2000), I estimated that parental ID8 cells have an estimated 5.5 mutations per million bases, within the range of most HGSOC tumors. ID8-IP cells had even fewer total mutations, though it is difficult to assess the exact mutational burden in these cells due to predicted differences in copy number alterations.

Next, I compared variants identified in WES between the ID8 parental cells and the ID8-IP aggressive cell line. While ID8-IP cells shared 40% of the

mutations identified in the parental ID8 line, about 38% of the total ID8-IP mutations were unique to the ID8-IP cells (Fig 3.1b). This suggests that the ID8 population itself is heterogeneous, and only a subset of the ID8 parental population formed the aggressive population that constitutes the ID8-IP cell line. Additionally, it raises the possibility that additional mutations acquired in the ID8-IP cells could be responsible for the increased aggressiveness of the ID8-IP line. To test this hypothesis, I filtered the unique ID8-IP mutations, keeping only transcribed nonsynonymous functional mutations. I also filtered mutations in dbSNP 138, as common SNPs are not likely to affect protein function. Two predicted single amino acid mutations remained, in *Atxn10* and *Xxylt1*. Although both mutations were predicted to be damaging by PROVEAN or SIFT analysis (Table 3.2) (Choi, Chan, and Craig 2015), neither gene is commonly mutated in ovarian cancer nor is in the TCGA Cancer Gene Census (Forbes et al. 2015). Therefore, acquired mutations are not a likely cause for the increased aggressiveness of the ID8-IP line.

As the filtering strategy may overlook highly mutated proteins that are no longer expressed on the RNA level, I examined mRNA expression levels of tumor suppressors commonly mutated, downregulated, or deleted in ovarian cancer (*Brca1, Brca2, Cdkn2a, Nf1, Pten, and Rb1*). Interestingly, all were expressed except *Cdkn2a* (1 read in ID8 cells, 0 reads in ID8-IP cells), which encodes the $p16^{INK4a}$ and $p19^{Arf}$ (equivalent to human $p14^{ARF}$) proteins. As a positive control, *Cdkn2a* was highly expressed in an unrelated MEF (mouse embryonic fibroblast) cell line run concurrently (4902 reads). *Cdkn2a* is

downregulated in about 30% and deleted in about 2% of ovarian cancer cases (TCGA Research Network 2011). While WES detected a number of synonymous and non-synonymous variants in *Cdkn2a*, none were predicted to encode a truncated protein. However, the low number of reads by WES at this locus suggests a small focal deletion (average of 16 reads, as compared to an average of ~1000 reads in nearby genes). These results are supported by a recent study that identified *Cdkn2a* deletion in ID8 cells using a combination of WES, array comparative genomic hybridization, and targeted sequencing (Mosely et al. 2017). Therefore, *Cdkn2a* expression is lost in both ID8 and ID8-IP cells, a common occurrence in HGSOC.

Analysis of ID8-IP copy number alterations

Copy number alterations (CNAs) predominate HGSOC genetic alterations (Bowtell et al. 2015). We used CNVkit to assess putative copy number alterations in ID8-IP cells as compared to ID8 parental cells (Fig 3.2a). Several copy number gains and losses were identified in ID8-IP cells that corresponded to the top 20 most significantly altered regions in HGSOC (Table 3.3) (TCGA Research Network 2011). Both the human and the ID8-IP murine amplified regions contain genes such as *Kras, Recql4, Myc,* and *Ptk2* (*FAK*). In support of this finding, ID8-IP cells express higher levels of total and active FAK pY397 (Fig 3.2b). Additionally, four deleted regions overlap with the most common focal deletions in HGSOC, containing the genes *Gna11, Map2k2, Tjp3, Map3k1, Ccnb1, Pik3r1,*

and Foxd1 (Table 3.3). In summary, these results reveal that ID8-IP cells have acquired additional CNAs as compared to parental ID8 cells, several of which correspond to the most common HGSOC gains and losses.

Analysis of p53 mutations and protein levels

Tumor repressor p53 (murine *Trp53*) is mutated in most cases of ovarian cancer. In support of previous findings, WES or RNA-Seq did not reveal *Trp53* exonic mutations in ID8 cells (Walton et al. 2016). Furthermore, no *Trp53* mutations were identified in ID8-IP cells. However, protein levels of both p53 and the p53 transcriptional target p21 (also known as Cdkn1a/Cip1) were undetectable in ID8-IP cells even upon treatment with the DNA-damaging chemotherapeutic drug cisplatin (Fig 3.2c). This suggests that p53 stability is altered despite the lack of mutations.

In normal conditions, p53 is constitutively ubiquitinated, primarily by the E3 ubiquitin ligase Mdm2. Monoubiquitination of p53 prevents p53 association with DNA, and polyubiquitination marks the protein for proteasomal degradation (Brooks, Li, and Gu 2007). In response to various types of stress, proteins such as $p19^{Arf}$ (alternate reading frame of the *Cdkn2a* locus) bind to Mdm2, preventing Mdm2 association with and ubiquitination of p53. As previously mentioned, *Cdkn2a* is not expressed in ID8 or ID8-IP cells, which may account for the lack of detectable p53 protein. We are currently investigating whether ubiquitinated p53

is detectable on the protein level in ID8 and ID8-IP cells, and whether treatment with the Mdm2 inhibitor nutlin-3 will stabilize levels of p53 protein.

Functional characteristics of the ID8-IP model

In anchorage-independent conditions, ID8-IP cells formed significantly more colonies from single cells as compared to ID8 cells (Fig 3.3a). To explore molecular mechanisms responsible for the increased tumorigenicity of ID8-IP cells *in vivo*, I queried the ChEA (Chip Enrichment Analysis) database (Lachmann et al. 2010) with the 346 genes differentially upregulated in the ID8-IP cells as compared to the ID8. Amongst the transcription factors with significantly overrepresented targets in the ID8-IP upregulated gene set were Sox2, Nanog, and Oct4, transcriptional regulators of the stem-cell signature (Table 3.4, Fig 3.3b). Therefore, ID8-IP cells exhibit a more stem-like transcriptional profile as compared to the ID8 cells.

Increased aldehyde dehydrogenase activity is one marker of cancer stem cells (CSC) in several solid tumors, including ovarian cancer (Silva et al. 2011). As such, ALDEFLUOR activity assays were performed with ID8 and ID8-IP cells (Figure 3.3c). When grown in anchorage-independent conditions, ID8-IP cells exhibited an >8-fold increase in total ALDH activity as compared to ID8 cells (Figure 3.3d). Together, these results provide transcriptional and functional support for the hypothesis that ID8-IP cells possess enhanced CSC-like properties.

3.3 Discussion

In this study, we reveal that the aggressive ID8-IP subline has a low mutational burden, and encodes no candidate driver mutations. By analyzing copy number alterations, we demonstrate that ID8-IP cells exhibit the genomic instability that is characteristic of HGSOC, and identify amplifications and deletions that correspond to some of the most common CNAs in HGSOC (TCGA Research Network 2011). While no mutations were identified in*Trp53*, ID8-IP cells do not express detectable levels of p53 protein. This may be due to the lack of expression of the tumor suppressor *Cdkn2a*, which regulates Mdm2-p53 interactions. Finally, we show that ID8-IP cells exhibit enhanced CSC-like transcriptional and functional characteristics as compared to parental ID8 cells.

Patients with HGSOC often present at clinic after tumors have spread into the peritoneal cavity. Targeting growth of peritoneal cancer spheroids is a key part of preventing tumor recurrence, as spheroids may survive initial cytoreductive surgery. Additionally, spheroids with CSC-like characteristics such as increased ALDH activity have been shown to be more aggressive and chemoresistant (Silva et al. 2011; Raha et al. 2014). The adoption of three-dimensional (3D) *in vitro* spheroid models is needed to interrogate molecular mechanisms that promote spheroid survival and chemoresistance. As ID8-IP cells grow more readily in 3D than ID8 parental cells (Fig 3.3a, (Ward et al.

2013)), and exhibit increased ALDEFLUOR activity, these cells represent a valuable model for *in vitro* and *in vivo* 3D spheroid growth.

ID8 cells are the most commonly used spontaneously transformed mouse ovarian cancer cell line. However, a common criticism of the model is the lack of p53 mutation. Here, we show that ID8-IP cells do not have detectable levels of p53 protein, even after cisplatin treatment. Currently, we are testing p53 protein in ID8 cells, as p53 accumulation after cisplatin treatment has been demonstrated by another lab (Walton et al. 2016). While no mutations were found in *Trp53* by WES or RNA-Seq, *Cdkn2a* transcripts are not expressed in either ID8 or ID8-IP cells, which may negatively affect p53 stability. Ongoing and future studies will use Sanger sequencing and immunoblotting to evaluate Cdkn2a ($p16^{INK4a}$ and $p19^{Arf}$) in ID8 and ID8-IP cells. Furthermore, future studies will use the Mdm2 inhibitor nutlin-3 and the proteasomal inhibitor MG-132 to determine whether p53 stability can be rescued by disrupting MDM2-p53 interactions.

It has been difficult to generate models of HGSOC that are also transplantable in immunocompetent mice. ID8-IP cells display increased aggressiveness and tumorsphere-generating capacity as compared to parental ID8 cells, and through passage in syngeneic C57Bl/6J mice ID8-IP cells have gained CNAs that reflect common deletions and amplifications seen in human HGSOC. Therefore, ID8-IP cells are a suitable model for *in vitro* and *in vivo* experiments to recapitulate human disease in immunocompetent mice. Use of ID8-IP cells may further our understanding of CSC-maintenance mechanisms,

chemoresistance, anchorage-independent growth, and the role of the immune TME in ovarian cancer progression.

3.4 Materials and Methods

Antibodies and reagents

Total FAK (EMD Millipore, clone 4.47), pY397 FAK (ThermoFisher, clone 141-9), p53 (Abcam, ab26), p21 (Santa Cruz sc-6246), and B-actin (Sigma, clone AC-74) antibodies were used for immunoblotting. Cisplatin (CP, 1 mg/ml, APP Pharmaceuticals) was from the UCSD Moores Cancer Center Pharmacy.

Cells

Murine ovarian ID8 cells were from Katherine Roby (University of Kansas Medical Center), and ID8-IP cells were isolated from ID8 peritoneal ascites as described (Ward et al. 2013). Lewis lung carcinoma cells were from ATCC (CRL-1642) and FAK-/-p21-/- mouse embryo fibroblasts were used as previously described (Lim et al. 2008). For adherent growth, cells were maintained in DMEM (Corning) supplemented with 10% FBS, 100 μM non-essential amino acids, 100 U/ml penicillin, and 100 μg/ml streptomycin on tissue culture-treated plastic plates (Corning). For tumorsphere colony assays, 1.0 $x10^4$ cells per well were suspended in 1% methylcellulose diluted in growth media and plated into 6-well ultra-low-attachment plates (Corning).

Exome sequencing and CNV calling:

Exome sequencing was performed by Novogene (Beijing, China), using genomic DNA isolated from ID8 or ID8-IP cells (n=1). Briefly, genomic DNA was sheared into 180-280 bp fragments using a Covaris sonicator. Exome enrichment and sequencing libraries were generated using Agilent SureSelect Mouse All Exon kit following manufacturer's recommendations. Each exome was sequenced using a 150 bp paired-end protocol on the Illumina HiSeq platform, generating 47M reads for the ID8 sample and 61M reads for the ID8-IP sample. Reads were aligned with BWA MEM 0.7.12 (Li and Durbin 2009) to mouse genome GRCm38_68. Variants were called with GATK 3.4 according to the Broad Institute's best practices (https://software.broadinstitute.org/gatk/best-practices) (McKenna et al. 2010). Subsequent processing after alignment was carried out with SAMtools v.1.1 (Li et al. 2009). Variants were annotated with ANNOVAR (Wang, Li, and Hakonarson 2010). CNVs were called from the same alignments with CNVkit (Talevich et al. 2016; Olshen et al. 2011) with standard parameters using the ID8 sample as the normal, and ID8-IP as the tumor sample. CNVs were visualized in the Integrative Genomics Viewer (Robinson et al. 2011; Thorvaldsdóttir, Robinson, and Mesirov 2013).

RNA-Seq and downstream analyses:

Total RNA was isolated from ID8 and ID8-IP cells growing on a 2D monolayer coated with 0.2% Matrigel (n=1) using PureLink RNA Mini Kit (ThermoFisher). RNA sequencing was performed by Novogene (Beijing, China).

RNA sample preparation was performed using NEB Next Ultra RNA Library Prep Kit (New England Biolabs) as per manufacturer recommendations. Each transcriptome was sequenced using a 150 bp paired-end protocol on the Illumina HiSeq platform, generating 54M and 57M clean reads for the ID8 and ID8-IP samples, respectively. Reads were mapped to the reference genome (reads for ID8 or ID8-IP were 89.4% and 89.2% mapped, respectively) using TopHat2 (Kim et al. 2013). Differentially expressed genes were classified as genes that had a > two-fold difference between samples and had a q-value < 0.005. ChEA (Lachmann et al. 2010) analysis was performed using Enrichr (Chen et al. 2013; Kuleshov et al. 2016). PROVEAN and SIFT analysis were analyzed using the online PROVEAN software (Choi, Chan, and Craig 2015).

ALDH activity

The ALDEFLUOR fluorescent reagent system (Stemcell Technologies) was used to measure cell-associated ALDH activity. Briefly, cells were cultured as spheroids, collected by centrifugation, dissociated by trypsinization, resuspended in ALDEFLUOR assay buffer containing ALDH substrate (BODIPY-aminoacetaldehyde), and incubated for 45 minutes at 37°C with or without the ALDH inhibitor diethylamino-benzaldehyde (DEAB). Individual gates were used to determine the percentage of ALDEFLUOR-positive cells per experimental point relative to DEAB-inhibitor treated controls.

Statistics

Statistical differences between pairs of data were determined using an unpaired two-tailed Student's t test using Prism (GraphPad Software, v7). *p*-values of <0.05 were considered significant.

3.5 References

Bowtell, D. D., S. Böhm, A. A. Ahmed, P.-J. Aspuria, R. C. Bast, V. Beral, J. S. Berek, et al. 2015. "Rethinking Ovarian Cancer II: Reducing Mortality from High-Grade Serous Ovarian Cancer." *Nat Rev Cancer* 15 (11): 668–79. doi.org/10.1038/nrc4019.

Brooks, C. L., M. Li, and W. Gu. 2007. "Mechanistic Studies of MDM2-Mediated Ubiquitination in p53 Regulation." *J Biol Chem* 282 (31): 22804–15. doi.org/10.1074/jbc.M700961200.

Chen, E. Y., C. M. Tan, Y. Kou, Q. Duan, Z. Wang, G. V. Meirelles, N. R. Clark, and A. Ma'ayan. 2013. "Enrichr: Interactive and Collaborative HTML5 Gene List Enrichment Analysis Tool." *BMC Bioinformatics* 14. doi.org/10.1186/1471-2105-14-128.

Choi, Y., A. P. Chan, and T. J. Craig. 2015. "Sequence Analysis PROVEAN Web Server : A Tool to Predict the Functional Effect of Amino Acid Substitutions and Indels" 31 (April): 2745–47. doi.org/10.1093/bioinformatics/btv195.

Cole, A. J., T. Dwight, A. J. Gill, K.-A. Dickson, Y. Zhu, A. Clarkson, G. B. Gard, et al. 2016. "Assessing Mutant p53 in Primary High-Grade Serous Ovarian Cancer Using Immunohistochemistry and Massively Parallel Sequencing." *Sci Rep* 6 (1): 26191. doi.org/10.1038/srep26191.

Domcke, S., R. Sinha, D. a Levine, C. Sander, and N. Schultz. 2013. "Evaluating Cell Lines as Tumour Models by Comparison of Genomic Profiles." *Nat Commun* 4 (January): 2126. doi.org/10.1038/ncomms3126.

Forbes, S. A., D. Beare, P. Gunasekaran, K. Leung, N. Bindal, H. Boutselakis, M. Ding, et al. 2015. "COSMIC : Exploring the World ' S Knowledge of Somatic Mutations in Human Cancer" 43 (October 2014): 805–11. doi.org/10.1093/nar/gku1075.

Horbach, S. P. J. M., and W. Halffman. 2017. “The Ghosts of HeLa: How Cell Line Misidentification Contaminates the Scientific Literature.” *PLoS One* 12 (10): 1–16. doi.org/10.1371/journal.pone.0186281.

Kim, D., G. Pertea, C. Trapnell, H. Pimentel, R. Kelley, and S. L. Salzberg. 2013. “TopHat2 : Accurate Alignment of Transcriptomes in the Presence of Insertions, Deletions and Gene Fusions.” *Genome Biol* 14. doi.org/10.1101/000851.

Kuleshov, M. V., M. R. Jones, A. D. Rouillard, N. F. Fernandez, Q. Duan, Z. Wang, S. Koplev, et al. 2016. “Enrichr: A Comprehensive Gene Set Enrichment Analysis Web Server 2016 Update.” *Nucleic Acids Res* 44 (W1): W90–97. doi.org/10.1093/nar/gkw377.

Lachmann, A., H. Xu, J. Krishnan, S. I. Berger, A. R. Mazloom, and A. Ma’ayan. 2010. “ChEA: Transcription Factor Regulation Inferred from Integrating Genome-Wide ChIP-X Experiments.” *Bioinformatics* 26 (19): 2438–44. doi.org/10.1093/bioinformatics/btq466.

Li, H., and R. Durbin. 2009. “Fast and Accurate Short Read Alignment with Burrows-Wheeler Transform.” *Bioinformatics* 25 (14): 1754–60. doi.org/10.1093/bioinformatics/btp324.

Li, H., B. Handsaker, A. Wysoker, T. Fennell, J. Ruan, N. Homer, G. Marth, G. Abecasis, and R. Durbin. 2009. “The Sequence Alignment/Map Format and SAMtools.” *Bioinformatics* 25 (16): 2078–79. doi.org/10.1093/bioinformatics/btp352.

Lim, S.-T., X. L. Chen, Y. Lim, D. A. Hanson, T.-T. Vo, K. Howerton, N. Larocque, S. J. Fisher, D. D. Schlaepfer, and D. Ilic. 2008. “Nuclear FAK Promotes Cell Proliferation and Survival through FERM-Enhanced p53 Degradation.” *Mol Cell* 29 (1): 9–22. doi.org/10.1016/j.molcel.2007.11.031.

McCloskey, C. W., R. L. Goldberg, L. E. Carter, L. F. Gamwell, E. M. Al-Hujaily, O. Collins, E. A. Macdonald, et al. 2014. “A New Spontaneously Transformed Syngeneic Model of High-Grade Serous Ovarian Cancer with a Tumor-Initiating Cell Population.” *Front Oncol* 4 (March): 53. doi.org/10.3389/fonc.2014.00053.

McCloskey, C. W., G. M. Rodriguez, K. J. C. Galpin, and B. C. Vanderhyden. 2018. “Ovarian Cancer Immunotherapy: Preclinical Models and Emerging Therapeutics.” *Cancers (Basel)* 10 (8): 1–30. doi.org/10.3390/cancers10080244.

McKenna, A., M. Hanna, E. Banks, A. Sivachenko, K. Cibulskis, A. Kernytsky, K. Garimella, et al. 2010. “The Genome Analysis Toolkit: A MapReduce Framework for Analyzing next-Generation DNA Sequencing Data.” *Genome Res* 20: 1297–1303. doi.org/10.1101/gr.107524.110.20.

Mosely, S. I. S., J. E. Prime, R. C. A. Sainson, J.-O. Koopmann, D. Y. Q. Wang, D. M. Greenawalt, M. J. Ahdesmaki, et al. 2017. “Rational Selection of Syngeneic Preclinical Tumor Models for Immunotherapeutic Drug Discovery.” *Cancer Immunol Res* 5 (1): 29–41. doi.org/10.1158/2326-6066.CIR-16-0114.

Olshen, A. B., H. Bengtsson, P. Neuvial, P. T. Spellman, R. A. Olshen, and V. E. Seshan. 2011. “Parent-Specific Copy Number in Paired Tumor-Normal Studies Using Circular Binary Segmentation.” *Bioinformatics* 27 (15): 2038–46. doi.org/10.1093/bioinformatics/btr329.

Raha, D., T. R. Wilson, J. Peng, D. Peterson, P. Yue, M. Evangelista, C. Wilson, M. Merchant, and J. Settleman. 2014. “The Cancer Stem Cell Marker Aldehyde Dehydrogenase Is Required to Maintain a Drug-Tolerant Tumor Cell Subpopulation.” *Cancer Res* 74 (13): 3579–90. doi.org/10.1158/0008-5472.CAN-13-3456.

Robinson, J. T., H. Thorvaldsdóttir, W. Winckler, M. Guttman, E. S. Lander, G. Getz, and J. P. Mesirov. 2011. “Integrative Genome Viewer.” *Nat Biotechnol* 29 (1): 24–26. doi.org/10.1038/nbt.1754.Integrative.

Roby, K. F., C. C. Taylor, J. P. Sweetwood, Y. Cheng, J. L. Pace, O. Tawfik, D. L. Persons, P. G. Smith, and P. F. Terranova. 2000. “Development of a Syngeneic Mouse Model for Events Related to Ovarian Cancer Athymic and Syngeneic Mice Resulted in Growth of Tumor” 21 (4): 585–91.

Silva, I. A., S. Bai, K. McLean, K. Yang, K. Griffith, D. Thomas, C. Ginestier, et al. 2011. “Aldehyde Dehydrogenase in Combination with CD133 Defines Angiogenic Ovarian Cancer Stem Cells That Portend Poor Patient Survival.” *Cancer Res* 71 (11): 3991–4001. doi.org/10.1158/0008-5472.CAN-10-3175.

Talevich, E., A. H. Shain, T. Botton, and B. C. Bastian. 2016. “CNVkit: Genome-Wide Copy Number Detection and Visualization from Targeted DNA Sequencing.” *PLoS Comput Biol* 12 (4): 1–18. doi.org/10.1371/journal.pcbi.1004873.

TCGA Research Network. 2011. “Integrated Genomic Analyses of Ovarian Carcinoma.” *Nature* 474 (7353): 609–15. doi.org/10.1038/nature10166.

Thorvaldsdóttir, H., J. T. Robinson, and J. P. Mesirov. 2013. “Integrative Genomics Viewer (IGV): High-Performance Genomics Data Visualization

and Exploration." *Brief Bioinform* 14 (2): 178–92. doi.org/10.1093/bib/bbs017.

Walton, J., J. Blagih, D. Ennis, E. Leung, S. Dowson, M. Farquharson, L. A. Tookman, et al. 2016. "CRISPR/Cas9-Mediated Trp53 and Brca2 Knockout to Generate Improved Murine Models of Ovarian High-Grade Serous Carcinoma." *Cancer Res* 76 (20): 6118–29. doi.org/10.1158/0008-5472.CAN-16-1272.

Wang, K., M. Li, and H. Hakonarson. 2010. "ANNOVAR: Functional Annotation of Genetic Variants from High-Throughput Sequencing Data." *Nucleic Acids Res* 38 (16): 1–7. doi.org/10.1093/nar/gkq603.

Ward, K. K., I. Tancioni, C. Lawson, N. L. G. Miller, C. Jean, X. L. Chen, S. Uryu, et al. 2013. "Inhibition of Focal Adhesion Kinase (FAK) Activity Prevents Anchorage-Independent Ovarian Carcinoma Cell Growth and Tumor Progression." *Clin Exp Metastasis* 30 (5): 579–94. doi.org/10.1007/s10585-012-9562-5.

3.6 Figures

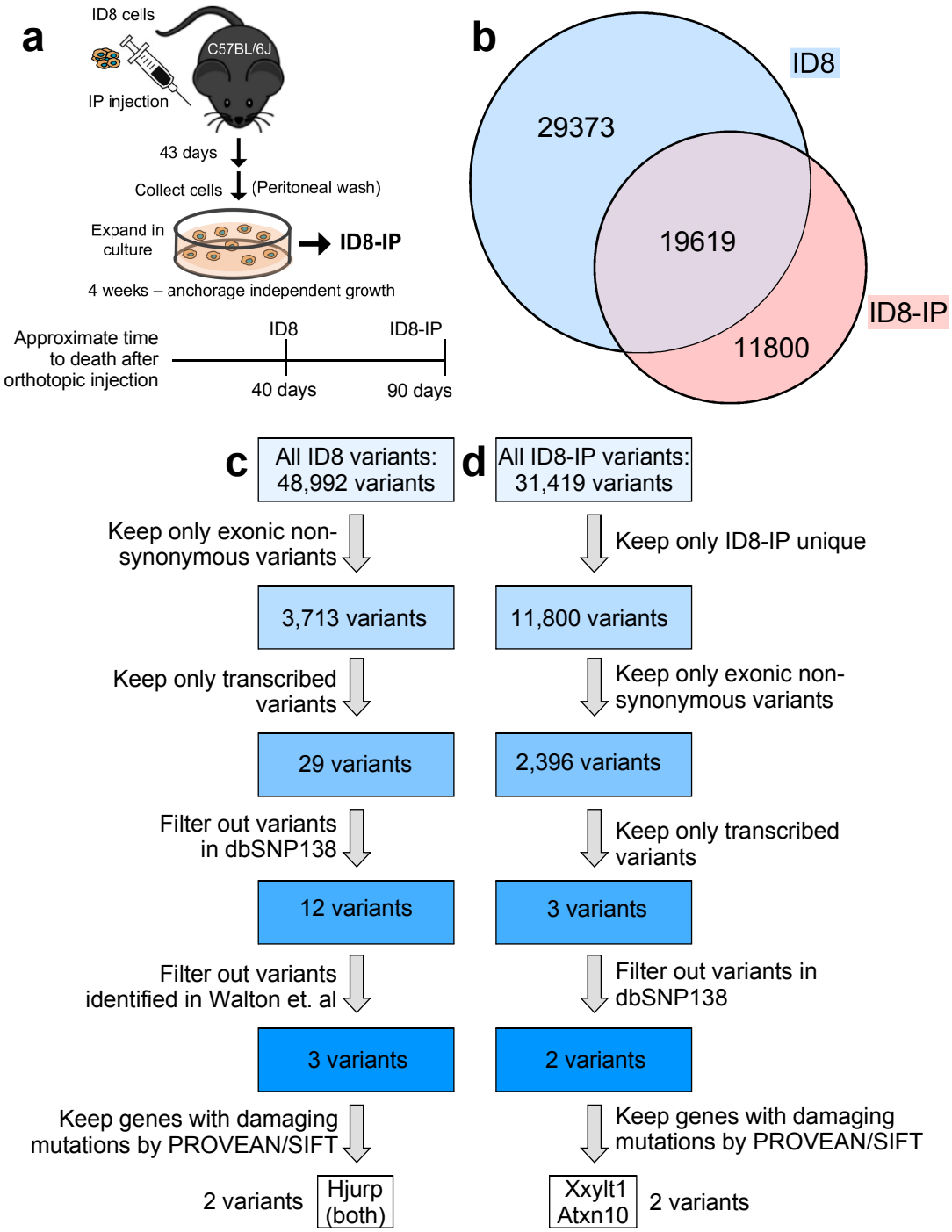

Figure 3.1: Exome sequencing of ID8 and ID8-IP cells. **(a)** Schematic of ID8-IP generation. ID8 cells were injected into the intraperitoneal (IP) cavity of syngeneic C57Bl6/J mice. **(b)** Variants identified by whole exome sequencing in either ID8 cells (blue), ID8-IP cells (pink), or shared between ID8 and ID8-IP cells (purple). **(c)** Filtering strategy to identify variants in ID8 parental cells that are not found in published ID8 sequencing results. **(d)** Filtering strategy to identify variants in ID8-IP cells that may cause an altered phenotype from parental ID8 cells.

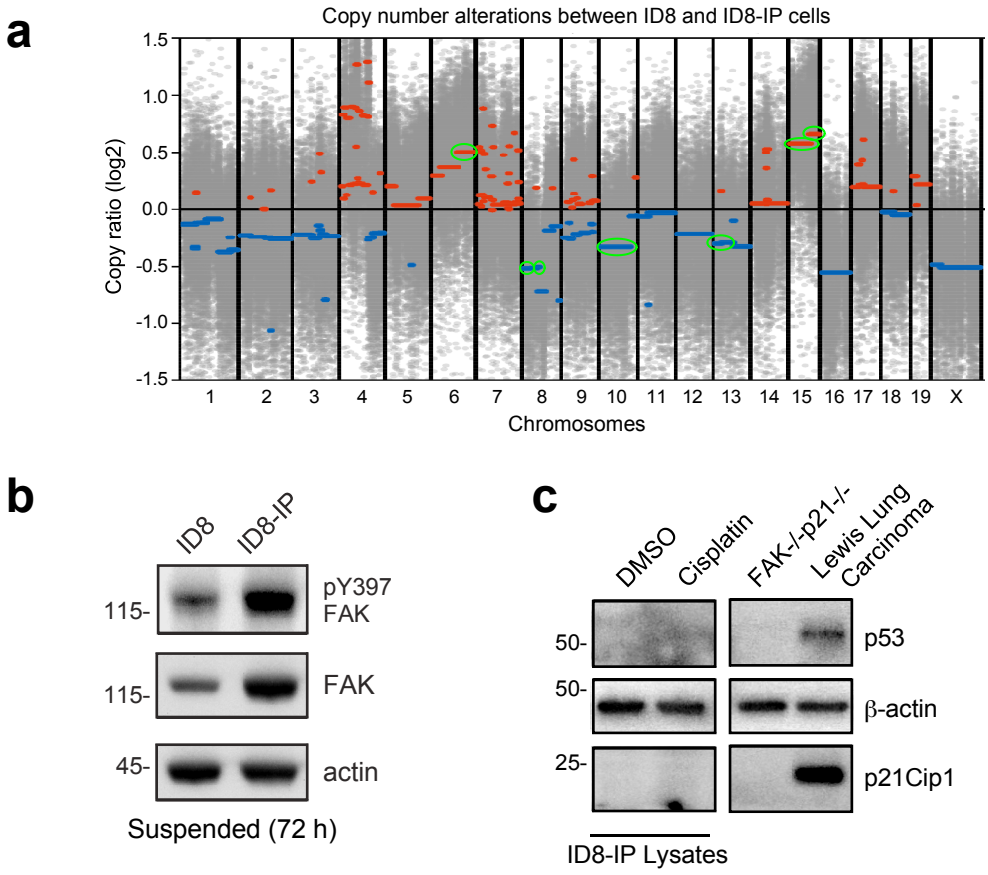

Figure 3.2: Characterization of ID8-IP copy number alterations and p53 status. **(a)** ID8-IP copy number ratio was determined from ID8 and ID8 IP exome sequencing using CNVkit software. Gains (red) and losses (blue) as compared to parental ID8 cells are denoted across chromosomes. Circled regions (green) correspond to shared genomic alterations between ID8-IP and human high-grade serous ovarian cancer (see Table 3.3). **(b)** ID8 and ID8-IP were grown in suspension and protein lysates analyzed for pY397 FAK, total FAK, and actin by immunoblotting. **(c)** ID8-IP cells were treated with DMSO or 10 uM cisplatin for 2 hours. ID8-IP lysates were analyzed alongside lysates from p21-deficient MEFs and positive-control Lewis lung carcinoma cells. Image is from one blot with same exposure.

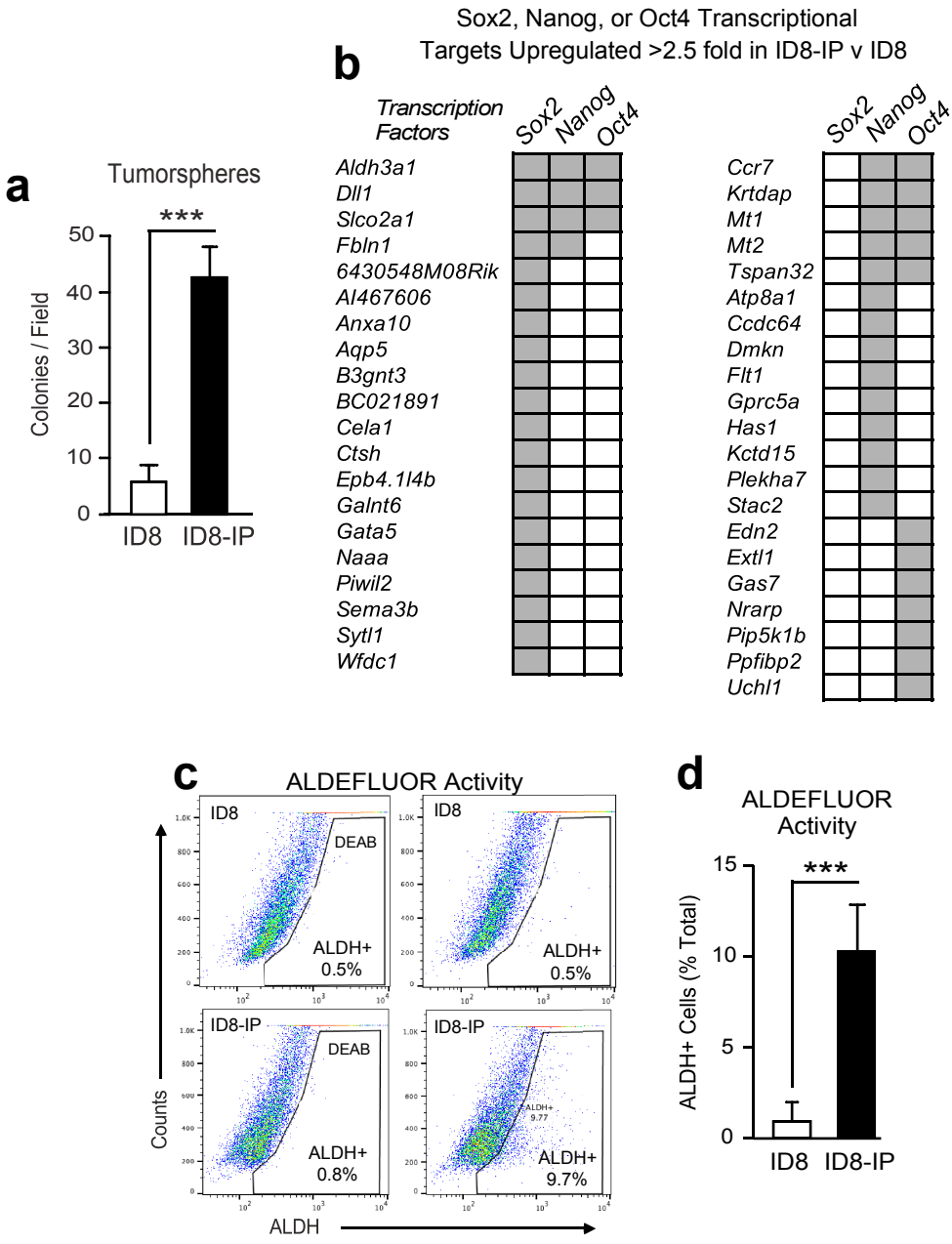

Figure 3.3: ID8-IP cells have more cancer stem cell-like characteristics. **(a)** Equal numbers of ID8 or ID8-IP cells were analyzed for tumorsphere formation in methylcellulose (18 days). Values are means (n=9) from 3 independent experiments (± SEM, *** $p \leq 0.001$). **(b)** The ChEA database was used to identify the most overrepresented transcription factor gene sets in the 346 genes differentially upregulated in the ID8-IP cells as compared the the ID8 parental cells. Common Sox2, Nanog, or Oct4 transcriptional mRNA targets up-regulated >2.5 fold in ID8-IP compared to ID8 cells are shown. **(c)** Representative flow cytometry profiles of ID8 and ID8-IP cells with or without N,N-diethylaminobenzaldehyde (DEAB) and analyzed by ALDEFLUOR assay to identify ALDH-bright (ALDH+) cells when grown as tumorspheres. (**d**) Percentage of ALDH+ ID8 or ID8-IP cells determined by ALDEFLUOR flow cytometry when grown as tumorspheres. Values (n=3) are means (± SD, *** P <0.001).

3.7: Tables

Table 3.1: Variants in ID8 or ID8-IP cells.

Chr	Start	End	Ref	Alt	Gene	AAChange	ID8 RNA	ID8-IP RNA	Shared ID8/ID8-IP DNA	Type	Walton et. al. 2016
1	88266524	88266524	-	T	Hjurp	Hjurp:NM_172505:exon5:c.432dupA:p.L145fs	x	x	x	INDEL	
1	88275050	88275050	A	T	Hjurp	Hjurp:NM_172505:exon3:c.T211A:p.Y71N	x	x	x	SNP	
1	149872754	149872754	C	T	Pla2g4a	Pla2g4a:NM_001305632:exon8:c.G678A:p.M226I	x		x	SNP	x
1	171271803	171271803	G	C	B4galt3	B4galt3:NM_020579:exon3:c.G61C:p.A21P	x	x	x	SNP	x
4	117912101	117912101	C	A	Ipo13	Ipo13:NM_146152:exon2:c.G493T:p.A165S	x	x	x	SNP	x
5	107903816	107903816	G	T	Rpl5	Rpl5:NM_016980:exon5:c.G475T:p.V159F	x	x	x	SNP	x
6	72556234	72556234	C	A	Capg	Capg:NM_001042534:exon5:c.C501A:p.F167L	x	x	x	SNP	x
8	48235956	48235956	G	C	Tenm3	Tenm3:NM_001145937:exon25:c.C6547G:p.R2183G	x	x	x	SNP	x
10	67225684	67225684	A	T	Jmjd1c	Jmjd1c:NM_001242396:exon9:c.A3272T:p.N1091I	x	x	x	SNP	x
10	80804018	80804018	C	T	Sf3a2	Sf3a2:NM_013651:exon9:c.C662T:p.P221L	x	x	x	SNP	x
14	47395949	47395949	C	T	Dlgap5	Dlgap5:NM_144553:exon14:c.G1619A:p.S540N	x	x	x	SNP	x
16	44217997	44217997	C	T	Usf3;Gm608	Usf3:NM_001029889:exon8:c.C2839T:p.P947S	x	x	x	SNP	
19	17125354	17125354	G	T	Prune2	Prune2:NM_181348:exon9:c.G7876T:p.D2626Y		x	x	SNP	x
3	151835507	151835507	G	C	Ptgfr	Ptgfr:NM_008966:exon2:c.C363G:p.C121W		x	x	SNP	x
15	85387021	85387021	G	T	Atxn10	Atxn10:NM_016843:exon7:c.G759T:p.K253N		x		SNP	
16	30957523	30957523	A	C	Xxylt1	Xxylt1:NM_198626:exon4:c.T994G:p.F332V		x		SNP	

Table 3.2: PROVEAN and SIFT analysis.

Cell line	Protein ID	Input	Gene	Pos	Ref	Alt	Type	PROVEAN prediction	SIFT prediction
ID8, ID8-IP	ENSMUSP00000112620	16,44217997,c,t	Usf3	947	P	S	Single AA	Neutral	Tolerated
ID8, ID8-IP	ENSMUSP00000128627	16,44217997,c,t	Usf3	947	P	S	Single AA	Neutral	Tolerated
ID8, ID8-IP	ENSMUSP00000054263	1,88275050,a,t	Hjurp	71	Y	N	Single AA	Neutral	Tolerated
ID8, ID8-IP	ENSMUSP00000070419	1,88275050,a,t	Hjurp	71	Y	N	Single AA	Neutral	Damaging
ID8, ID8-IP	ENSMUSP00000120753	1,88275050,a,t	Hjurp	71	Y	N	Single AA	Neutral	Tolerated
ID8, ID8-IP	ENSMUSP00000054263	1,88266524,g,gt	Hjurp				Frameshift	NA	NA
ID8, ID8-IP	ENSMUSP00000070419	1,88266524,g,gt	Hjurp				Frameshift	NA	NA
ID8, ID8-IP	ENSMUSP00000118659	1,88266524,g,gt	Hjurp				Frameshift	NA	NA
ID8-IP	ENSMUSP00000132450	15,85387021,g,t	Atxn10	253	K	N	Single AA	Neutral	Damaging
ID8-IP	ENSMUSP00000050246	16,30957523,a,c	Xxylt1	332	F	V	Single AA	Deleterious	Damaging

Table 3.3: Shared genetic alterations between murine ID8-IP cells and human HGSOC.

Mouse cytobands	Human cytobands[a]	Amp/ Del	Genes in common	Pathway
6qD1-G3	12p12.1	Amp	*Kras*	RAS/MAPK
15qD3-F3	8q24.3	Amp	*Recql4*	Cell cycle
15qA1-D3	8q24.21, 8q24.3	Amp	*Myc, Ptk2*	MYC, adhesion
8qA1.1-1.3	8p23.3	Del		
8qB1.1-1.2	4q34.3	Del		
10qA1-D1	19p13.3	Del	*Gna11, Map2k2, Tjp3*	GPCRs, MAPK
13qB3-D2.3	5q11.2, 5q13.1	Del	*Map3k1, Ccnb1, Pik3r1, Foxd1*	MAPK, Cell cycle, PI3K/AKT

[a]Shared copy number alterations with top 20 most significant amplified and deletions in HGSOC (see reference 26).

Table 3.4: ChEA analysis of ID8-IP mRNA transcripts.

Term	Overlap	Adjusted P-value	Combined Score
SUZ12	136/4356	2.54337E-11	27.89927623
SOX2	77/2000	2.33661E-09	37.60163692
MTF2	98/2981	9.88608E-09	29.5941184
GATA1	68/1834	1.24552E-07	34.49691383
PRDM14	63/1944	6.68816E-05	21.95542951
NANOG	63/1989	0.00012708	22.09577731
WT1	54/1663	0.000242235	23.34849885
LMO2	61/2000	0.000340508	17.2918645
SOX9	46/1384	0.000604792	17.21930015
STAT3	55/1788	0.000674034	15.78097869
PPARG	55/1807	0.000858028	15.63751369
NRF2	43/1331	0.001255081	16.54518721
RNF2	42/1302	0.001490571	18.0646686
EZH2	42/1302	0.001490571	18.00219816
SMARCA4	68/2522	0.002273759	11.07504443
TEAD4	63/2293	0.002444755	12.17267638
RCOR3	74/2851	0.003160964	8.754024778
EP300	57/2093	0.005051091	18.7116368
MYB	31/923	0.005051091	14.39424585
TBX20	55/2000	0.005051091	9.920330374
SMAD3	33/1020	0.005616111	13.77567981
YAP1	61/2329	0.007520797	8.19846534
ZFP281	54/2004	0.008085357	13.77968507
TAL1	51/1875	0.00911886	9.412960112
CEBPD	48/1735	0.00911886	8.974846104
STAT5	36/1197	0.009908752	11.46676647
JARID2	34/1117	0.01092095	11.68338314
OCT4	53/1992	0.01092095	8.143481987
TET1	53/1994	0.010925953	6.901438162
PPARA	53/2000	0.011014886	7.582040819

3.8 Acknowledgements

Chapter 3 is an adaptation of material in preparation for submission in collaboration with Carlos Díaz-Osterman, Allison Barrie, Adam Mark, and Kathleen Fisch. The dissertation author was a co-primary investigator and author of this material.

The dissertation author designed, performed, and analyzed all experiments included in this chapter except those listed below. Carlos Díaz-Osterman performed the tumorsphere growth assay, immunoblotting for FAK levels, and ALDEFLUOR assay. Allison Barrie performed immunoblotting for p53/p21. Katie Fisch and Adam Mark performed calling of exome variants and generated the CNA plot.

Chapter 4

Conclusions and Future Directions

4.1 Summary of the thesis

In Chapter 3, I characterized the ID8-IP murine model of ovarian cancer. These cells were generated by passage of ID8 parental cells in C57Bl/6J mice, followed by recovery of ascites-associated cells and expansion in anchorage-independent conditions (Ward et al. 2013). Selective pressure generated from peritoneal and anchorage-independent growth resulted in an aggressive ID8-IP subline, which exhibits increased metastatic growth as compared to the ID8 parental line. I sought to characterize the suitability of these cells as an HGSOC model, and to identify genomic alterations that may account for the ID8-IP phenotype. Using whole exome sequencing and whole transcriptome sequencing, I demonstrated that these cells exhibit many of the hallmarks of HGSOC: low mutational burden, no predicted tumor-driver mutations, and a similar copy number alteration profile.

ID8-IP cells also exhibit some characteristics of cancer stem cells. This includes the upregulation of Sox2-, Oct4-, and Nanog-regulated transcripts, increased growth as tumorspheres, and increased ALDEFLUOR activity as compared to parental ID8 cells. Cells with cancer stem cell (CSC)-like properties are more chemoresistant, and elimination of the ovarian CSC population may provide therapeutic benefit (Roy and Dahl 2018). ID8-IP cells represent a promising model of ovarian cancer stem cells. Future studies will focus on targeting genes amplified in ID8-IP cells, such as *MYC* and *FAK*, to determine whether these genes contribute to the more aggressive and CSC-like phenotype.

Intriguingly, preliminary analysis suggests that ID8-IP cells express low levels of p53 even after genotoxic stress is induced. Loss of expression at the *Cdkn2a* locus may partially account for this result. An alternate reading frame at this locus produces the protein $p19^{Arf}$ (equivalent to human $p14^{ARF}$), which inhibits the E3 ubiquitin ligase Mdm2 under conditions of cell stress, leading to p53 stabilization (Harris and Levine 2005). Thus, transcriptional loss of *Cdkn2a* may lead to elevated Mdm2-promoted p53 degradation under all conditions. Future studies will explore whether there are p53 expression differences between ID8 and ID8-IP cells. If p53 protein levels increase upon treatment with MG-132 proteasomal inhibitor, nutlin-3 Mdm2 inhibitor, or transient expression of $p19^{Arf}$, this would support the hypothesis that loss of *Cdkn2a* in ID8 and/or ID8-IP cells promotes constitutive p53 ubiquitination and degradation.

In Chapter 2, I explored a novel role for Rgnef in ovarian cancer progression. I observe that Rgnef is overexpressed in late-stage serous ovarian cancer, and high Rgnef expression corresponds to poor prognosis in late-stage patients. Using a genetically engineered mouse model and ID8-IP cells, I establish that Rgnef expression promotes primary tumor growth and metastasis *in vivo*, and promotes anchorage-independent spheroid growth *in vitro*.

RNA-Seq reveals that Rgnef-expressing cells express higher levels of endogenous antioxidant gene expression than Rgnef-KO cells, and correspondingly Rgnef-KO cells have higher levels of total cellular ROS in suspension. Both ROS levels and cellular growth defects in Rgnef-KO cells were rescued with administration of the antioxidant Trolox. A topic for future study will

be whether high ROS levels promote cell senescence, or whether high ROS triggers apoptosis in ovarian cancer cells. Additionally, it would be beneficial to evaluate whether administration of Trolox in mice rescues Rgnef-KO ovarian tumor growth.

I also demonstrated that transient overexpression of Rgnef induces IL-6 transcriptional activation in an NF-kB-dependent manner. Many genes in the antioxidant gene signature are under the control of NF-kB. Pretreatment with NF-kB inhibitors in adherent conditions prevented growth when cells were transferred to anchorage-independent conditions. This suggests that NF-kB activation downstream of Rgnef promotes an antioxidant gene signature, and that Rgnef-expressing cells have an increased capacity to mitigate increased ROS upon loss of cell adhesion. Future studies will focus on the molecular pathways that connect Rgnef to NF-kB.

4.2 Ongoing studies

As a guanine nucleotide exchange factor (GEF), Rgnef activates Rho GTPases (Miller et al. 2012). In a GEF-independent manner, Rgnef binds to FAK, promoting FAK activation and recruitment to nascent adhesions (Miller et al. 2013). However, it remains unclear how Rho GTPase activation and FAK contribute to the tumorigenic phenotypes outlined in Chapter 2. Overexpression of a dominant negative C-terminal Rgnef mutant prevents the endogenous Rgnef-FAK interaction and impairs colon carcinoma primary tumor growth and

invasiveness (Yu et al. 2011). Therefore, I hypothesized that the FAK-Rgnef interaction is also important for promoting a metastatic phenotype in ovarian carcinoma cells.

Rgnef requires FAK binding for tumorigenic growth and contractility in extracellular matrix

In Chapter 2, I demonstrated that CRISPR/Cas9-mediated Rgnef knockout in ID8-IP cells impairs colony formation from single cells embedded in Matrigel. To elucidate the role of the Rgnef-FAK interaction in colony formation, I transduced ID8-IP Rgnef-KO cells with either GFP-Rgnef-WT or a Rgnef mutant with a deletion in the FAK-binding domain (amino acids 1292-1301) (Fig. 4.1a-b). The GFP-Rgnef-Δ1292 mutant retains its canonical guanine nucleotide exchange (GEF) activity, but is unable to bind FAK (Miller et al. 2013). Stable expression of GFP-Rgnef-WT significantly enhanced colony formation as compared to Rgnef-KO or GFP-Rgnef-Δ1292 re-expressing cells (Fig 4.1c). Furthermore, in a focus formation assay performed on Matrigel-coated wells, ID8-IP cells expressing GFP-Rgnef-WT formed significantly more multilayered foci than cells with Rgnef knockout or re-expressing Rgnef-Δ1292. These results suggest that the Rgnef-FAK interaction is necessary for growth as 3D colonies or as multilayered foci, and that Rgnef GEF activity alone is not sufficient to promote this phenotype.

Both Rgnef and FAK play a role in regulating cell contractility (Yu et al. 2011; Gebbink et al. 1997; Mitra, Hanson, and Schlaepfer 2005). To define the

contribution of Rgnef-FAK connection to three-dimensional contractility, ID8-IP cells were seeded in a collagen I gel, which was allowed to contract freely after polymerization. Collagen gels embedded with ID8-IP GFP-Rgnef-WT cells contracted significantly more after 4 days than gels seeded with ID8-IP Rgnef-KO cells or cells re-expressing the GFP-Rgnef-Δ1292 mutant (Fig 4.1e). This suggests that the Rgnef-FAK connection is also required for contractility in 3D, ECM-attached conditions.

The Rgnef-FAK interaction is dispensable in ECM-independent conditions

In Chapter 2, I demonstrated that Rgnef knockout impairs suspended cell growth in ID8-IP cells. Since re-expression of the GFP-Rgnef-Δ1292 mutant did not rescue three-dimensional colony growth in Matrigel (Fig 4.1c), I hypothesized that the Rgnef-FAK connection was also necessary for efficient growth in suspension. Surprisingly, re-expression of GFP-Rgnef-Δ1292 in ID8-IP Rgnef-KO cells rescued anchorage-independent growth in suspension (Fig 4.1f). This suggests that while cells grown in ECM-attached conditions require Rgnef-FAK binding, this interaction is dispensable for three-dimensional growth without ECM attachment.

4.3 Summary

Interestingly, while both colony formation in Matrigel and collagen contractility require Rgnef-FAK binding (Fig 4.1c-d), ongoing studies suggest that the FAK-Rgnef interaction is not necessary for growth in ECM-detached suspended conditions (Fig 4.1f). One possible explanation for this divergence may be that Rgnef requires localization to the plasma membrane downstream of integrin engagement in order to bind FAK.

I propose a model (Fig 4.2) in which Rgnef plays dual roles in ovarian cancer tumorigenesis. In matrix-attached conditions (Fig 4.2a) integrin stimulation promotes Rgnef membrane localization, followed by FAK recruitment. This Rgnef-FAK interaction can promote contractility and growth as three-dimensional colonies. While NF-kB is activated downstream of Rgnef in both adherent and suspended conditions (Fig 4.2b), this pathway is not required for growth in adherent conditions when ROS levels are low. However, upon detachment from extracellular matrix, Rgnef-expressing cells have an increased capacity to buffer increased ROS and protect cells from oxidative stress. These dual roles of Rgnef ultimately promote ovarian tumor progression.

4.4 Materials and Methods

Cells, plasmids, and chemicals.

Murine ID8-IP cells were isolated from ascites-associated cells as described (Ward et al. 2013). For adherent growth, cells were maintained in DMEM (Corning) supplemented with 10% FBS, 100 μM non-essential amino acids, 100 U/ml penicillin, and 100 μg/ml streptomycin on tissue culture-treated plastic plates (Corning). For anchorage-independent growth, cells were seeded at 50k/well in ultra-low attachment plates (Corning) in serum-free Tumorsphere Medium XF (PromoCell). pCDH-CMV-MCS1-GFP-Rgnef and pCDH-CMV-MCS1-GFP-Rgnef- Δ1292 were used to produce lentivirus as described (Lim et al. 2008) and cells were transduced according to standard methods (System Biosciences) and enriched by fluorescence-activated cell sorting.

3D colony formation assay

Protocol was adapted from (Shapiro et al. 2014), Matrigel-on-top assay. A dense layer of Matrigel was diluted 1:1 with culture media and allowed to solidify. A single-cell suspension consisting of cells diluted at 3000 cells/cm^2 in a 1:50 Matrigel:culture medium dilution was prepared, and added on top of the base layer at twice the volume of the base layer.

Collagen contraction assay

Neutralized collagen I was prepared per manufacturer recommendations (Corning #354249) to a concentration of 3 mg/mL. Neutralized collagen I was added to cells diluted in culture medium at 150k cells/mL in a ratio of 1:2. This mixture was allowed to solidify in multiwell plates at room temperature for 15 minutes, then at 37°C for a further 45 minutes. After this time, gel edges were freed using a pipette tip, and an equal volume of culture medium was added atop the gel. Images were taken on an Olympus CKX31 inverted microscope, 1.25X objective. Percent contraction was measured by ImageJ software.

Focus formation assay

Cytosoft plates (Advanced BioMatrix) with an elastic modulus of 32 kPa were coated with 100 ug/mL Matrigel (Corning) diluted in PBS (ThermoFisher) for one hour at 37°C. Cells were seeded at 30k/well and incubated for 10 days. Adherent cells were fixed-stained with 0.1% crystal violet in 20% methanol-PBS for 30 mins, washed in tap water, and imaged in phase contrast using an Olympus CKX31 inverted microscope, 1.25X objective. Experiment performed in duplicate, and one representative picture is shown.

4.5 References

Gebbink, M. F., O. Kranenburg, M. Poland, F. P. van Horck, B. Houssa, and W. H. Moolenaar. 1997. “Identification of a Novel, Putative Rho-Specific GDP/GTP Exchange Factor and a RhoA-Binding Protein: Control of Neuronal Morphology.” *J Cell Biol* 137 (7): 1603–13.

Harris, S. L., and A. J. Levine. 2005. “The p53 Pathway: Positive and Negative Feedback Loops.” *Oncogene* 24 (17): 2899–2908. doi.org/10.1038/sj.onc.1208615.

Lim, Y., S.-T. Lim, A. Tomar, M. Gardel, J. a Bernard-Trifilo, X. L. Chen, S. a Uryu, et al. 2008. “PyK2 and FAK Connections to p190Rho Guanine Nucleotide Exchange Factor Regulate RhoA Activity, Focal Adhesion Formation, and Cell Motility.” *J Cell Biol* 180 (1): 187–203. doi.org/10.1083/jcb.200708194.

Miller, N. L. G., C. Lawson, X. L. Chen, S.-T. Lim, and D. D. Schlaepfer. 2012. “Rgnef (p190RhoGEF) Knockout Inhibits RhoA Activity, Focal Adhesion Establishment, and Cell Motility Downstream of Integrins.” *PLoS One* 7 (5): e37830. doi.org/10.1371/journal.pone.0037830.

Miller, N. L. G., C. Lawson, E. G. Kleinschmidt, I. Tancioni, S. Uryu, and D. D. Schlaepfer. 2013. “A Non-Canonical Role for Rgnef in Promoting Integrin-Stimulated Focal Adhesion Kinase Activation.” *J Cell Sci* 126 (Pt 21): 5074–85. doi.org/10.1242/jcs.135509.

Mitra, S. K., D. a Hanson, and D. D. Schlaepfer. 2005. “Focal Adhesion Kinase: In Command and Control of Cell Motility.” *Nat Rev Mol Cell Biol* 6 (1): 56–68. doi.org/10.1038/nrm1549.

Roy, L., and K. D. C. Dahl. 2018. “Can Stemness and Chemoresistance Be Therapeutically Targeted via Signaling Pathways in Ovarian Cancer?” *Cancers (Basel)* 10 (8): 1–23. doi.org/10.3390/cancers10080241.

Shapiro, I. M., V. N. Kolev, C. M. Vidal, Y. Kadariya, J. E. Ring, Q. Wright, D. T. Weaver, et al. 2014. “Merlin Deficiency Predicts FAK Inhibitor Sensitivity: A Synthetic Lethal Relationship.” *Sci Transl Med* 6 (237): 1–12. doi.org/10.1126/scitranslmed.3008639.

Ward, K. K., I. Tancioni, C. Lawson, N. L. G. Miller, C. Jean, X. L. Chen, S. Uryu, et al. 2013. “Inhibition of Focal Adhesion Kinase (FAK) Activity Prevents Anchorage-Independent Ovarian Carcinoma Cell Growth and Tumor

Progression." *Clin Exp Metastasis* 30 (5): 579–94. doi.org/10.1007/s10585-012-9562-5.

Yu, H.-G., J.-O. Nam, N. L. G. Miller, I. Tanjoni, C. Walsh, L. Shi, L. Kim, et al. 2011. "p190RhoGEF (Rgnef) Promotes Colon Carcinoma Tumor Progression via Interaction with Focal Adhesion Kinase." *Cancer Res* 71 (2): 360–70. doi.org/10.1158/0008-5472.CAN-10-2894.

4.6 Figures

Figure 4.1: The Rgnef-FAK connection promotes colony growth and contractility in extracellular matrix. **(a)** Expression of GFP-Rgnef and GFP-Rgnef FAK-binding mutant (d1292). **(b)** Schematic models of Rgnef full-length and FAK-binding mutant protein structure. **(c)** ID8-IP Rgnef-KO and -d1292 cells have significantly impaired colony growth by day 10 in Matrigel as compared to cells re-expressing GFP-Rgnef-WT. Also shown are representative pictures from day 9, right. (****p≤0.0001, n.s.=no significance). **(d)** ID8-IP Rgnef-KO and re-expressing cells were seeded onto a 32 kPa Matrigel-coated surface, and foci were visualized by crystal violet staining after 10 days. Experiment was performed in duplicate, with one representative image shown. **(e)** ID8-IP Rgnef-KO or re-expressing cells were seeded in collagen I gels and allowed to contract freely for 4 days. Also shown are representative pictures from Day 4 (*p≤0.05, n=2 biological replicates). **(f)** ID8-IP cells were grown in anchorage-independent conditions. 50k cells were seeded on day 0 and cells were counted at day 7 (**p≤0.01, ***p≤0.001, n.s. = no significance).

Figure 4.1

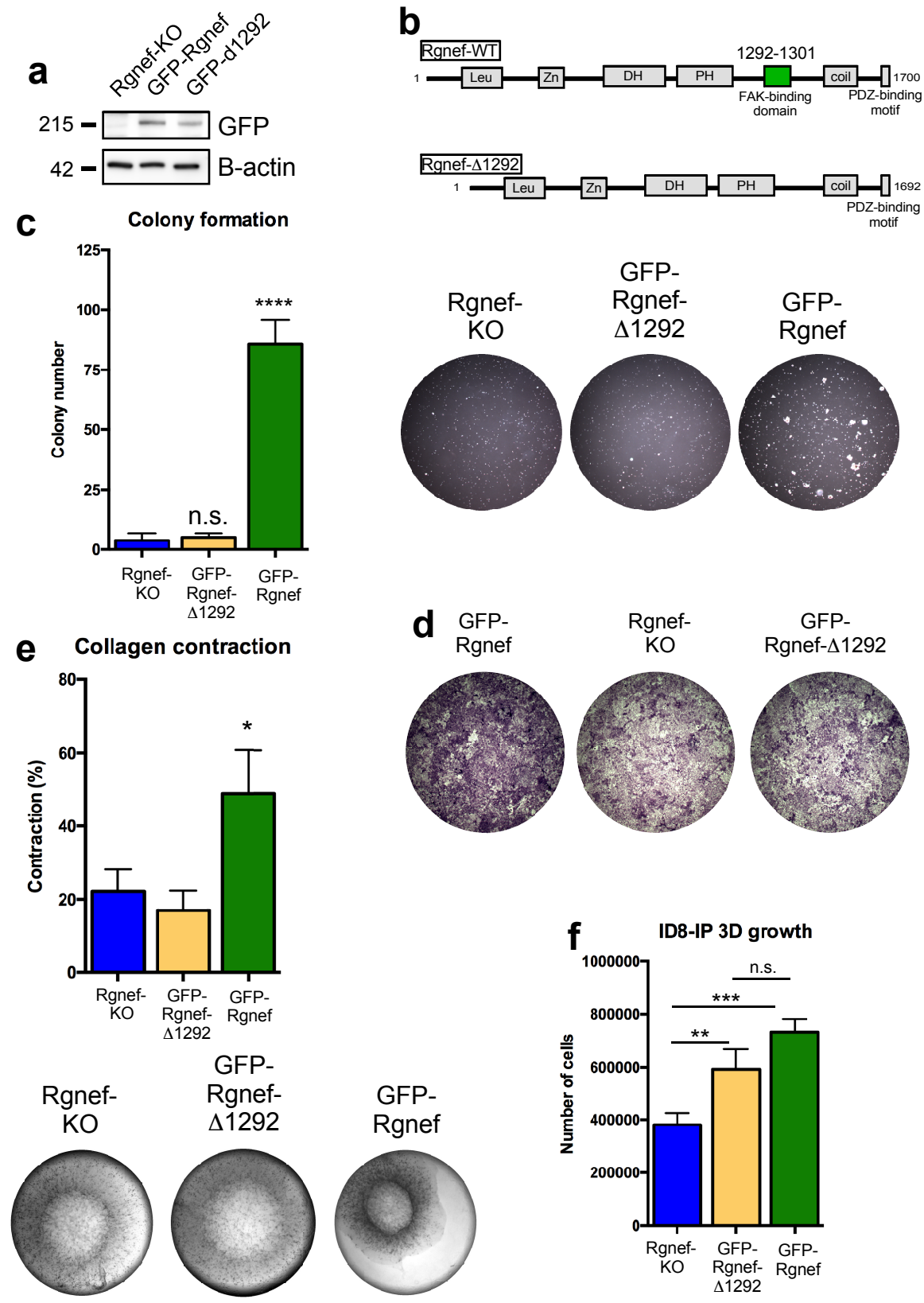
a
Rgnef-KO
GFP-Rgnef
GFP-d1292
215
GFP
42
B-actin
b
Rgnef-WT
1292-1301
1
Leu
Zn
DH
PH
coil
1700
FAK-binding domain
PDZ-binding motif
Rgnef-Δ1292
1
Leu
Zn
DH
PH
coil
1692
PDZ-binding motif
c
Colony formation
Colony number
125
100
75
50
25
0
****
n.s.
Rgnef-KO
GFP-Rgnef-Δ1292
GFP-Rgnef
Rgnef-KO
GFP-Rgnef-Δ1292
GFP-Rgnef
d
GFP-Rgnef
Rgnef-KO
GFP-Rgnef-Δ1292
e
Collagen contraction
Contraction (%)
80
60
40
20
0
*
Rgnef-KO
GFP-Rgnef-Δ1292
GFP-Rgnef
Rgnef-KO
GFP-Rgnef-Δ1292
GFP-Rgnef
f
ID8-IP 3D growth
Number of cells
1000000
800000
600000
400000
200000
0
n.s.
***
**
Rgnef-KO
GFP-Rgnef-Δ1292
GFP-Rgnef

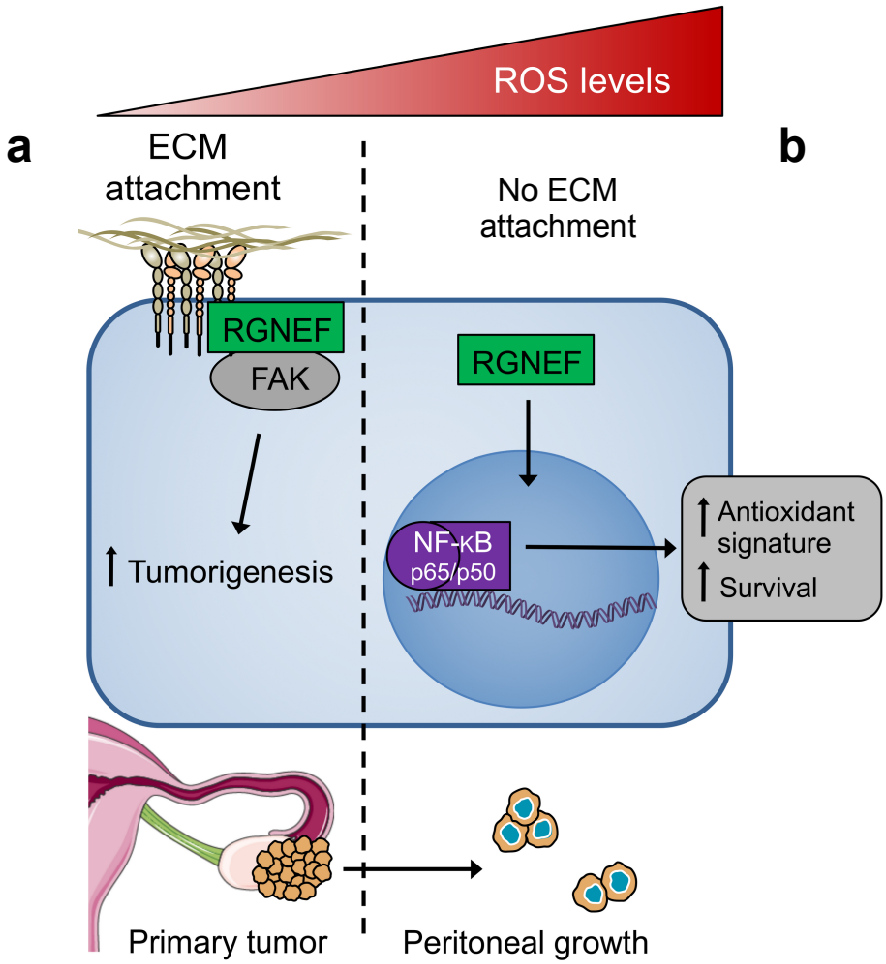

Figure 4.2: A unified proposed model of Rgnef in tumor progression. **(a)** When cells are attached to the ECM, Rgnef-FAK signaling is required for increased tumorigenesis. **(b)** ROS is increased upon loss of ECM attachment, as in shedding of tumor cells into the peritoneal cavity. In this context, Rgnef-dependent transcription of an NF-KB-driven antioxidant signature is critical to counteract increased ROS and promote peritoneal survival.